VI. NEW CALORIMETER DESIGN STUDIES

In the previous sections various issues of calorimeter utility and design have been considered at length. We have dealt with the physics to be accomplished, the spatial and energy resolutions desired, the various geometries which might be used, and the technologies available for building practical devices.

In this section we explore several examples of how these ideas can be brought together in a real detector. In this way we hope to begin an evaluation of various competing configurations and techniques. Some of the strengths and weaknesses of the various techniques will be clarified. In addition, these examples should help point out the areas of testing that will be necessary to assure the desired performance.

We have six examples which substantially span the space of available or anticipated technology:

* a drift-collection calorimeter
* hybrid readout proportional chamber calorimeter
* uranium-scintillator calorimeter
* liquid argon calorimeter
* hybrid readout drift-collection calorimeter
* compact calorimeter

A. Drift-collection Calorimeter

1. Introduction

Gas-sampling calorimeters based on drifting in long channels imbedded in radiator material have been investigated recently with considerable success. These systems include the drift-collection calorimeter[1] with drifting between parallel plates and the time projection quantameter[2] with drifting in channels normal to the radiator plates. The drifting ionization electrons are detected on proportional wires at the ends of

the drift channels. This readout can be done in narrow time buckets so that high spatial resolution and fine segmentation can be achieved with a modest number of readout channels. Information about the spatial structure of the shower can probably be used to enhance the energy resolution, at least for electromagnetic calorimeters.

A calorimeter based on long drift paths seems well suited to the low repetition rate of the SLC, which will obviate confusion between particles from successive beam crossings. The fact that in a general purpose detector some portion of the calorimeter must operate in a magnetic field complicates the use of long drift paths. However, as we discuss in the next section, the resulting constraints are tolerable. They do lead to a choice of the parallel plate or drift-collection calorimeter geometry.

In the remainder of this note, we first discuss the effects of magnetic fields and then present a specific calorimeter design suitable for use at SLC energies.

2. Drifting in Magnetic Fields

The calorimeter presented below has an electromagnetic part inside a solenoidal magnet coil and therefore in the full magnetic field of the detector. The hadronic portion of the calorimeter is partly outside the coil, where it is subjected to smaller, but less predictably oriented magnetic fields. Can drift-collection calorimeters coexist with real magnetic fields?

Two directions of drift are proposed below: axial drift between cylindrical plates in the barrel region; and radial drift between plates perpendicular to the magnet axis in the endcap region. The solenoidal field in which the drifting takes place is primarily axial, with a

smaller radial component. In addition there will be small azimuthal components arising from lack of cylindrical symmetry in the coil and flux return iron. The motion of drifting electrons is governed by the Lorentz force $F = e(E + v \times B)$, where v is the instantaneous velocity. Although the actual motion of the electrons is discontinuous and punctuated by frequent collisions with gas molecules, an adequate approximation is obtained by assuming a constant velocity $\langle v \rangle$ in the direction

$$(E + \langle v \rangle \times B). \qquad (1)$$

With this approximation we can now discuss drifting in the barrel and endcap portions of the calorimeter. In the barrel, the large axial component of the magnetic field is not troublesome, as the electrons drift along it. Further, radial fields produce an azimuthal component of drift, which is still acceptable in a cylindrical drift gap. It can be largely eliminated by pitching the drift electric field so that $(E + \langle v \rangle \times B)$ is still axial. If the compensation is not exact, the result will be an azimuthal distortion of position at the readout wires which can be corrected. Thus, only the azimuthal component of magnetic field--which produces radial components of drift velocity and hence tends to lose drifting electrons on the plates--is damaging, and it can be kept small by proper design of the magnet.

In the endcap portion of the calorimeter, the radial component of B is along the direction of drift, while the main axial component produces an azimuthal component of drift velocity, which as above is tolerable and largely correctable by the direction of the electric field. Here again it is the azimuthal magnetic field which produces drift into the plates, now with an axial motion.

We can use the approximate direction of Equation (1) to calculate a limit on the azimuthal magnetic field. The parameters below are such that half of the drifting charge will be lost if the angle of drift toward the plates is 0.005 radians. We equate this angle to $\langle v \rangle B_{phi}/E$, where B_{phi} is the azimuthal component of B. If we take typical values of $\langle v \rangle = 1 \times 10^4$ m/sec and $E = 2 \times 10^6$ v/m (e.g. in 90% Ar, 10% CO_2) we find B_{phi} = 0.01 Tesla = 100 gauss. In an axial field of, say, 5 kG, this should be attainable. This analysis of drift directions agrees within about 25% with measured drift angles in magnetic fields[3]. The disagreement with measurements, and indeed with a fuller analysis--are such that our calculations from (1) overestimate the effect of azimuthal fields.

An interesting possibility lies in the use of focusing electric fields[1]. In this case, the electric field at the plates always has a component toward the center of the drift gap, which tends to lessen the effect of azimuthal magnetic fields and of diffusion in the gas. In this case the tolerable B_{phi} can realistically be 300 gauss.

3. Construction

The calorimeter system suggested here is shown in Figure 1. It consists of an inner electromagnetic part and an outer hadronic part. In the barrel region, the electromagnetic part is shown inside the coil and the hadronic part is shown outside. Radiator plates are cylinders about the beam line in the barrel region and planes perpendicular to the beam line in the endcap region. The gaps between radiator plates are filled with a suitable drift chamber gas, such as 90% Ar + 10% CO_2, and electrodes on an insulating sheet mounted on the radiator plates establish an electric field to drift ionization electrons to one end of

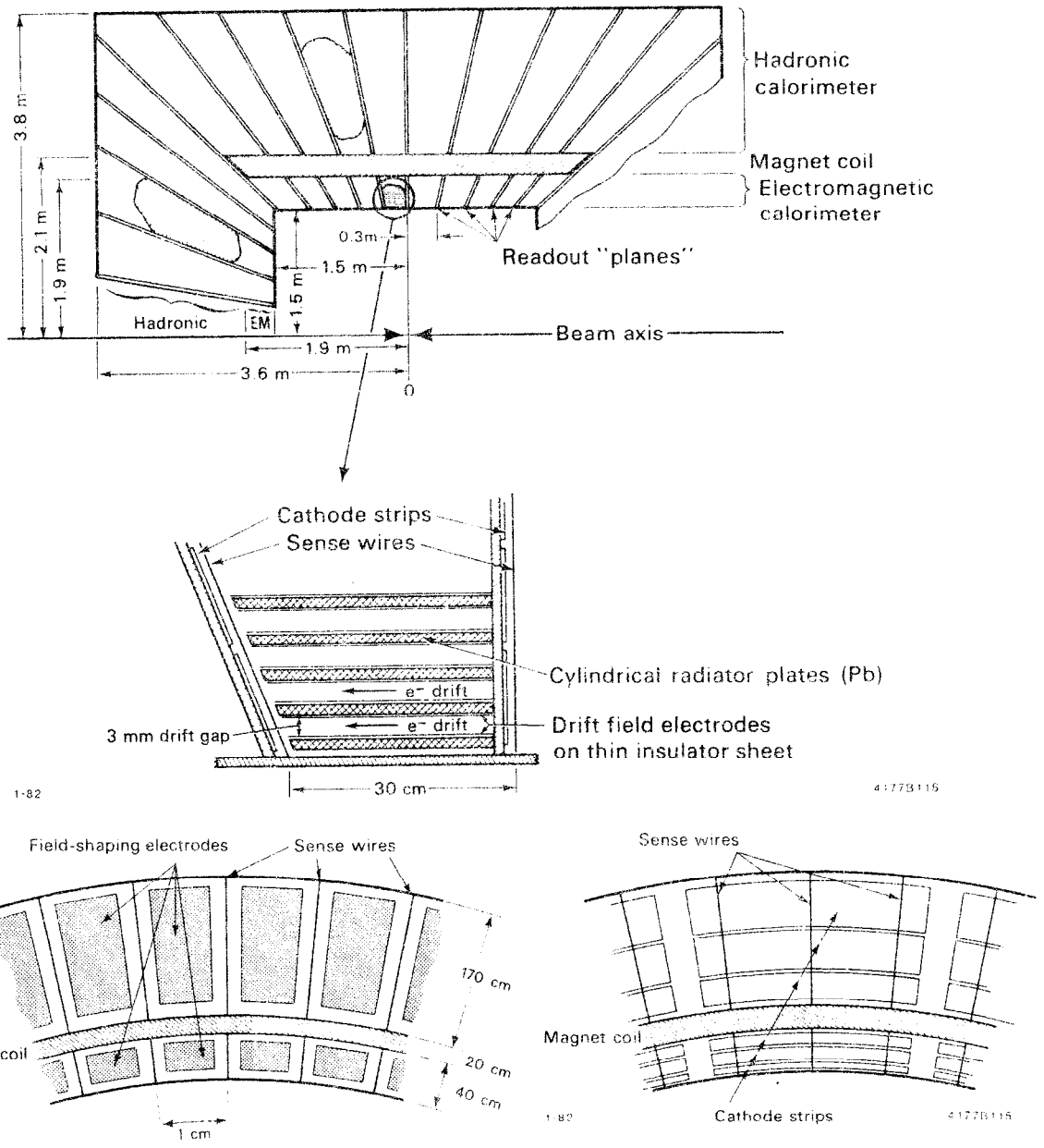

Not to scale

FIG. 1,2,3. Components of a drift-collection calorimeter.

a set of plates, where they are detected on proportional wires. The plates are assembled into modules with projective geometry, whose length is chosen to give a convenient drift distance. Suggested parameters are given in Table I. The system could be used either with uranium plates throughout or with lead plates in the electromagnetic part and iron plates in the hadronic part.

Read-out proportional wires are located in thin gaps (≃1 cm) between modules. These readout gaps are approximately radial and therefore form sections of cones. It seems necessary to run the wires radially, so that some care must be taken to obtain constant gain from the wires, since their spacing is not constant. A method of doing this with field-shaping electrodes between the anode wires is shown in Figure 2. The actual readout is from cathode pads adjacent to the wires, whose number and shape are chosen to give the desired azimuthal and longitudinal segmentation (see Table I). The arrangement of wires and cathode pads is shown in Figure 3.

Table I

Suggested Parameters

		ELECTROMAGNETIC	HADRONIC
Plate thickness		0.2 X_0	0.2 Λ_i
Drift gap		3 mm	6 mm
Drift distance		30 cm	40-70 cm
Total thickness		15 X_0	5 Λ_i
Polar segmentation (drift)		1.5 mrad	1.5 mrad
Azimuthal segmentation		25 mrad	25 mrad
Longitudinal segmentation		3 segments	3 segments
Channels	Barrel:	7500	7500
	Endcap:	4250	4250
Energy resolution x $\sqrt{E}$		0.12	Fe: 0.60 U: 0.35
Drift Electric Field		200 V/cm	
Drift chamber gas		90% Ar, 10% CO_2	
Drift velocity		1 cm/μsec	

X_0 = radiation lengths
Λ_i = nuclear interaction lengths

References

1. L. E. Price, Contribution to the International Conference on Instrumentation at LEP, Uppsala, Sweden, 1980, Physica Scripta 23, 685(1981);
L. E. Price and I. Ambats, IEEE Trans. Nucl. Sci. NS-28, 506 (1981).

2. H. G. Fischer and O. Ullaland, IEEE Trans. Nucl. Sci. NS-27, 38 (1980).

3. H. Daum, et al., NIM 152, 541 (1978).

B. A Hybrid Readout Calorimeter

We choose to push this particular example of proportional wire calorimeter technology to an extreme in order to illustrate a multiple stereo-view hybrid system. Two independent measurements of the shower energy are made, and this information is read out in two geometries.

The gross features of both the barrel and end cap calorimeters are: a total of 18 radiation lengths of lead plates, sampled by 4-mm gas gaps every 0.2 to 0.3 X_0. The radiators are made of lead-G10-aluminum sandwiches, so that the strip and tower cathodes can be cut out of the aluminum cladding on the G10 insulator. (This has been done for strips in the TPC barrel calorimeter for 6 foot by 12 foot sheets.) There should be at least two sections in depth, and preferably three, for improved pion-electron separation. The lead radiators could also be tailored for improved energy resolution. These details are not the central theme of this note, and will not be addressed.

The detailed geometric features are different for odd-numbered and even-numbered gaps. In the odd gaps there are proportional wires aligned axially, allowing either a modular construction or a monolithic cylinder construction depending upon mechanical support constraints. Cathode strips which pick up the induced signal from the proportional avalanche are aligned at +60° to the wires on one side of the gap, and at -60° to the wires on the other side. Thus, the odd gaps alone comprise a complete calorimeter with three stereo views.

The even gaps again have axial wires, but with cathode strips at 90° to the wires on one side of the gap, and rectangular pads on the other side. The gap width and pad sizes are chosen so that an integral number of strips covers one pad in both the wire and 90° cathode views. These

even gaps also comprise a complete calorimeter system, with two stereo views and towers. These are illustrated in figures 1, 2a and 2b.

The electrical grouping of these wires and cathodes into electronic channels can be done on the edges of the modules, or at one or two seams if the barrel is monolithic. There is a routing problem with the tower signals, which at least can be solved by introducing an additional insulating layer in the laminate which carries the tower pads.

All channels are projective; this is easy for the cathodes, and possible with the wires, since at reasonable gains the gain variation is very small for changes in wire separation.

A slight economy in the number, s, of channels can be obtained by varying the strip width and tower size so that each subtend a constant angle when viewed from the interaction point. This is also a nice feature in the physics analysis since the angular resolution on a reconstructed shower is roughly independent of where it is in the system.

The electrical grouping of the wires and cathodes into electronic channels produces one set of channels for the towers, one set each for the +60°, -60°, and 90° cathodes; and one set each for the wire channels in the odd and even gaps. In this way we make two measurements of the shower energy--one in the even gaps and one in the odd. The respective cathodes in each gap just pick up the induced signal from the avalanche, and this coupling is good to about 2% rms precision. This coupled-energy information is read out along three stereo views in the odd gaps, and along two stereo views and one tower view in the even gaps. The correlation between the energy measurements in the odd and even gaps is a function of shower energy, typically 90% at 10 GeV and 50% at 1 GeV.

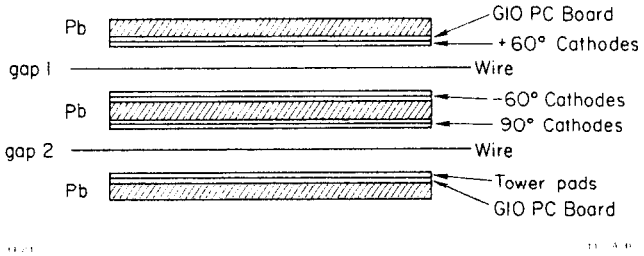

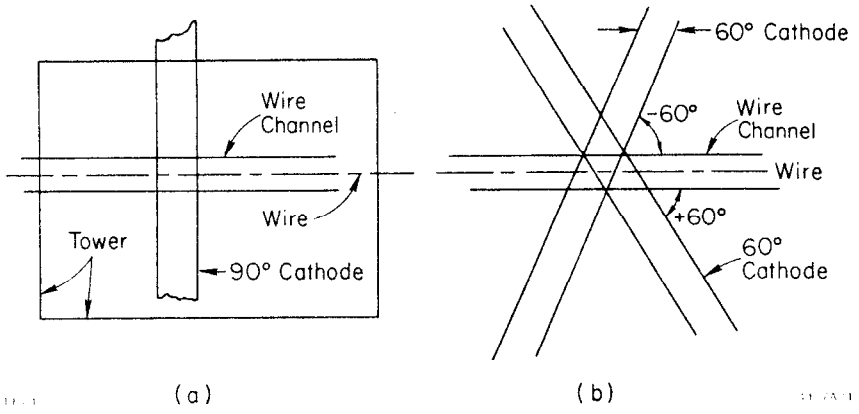

FIG. 1,2a,2b. Components of a hybrid readout calorimeter.

This can be used in addition to the over-constrained geometry in the reconstruction.

Along the wire stereo view one can make more precise measurements of energy for those showers which do not share a wire channel with any other shower by using the smaller of the two interleaved wire signals. This preferentially throws away those channels with large delta ray fluctuations in them, and gains back some of the energy resolution lost in a gas calorimeter.

This calorimeter could only reasonably be run at one atmosphere so the rms energy resolution would be about $16\%/\sqrt{E}$; the strips would be about one cm wide, well-matched to the intrinsic width of electromagnetic showers in a calorimeter of this sampling frequency. The towers would be about 15 to 20 centimeters on a side. The cost can be reduced with little effect on the performance by doubling or tripling the channel widths near the back of the calorimeter where the showers are wider. In addition, one could choose not to segment the even gaps (90° cathodes and towers) in depth, since the 60° views of the odd gaps would contain information in two or three depth sections.The point is that there are many choices for readout which can be implemented since the connections would be made using wire-wrap pins to tie the sets of wires or cathodes into electronic channels.

A calorimeter with such tight control over the geometry would be easy to analyze and powerful in its ability to resolve detail and unravel events. Clearly, there is a lot of information in a calorimeter of this sort.

The problems of building a wire proportional system are severe for such a large system; however, the TPC pole-tip calorimeters have

achieved a wire-to-wire gain variation of about 12% for an Fe^{55} source, and this is quite adequate.

C. Uranium and Scintillator Calorimeter

We consider here a scintillator and uranium-plate detector based on towers subdivided by orthogonal x and y strips. The towers are constructed so that they maintain projective geometry in both the shower chamber and hadronic calorimeter section. A tower cross section is shown in Figure 1 and a cut-away of the detector is shown in Figure 2.

We advocate the use of uranium plates in order to achieve the best hadronic energy resolution and to minimize the problem of energy calibration between photons and hadrons. In the shower chamber the plates would be about one half a radiation length thick (1.5 mm) and in the hadron calorimeter they would be about 3 mm thick. These 3 mm plates would be alternated with 5 mm thick copper plates after every two uranium plates. The shower chamber would be about 14 radiation lengths in total thickness and be located inside the coil. This configuration is desired to minimize the hadronic confusion in the shower chamber. The hadron calorimeter would be about five absorption lengths in total thickness--thick enough for the missing energy studies. The outer two absorption lengths could probably be made of pure copper which would save a substantial amount of money.

The inner section of the shower chamber, shown in Figure 3, is designed to locate each photon by digitizing the conversion vertex. This is done by drifting the ionization into small-angle stereo anode wires. Perhaps three anode wires between radiator plates will be necessary to handle the frequent occurrence of oblique tracks. Each gap

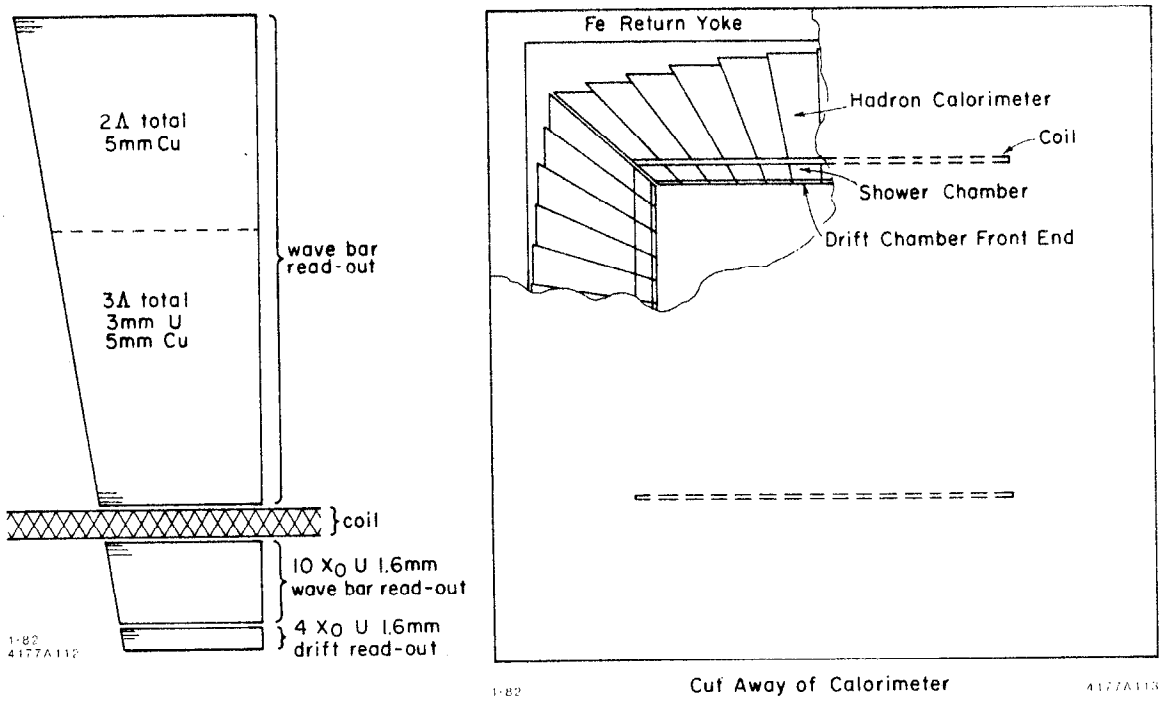

Cut Away of Calorimeter

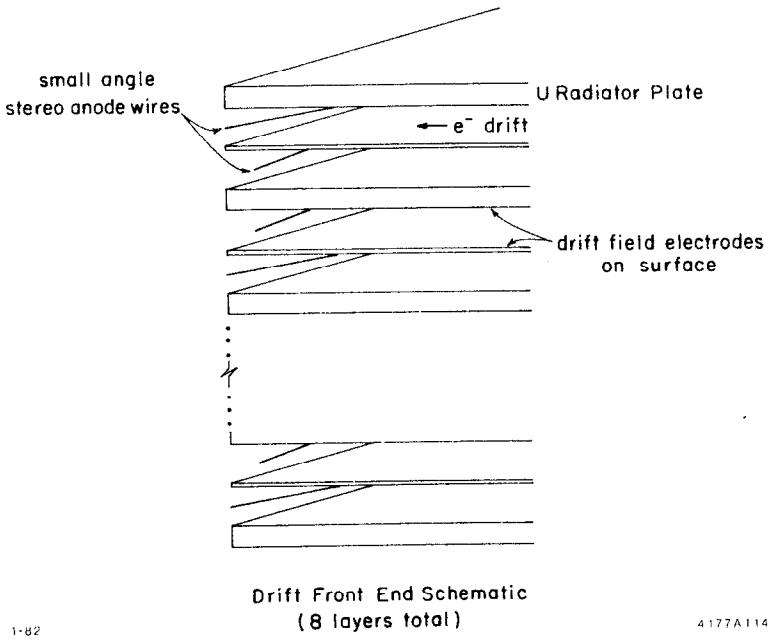

Drift Front End Schematic
(8 layers total)

FIG 1,2,3. Components of a uranium-scintillator calorimeter.

is independently digitized so that the conversion vertex can be determined.

An accurate measurement of the conversion vertex can greatly improve the pattern recognition of showers and their energy measurement in the presence of nearby showers. This measurement will also provide a substantial improvement in π/e separation by rejecting apparent electron showers caused by nearby photons.

It appears that micro-channel plate photomultipliers (MCPPMT's) would be a technically feasible and economically advantageous method of reading out the shower chambers. These devices have been used in magnetic fields of up to 7 kilogauss without appreciable loss of gain so they could be used inside the coil without long and cumbersome light pipes. Hamamatsu is developing a single step MCPPMT which would lower the price by perhaps a factor of 10. Furthermore, multiple anodes are easy to construct, and several wave bars could be read by one MCPPMT.

Perhaps the most important aspect is the fabrication of the uranium plates at reasonable cost. There is sufficient metal available but it is stored in the form of UF_4 and UF_6, so very expensive processing is required to make it into ingots. There is some scrap, but much of it is high in carbon and is very difficult to fabricate. The Rocky Flats uranium fabrication facility expects to produce abut 100 tons per year of uranium shavings. The Department of Energy is currently considering other possibilities of disposing of these shavings which are now burned and buried. One option is to build a plant that would allow the recycling of these shavings into plates for high energy physics.

The resolution obtained from the small angle stereo drift chamber needs to be studied. Shower simulations (from the EGS program) indicate

that good resolution can be obtained, but the real world may be different. The micro-channel plate devices have yet to be built in the desired configuraion. The precise resolution obtainable needs study.

A summary of the calorimeter construction cost and performance is contained in the following table. The cost estimates are very tenuous, especially concerning the uranium plates. Although it seems possible to use liquid scintillator, plastic strips cut with lasers or diamond saws may be more attractive.

Tower-Strip Hybrid Summary

700 Towers covering a central detector
3 meters in diameter and 3 meters long

Tower Design

a 25 X 25 cm^2 at inner face
b 5 X 25 cm^2 strips of scintillator, projectively larger
c 3 radial sections read out

1. 4 X_0 with drift readout and small-angle stereo
2. 10 X_0 U/Scintillator with wave-bar readout
3. 5 absorption length hadron section (3 U/Cu, 2 Cu)

Costs (in M$)

a	10 X_0 U shower chamber	.5
b	3 absorption length U/Cu	6.0
c	2 " " Cu	.5
d	Liquid scintillator	.5
e	14,000 PMT channels	1.0
f	11,000 TDC's	.3
g	7,000 ADC's	.5

Goals

a Equivalent E_γ and E_h response
b Good resolution
1. $10\%/\sqrt{E}$ electrons and photons
2. $36\%/\sqrt{E}$ hadrons

c precise location of converted γ's
d good e/π separation
e projective geometry and easy jet analysis

D. Liquid Argon Systems

This note discusses the salient characteristics of a calorimeter system which is based on liquid argon as the active medium.

We will consider some of the virtues of a liquid argon system, some of the problems, and a simplified design which will illustrate what can be accomplished.

The SLC event environment presents extreme challenges to a calorimeter design in several areas. We have spent a good deal of time discussing geometry, i.e., strips versus towers versus combinations. A liquid argon system allows readout in just about any geometry and is as flexible in this regard as any other technique we have considered. It is likely that we will settle on a combination of strips and towers as the best geometry for a calorimeter--projective geometry will have substantial benefits, although it introduces added complexity in mechanical construction. Such a radiator configuration can be realized in a liquid argon device in a natural way and without compromise.

Since a liquid argon detector is just a series of parallel plate ionization collectors, it is easy to see that radiator material can be arranged in any way which suits the physics, subject to strength of materials and structural integrity considerations. This can be done without regard to constraints imposed by stringing fine wires or guiding light to PMT's or channel plates. Supports will generate dead space of a few percent, but this is likely to be less than in other systems. The fact that charge is collected without gain in the medium and with a collection distance of a few millimeters results in uniform system response without the necessity to correct for light attenuation, wire gain variations (with time or along the wire length), or loss of charge

in a long drift space. This means that the ideal system resolution can be more closely approached in a liquid argon detector than in other types of devices. The experience of the Mark II versus other PEP detectors bears this out. The obtainable energy resolution of a sampling detector is often characterized by the plate thickness in radiation lengths. This resolution is never realized in practice for a variety of reasons. Gas sampling has the problem that the statistics of energy loss in the sampling medium dominates shower statistics. Scintillator sampling has a problem with photoelectron statistics as well as with uniformity of light collection. The analogous problem in liquid argon is the contribution of electronic noise. This is a negligible contribution to the energy resolution for the Mark II at PEP and would be even less significant at the SLC.

Another limitation on actual system performance is interchannel calibration and gain stability. In a liquid argon system, interchannel gain variations are determined with a precision pulser system to 1%. This takes a minute or two and thus can be done as often as desired. Other systems are in general much more difficult to calibrate, which means that there is a very real degradation of system performance.

The choice of medium has other important ramifications. Dynamic range requirements at the SLC are extreme. For the electromagnetic calorimeter a range of from 0.1 to 50 GeV is required. When fluctuations in energy deposition into individual channels are considered, the required dynamic range becomes more than 1000. All types of systems will find this difficult but possible to realize at the amplifier/ digitizer end, but saturation of proportional wire gain or scintillator light output must also be considered. There is no such

problem in a liquid argon system. In a hadron calorimeter the presence of both minimum ionizing particles and heavily ionizing nuclear fragments only aggravates this problem in other systems.

If a liquid argon system is so great, why is it not everyone's universal choice? The answer lies in the complexity of a liquid argon detector and in the size of the cryogenic system needed for a liquid argon based hadron calorimeter. The necessity of uniformly cooling large masses of material results in a large cryogenic system consisting of vacuum tanks, insulated transfer lines, high-integrity containers for the radiator/argon stacks, and large argon and nitrogen storage vessels. All the problems posed by such a system have been solved in the Mark II. A system incorporating a hadron calorimeter is a good deal larger (see below). It seems worth debating whether the performance benefits of a liquid argon system justify its complexity. It is possible that given the knowledge gained with the Mark II, certain simplifications in mechanical construction can be envisioned. For example, the Mark II barrel region was built as eight separate modules due to uncertainties in reliability. This allowed running with a certain number of modules out of action at any given time. This happened only once--very early on-- and a compartmentalized system may not be warranted. This could result both in simplified mechanical construction and in reduction of dead spaces in azimuth, which could be particularly important at the SLC.

In a new detector both electromagnetic and hadronic calorimeters should be considered together. They would be built in the same dewar, have a single cryogenic system, and use identical electronics.

The objective is to design the highest quality electromagnetic

calorimeter possible in the context of a general purpose detector. This means a device with excellent spatial and energy resolution, any degree of segmentation--both longitudinal and transverse--required by the physics environment, and the ability to realize the small scale performance characteristics in the context of a large system.

In the electromagnetic sector, radiator plates are uranium 1 mm (0.3 X_0) thick. In the hadronic section, plates are alternately 3 mm uranium and 3.7 mm copper, both corresponding to 0.025 absorption lengths. Total thickness of the electromagnetic section is 60 plates providing 18 radiation lengths and 0.5 absorption lengths. The hadron section has 180 plates, providing an additional 4.5 absorption lengths. With a liquid argon gap of 3 mm, the total thickness of the stack is 1.38 meters. Energy resolution on the basis of radiator thickness would be $8\%/\sqrt{E}$ for photons and electrons and $38\%/\sqrt{E}$ for hadrons.

Nitrogen consumption for the 800 ton device would be several times that of the Mark II, and the amount of nitrogen used for cooldown would be increased by a factor of five or so, but neither of these costs is prohibitive.

A combined strips/towers geometry would be complicated to build using any readout technique, but it may be easier in a liquid argon device than in some other approaches. A proportional chamber system with cathode strips and tower pads can be realized with any desired dimensions and can easily incorporate projective geometry. Interconnection of individual elements is difficult and tolerances on gap thickness and wire uniformity are extreme. Such a device would also be very thick, since gaps have to be large (1 cm) so as to be able to meet reasonable construction tolerances. In addition, energy

resolution, particularly in the electromagnetic section, is severely compromised by Landau fluctuations in energy deposition in the gas and by problems of calibration and gain stability. A calorimeter based on long drift spaces has the resolution limitations of any gas sampling device. It also presents the problem of providing carefully graded electric fields over acres of surface and maintaining efficient charge collection in different orientations in the face of ExB forces. This is a particular problem in the endcap region. This type of device is also likely to have large dead spaces. Further, a strip/tower scheme seems difficult to implement.

Dead spaces are also a problem with a scintillator/wave bar design. Another difficulty would occur in simultaneously providing strips, towers and projective geometry. Readout of several layers in depth could also be awkward. Resolution is likely to be compromised by photon statistics.

The stack structure in a liquid argon calorimeter could be constructed as a series of alternate,large ground-plane layers and layers with radiator cut into appropriate strip or tower elements, forming parallel plate capacitors. Since each grouping forms only a parallel plate ionization chamber, construction tolerances are quite loose. For example, while displacing a cathode plane in a proportional chamber results in two gaps with radically different gains, such a displacement in an ionization chamber has no strong effect on the response of either gap. Construction of the stack in this way is compatible with a cylindrical annulus design for the barrel, which results in no ϕ dead spaces, as well as a planar endcap design. The most difficult problem would be to interconnect the appropriate elements

reliably in different layers to form a single electronic channel. In the eight module strip geometry design of the Mark II, all connections could be made at the outer edge of the stack. This is not possible in the more complex geometry under discussion for the SLC. All the strip/tower systems have the same problem with interconnections. It is worth noting that the Young's modulus of uranium is close to that of steel, so that many of the construction problems due to the use of lead would disappear. Capacitance of a given electronic channel can get as large as 50 nF. In a storage ring this could be a problem, since amplifier time constants would be constrained by the collision frequency to be of the order of one microsecond. This would result in equivalent noise contributions of 15-25 MeV per channel, and would necessitate cumbersome low inductance connections. With the 180 pps repetition rate of the SLC, very long time constants can be used, resulting in negligible noise. Thus a liquid argon calorimeter in the SLC environment would not have to cope with a signal to noise problem, and low energy photon efficiency would be affected only by material before the counter, as is true in other approaches.

A cost estimate of the liquid argon calorimeter may be made by scaling from Mark II. The uranium and copper radiator material would cost 4M$, the stack fabrication 2M$, the electronics 2M$, the cryostats 1.5M$ and the cryogenics (tanks, transfer lines, controls) 2.5M$, for a total of 12M$. This may be somewhat more costly than some other techniques, but not by a large factor.

E. Hybrid Drift Calorimeter

This is a conceptual design elaborated in the course of the study of

a subgroup charged with investigating the division of tasks between electromagnetic and hadron calorimeters. The four design considerations are:

* Precise trajectory information is more informative than precise energy information.
* For a calorimeter that surrounds a tracking device inside a magnetic volume, the differential showers/cascade buildup pattern is the most valuable tool for e/hadron, μ/hadron, γ/hadron rejection, etc. Hence a good fraction of the available means should be spent on optimal instrumentation of that calorimeter section.
* There should be minimal material thickness between interaction point and shower buildup section. That puts at least this section of the calorimeter inside the coil for the standard solenoid magnet.
* The presence of a hadron calorimeter is essential for a number of vital functions: few, however, are going to suffer severely if the hadrometer section (i.e., the hadron calorimeter part that follows the electromagnetic shower detector and which acts as the buildup phase for many of the hadron cascades) is "skimpily" instrumented, as long as good position determination is assured.

Based on these concepts, the following rudimentary design is proposed as reasonable in cost but effective for most known applications.

1. Assume good charged-particle tracking in a cylindrical drift chamber volume of 1.5 m radius; particle identification by dE/dx and TOF. Minimal mass, low Z_{eff}
2. Shower buildup sections: 4 X_0 finely layered Pb (or preferably U)/drift chamber device; modified tower structure; high spatial resolution; good pattern recognition at moderate cost through the

use of large drift cells (drift lengths of up to 30 cm).

3. 16 X_0 more-crudely-layered shower counters; similar basic structure; thicker layers, readout ganging. Overall $\delta E(sh)/E$ = (15-20%)$\sqrt{E}$.

4. Coil (assume less than 1 X_0 thickness).

5. Hadrometer Fe-drift chamber principle: crude radial segmentation (3 times 1.5λ); but good position measurement for π/μ rejection.

The scheme is indicated schematically in Fig. 1. Clearly, many variants are possible. If the radial dimension inside the coil becomes critical, Part 3 above can be moved outside the coil. The basic drift chamber technology can be replaced by scintillator/BBQ wave bar units in all but the first 4 X_0 of the electromagnetic section, but at some cost in precision of localization. If liquid argon is desirable as an ionizing medium, the often-quoted boundary conditions that there has to be one cryogenic volume can probably be circumvented by incorporating the "buildup phase" 4 X_0 (section 2 above) into the cold shield for a superconducting magnet coil, which is in a convenient temperature range.

We stress the following points, referring to the subsystems 1-5 above:

* A fairly standard central drift chamber will provide good momentum measurement for charged particles up to momenta of $\simeq$ 10 GeV. The inherent limitations of a layered gas discharge detector, therefore, do not seriously limit electron energy determination.

* The shower buildup section which samples the first 4 X_0 at frequent intervals (e.g., every 0.3 X_0) provides both excellent localization of photon conversion and a considerable factor in π/e discrimination

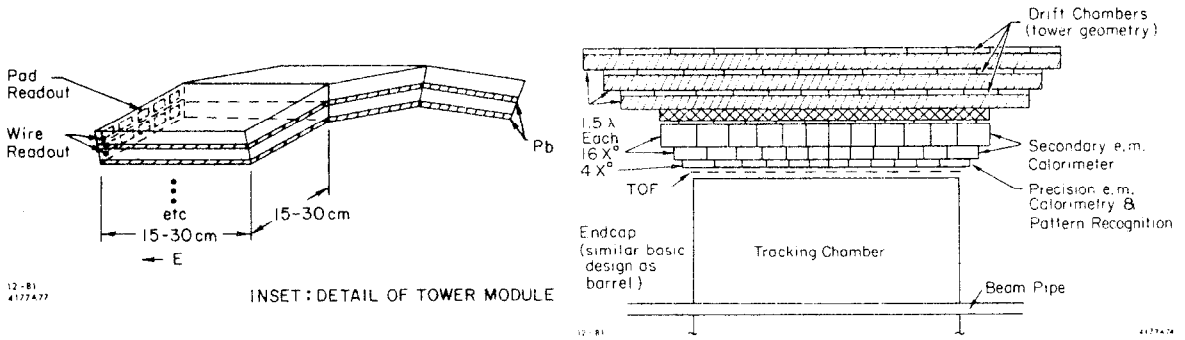

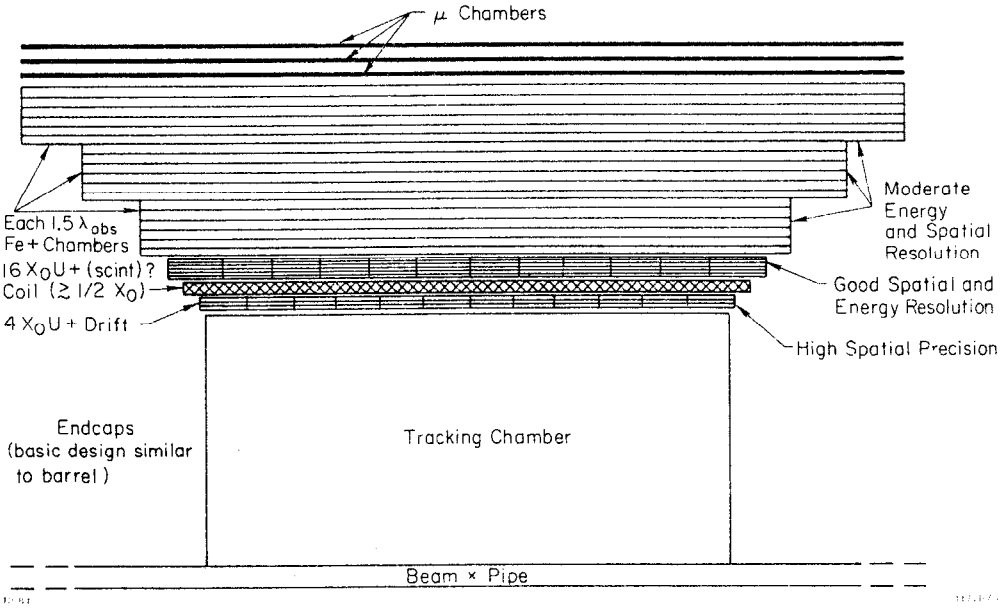

FIG. 1,2. Components of a hybrid drift calorimeter.

(at least 20).

* Both in this section and in 2) above, ganging of the pulse height information will have to be judiciously used to limit the number of electronic readout channels without the loss of vital information. This section may, if needed, be moved outside the coil; in that case, it will be necessary to seek the thinnest coil possible to limit shower spread and unobserved energy deposition.

* The coil may be conventional or superconducting. If the latter, its total geometrical thickness may be hard to keep acceptable for a split shower calorimeters arrangement.

* While there is some argument that a hadrometer arrangement, as sketched in Fig. 1, will be sufficient for most presumed physics needs, we point out that: (a) the localization in this section has to be kept well defined, to assist in π/μ rejection; (b) for the same purpose, two consecutive chambers outside the last iron absorbers will help to depress punch-through by determining the exact line-up and direction of particles. On the other hand, it may well be advisable--whether economically feasible or not--to break up the hadrometer into some or many more layers (Fig.2). Radial ganging of readout information then becomes mandatory on economic grounds.

F. A Compact Calorimeter

A relatively inexpensive compact detector system is considered for physics in the region of the Z^0. The detector is based on fieldless calorimetry, using a precision electromagnetic calorimeter made of bismuth germanate crystals (BGO) and a moderately good iron hadrometer. The physics strengths and weaknesses of such a design are discussed.

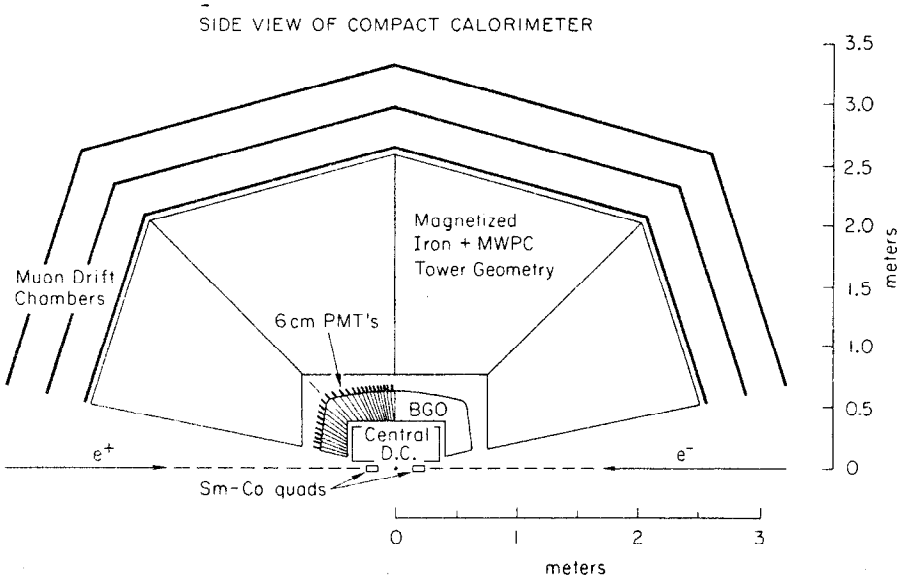

FIG 1. Schematic of a compact calorimeter.

The conclusion is that such a detector serves as a useful complement to more traditional solenoidal magnet designs.

1. Design Philosophy

There has been much discussion of the severe constraints placed on SLC detector design by the very high multiplicities, collimated geometries and wide range of particle energies expected to be present. Traditional solenoidal detectors either become very expensive or must optimize for physics not dependent on penetration to the jet core or on total event reconstruction. It thus becomes apparent that much of the physics to be done at the Z^0 does not necessarily require the traditional strong points of the solenoidal design.

Given the pragmatic difficulties of financing and building several large calorimeters for SLC, we consider the alternative of abandoning the large magnetic volume in conventional solenoids and using a fieldless compact design. The compactness is augmented by the use (in this example) of BGO ($Bi_4Ge_3O_{12}$) crystals as the electromagnetic calorimeter. We do not use the most compact and precise hadron calorimetry available (uranium) on the grounds that magnetized iron allows a handle on muon charge and momentum not afforded by the higher precision uranium.

In addition, the precision in energy and angle of a BGO shower counter opens up some physics possibilities precluded by conventional electromagnetic calorimeters, because of the superb energy resolution and the sensitivity to low energy γ's. We consider this a bonus added to the primary objective of keeping the size and complexity of the hadron calorimeter under control.

The total thickness of the iron and sampling detectors in the hadron

calorimeter in this exercise is 1.8 m, starting at 75 cm from the IR. Thus our definition of a "compactness" results in a radius of about 2.5 m for the high-density part of the detector. This does not include the external drift chamber system necessary to measure the muon momenta up to 50 GeV; this would add >1 m to the total radius. Both calorimeters would cover as much total angle as practical--the Sm-Co quads providing a limit for the electromagnetic calorimeter of $\Omega/4\pi$ = 99%. A schematic drawing of the calorimeters is given in Fig. 1 (above).

2. Description of the Calorimeter

a) Electromagnetic Calorimeter

Since BGO is relatively unknown as a particle detector, we summarize the relevant parameters in Table 1, using NaI(Tl) for comparison.

Electromagnetic shower containment to the 98% level for 10 GeV showering particles dictates a thickness of 20 X_0 (=22.4 cm) for the BGO calorimeter. The next parameter to be specified is the inner radius, which we choose to be 40 cm--mainly due to cost considerations. Experience with the Crystal Ball detector at SPEAR leads to a preference for projective tower geometry for the segments of the BGO shell, and a cylindrical shape for the inner cavity, for more effective usage of the limited space available for charged particle tracking. The θ/ϕ segmentation comes out naturally at a total of about 10,000 crystals (each axially viewed by a photomultiplier) from a number of practical considerations such as available phototube diameters as well as the wish not to degrade severely the potentially excellent angular resolution of the material. Each of the 10,000 modules would have an inner side of 1.4 x 1.4 cm^2 and an outer side of 2.2 x 2.2 cm^2. A somewhat surprising fact is that a module of this size will contain typically more than one

TABLE I

BGO - NaT(Tℓ) COMPARISON

	BGO	NaI(Tℓ)
Mechanical		
Specific Gravity	7.13	3.67
Hardness	~5 (soft glass)	~2 (rock salt)
Stability	rugged	cleaves, shatters easily
Behavior Near Melting	"crystalline"	"amorphous"
Chemical		
Stability	good	poor
Solubility (H_2O)	none	very hygroscopic
Optical		
Refractive Index	2.13	1.85
Absorption Length	?	?
Scintillation		
λ_{max} Emission	480 nm	420 nm
Rise, Fall Times	~50,300 ns	50,250 ns
Photoelectrons/MeV Deposited	300-500 (tube depn'd't)	
Relative Pulse Height (on PMT)	8-13	100
Temp. Coeff. of Light Output	~1.7%/°C	~.8%/°C
Nuclear		
Relative Neutron Cross Section	.25	1
Nuclear Absorption Length	~23 cm	~41 cm
Relative Radiation Hardness	?	1
Shower Detector		
Radiation Length, X_o	1.12 cm	2.59 cm
Critical Energy	10.5 MeV	12.5 MeV
Moliere Radius	2.24 cm	4.4 cm
dE/dx (min)	~8 MeV/cm	4.8 MeV/cm
E-Resolution (σ/E) at .67 MeV (best)	4.3%	2.6%
E-Resolution (σ/E) of Practical Detector (~16 R.L. thick)	$E < .1$ $.2\%/\sqrt{E}$ $.1 < E < 1$ 1% $E > 1$ $1\%/\sqrt[4]{E}$	$\sim \frac{2.6\%}{\sqrt[4]{E_{GeV}}}$
Angular Resolution of Practical Detector	~6 mr Monte Carlo	~20 mr Crystal Ball
Economic		
Cost/Liter (small quantities)	15 K$	---
(large quantities)	6 K$ (projected)	1.8 K$
Cost/X_o^3 (large quantities)	9K$ (projected)	28 $

half the energy of a 10 GeV photon. This dictates a large dynamic range (10^5) and low gain (i.e. <10 dynodes) for the PMT; a prototype under development for a Munich Max-Planck-Institut group[1] is only 6 cm long (without base) and would thus keep the hadron calorimeter as compact as possible.

b) Magnetized iron calorimeter

This section is not designed in detail but the basic dimensions of this piece can be chosen for setting the overall scale and for compatibility with the physics aims of calorimetry at SLC energies.

The inner cylindrical cavity has a radius of 75 cm and a length (along the beams) of 2 x 75 cm. The total radial depth of 1.8 m (1.2 m Fe + 0.6 m of proportional chambers or scintillator) need be instrumented only for the first four or five absorption lengths. The 1.2 m thickness of iron is required for muon filtering. The iron, toroidally magnetized, should be divided in four sectors in θ and six or eight sectors in ϕ to save on the total volume. The choice of the sampling material needs further investigation. Consider two possibilities:

* Scintillator with wavebar readout. Two extensive studies of the resolution of iron-scintillator calorimetry were carried out at CERN[2] and at Fermilab with neutrino detectors[3]. The CDHS group at CERN obtains $\sigma/E = 0.58/\sqrt{E}$ with 2.5 cm Fe absorber thickness. Further improvement can be obtained by reducing the iron thickness to 1 cm [4]. We have not investigated whether wavebar readout would deteriorate the resolution appreciably.

* Proportional tubes used in self-quenching streamer mode. Unpublished work by M. Atac at Fermilab[5] shows that this detector

produces large pulse heights (eliminating the need for local preamplifiers). The energy resolution could be as good as $\sigma/E = 0.6/\sqrt{E}$, but this number awaits confirmation.

In any case, a significant improvement over the standard $0.8/\sqrt{E}$ figure for Fe sampling calorimeters seems achievable.

In projective tower geometry, the useful limit on tower segmentation is set by the transverse development of hadronic showers in iron, where after one absorption length 95% of a hadron shower is contained in a cone 7 cm wide[4]. The BGO calorimeter is 1 nuclear absorption length thick and should thus spread out about 60% of the hadrons by this amount. This in turn suggests that the first absorption length of iron might be usefully segmented in 1 cm radial layers and somewhat more finely than 7 x 7 cm^2 in θ-ϕ to improve the energy/angle measurement for hadrons that did not interact in BGO.

With 5 x 5 cm^2 towers in the inner, more finely segmented part, followed by wider towers with 2.5 cm absorber thickness (each covering the four inner, finer towers)) we obtain a total of about 3700 individually-read-out towers.

3. Performance Parameters

a) Central tracker:

Although this section is not concerned with the design of a tracking chamber, one might question the precision available in a 40 cm radius device. Since there is no field, one need only provide a good match to the calorimeters. Trackers have been produced which give $\sigma(\theta,\phi) = 6$ to 17 mr (depending on θ) in 25 cm of spherical geometry. Scaling suggests that 3 to 10 mr in 40 cm of cylindrical space is quite reasonable. This will be an adequate match to the calorimeters.

b) Electromagnetic and hadron calorimeters:

The energy resolution of a BGO calorimeter module has been investigated both experimentally[7] and through the use of the EGS Monte Carlo. The behavior as a function of energy is complex and very detector-dependent. It is dominated by photoelectron statistics up to about 100 MeV and for a practical detector is parametrized by $\sigma(E)/E = 0.2\%/\sqrt{E}$, where $E<0.1$ GeV. For $0.10<E<1.0$ GeV a transition region is encountered as the photopeak disappears (shower leakage). Here, $\sigma(E)/E$ = 1% independent of E. At $E>1$ GeV leakage fluctuations dominate. Then $\sigma(E)/E \rightarrow 1\%/E^{.25}$, E in GeV.

The angular resolution expected for a single photon can be scaled from the Crystal Ball result, using the larger radius of the BGO shell and the smaller Moliere radius (see Table 1). This gives exactly the result of a Monte Carlo calculation of G. Blanar et. al.[1], and yields for this geometry: $\sigma(\theta_\gamma) = 6$ mr. This is limited by the segmentation and <3 mr is possible in principle.

For a single noninteracting particle the track is typically contained within a single crystal (entrance face dimension averages 1.4 cm) and the resolution in angle is given classically by $\sigma(\theta(\text{charged})) = (1.4\text{cm}/\sqrt{(12)})/40$ cm = 10 mr (or <7 mr with finer segmentation).

If the hadron interacts within the BGO (as about 60% will), then --assuming it can be recognized as such-- $\sigma(\theta(\text{charged}))$ might deteriorate to 20 mr. If it does not interact in BGO, it will shower in the finer-grained towers of the hadron calorimeter and will have an independent measurement with $\sigma(\theta(\text{charged})) = 20$ mr. The value 20 mr is assumed throughout, although 40% could have better determinations.

The ability to separate two showering particles (such as independent

γ's randomly overlapping, or correlated γ's from a π^0) depends on their relative energy and on the compactness of their (fluctuating) shower pattern. Here the quality of BGO far exceeds that of NaI because of the smaller Moliere radius of BGO. More precisely, the experience with the Crystal Ball may be used to define how well such overlapping γ's can be distinguished and how they scale with radiation length: the smallest opening angle needed to recognize photon pairs for the BGO shell should be about is 17 mr. This translates to $p(\pi^0) \leq 8$ GeV/c.

For the reconstruction of π^0's the device will have the usual large combinatorial background due to the high γ multiplicity. For unambiguous π^0's the energy of the π^0 will be very precise, being just $E(\gamma 1) + E(\gamma 2)$. The error on the π^0 reconstructed mass will be dominated by the angular errors, but will be a factor of about 4 improved relative to the Crystal Ball. At the mean pion momentum of 2.5 GeV/c it will be $\sigma(\pi^0 \text{ mass}) = 6\% \cdot \text{mass}$, deteriorating rapidly for higher momenta. The mass resolution for heavy objects decaying into two photons will be much better (see section 4 b).

The general problem of overlap of particles in the combined calorimeter is very model-dependent. The typical showering particle will light up about $\pi r_m^2/\pi r_{in}^2 = 0.1\%$ of 4π ster, or about 8 crystals (r_m=Moliere radius, r_{in}=inner radius). A non-interacting charged particle is contained in 0.01% of 4π(1 crystal). Interacting hadrons have greater variations in pattern, but should also light up $\approx$0.1% of 4π. Thus, the average two-jet event with 10 showering, 4 non-interacting and 6 interacting particles per jet will light up only 1.4% (per jet) of the available 50% of 4π. This fraction seems small enough to guarantee particle separation, except for the dense jet core.

For example, the one-third of all particles in a given jet that will lie within a ±200 mr cone (1% of 4π per jet) will light up 0.5% of the 4π of BGO. Each cone will have 7 particles in 100 crystals; ambiguities will abound. The situation does not improve with greater segmentation.

In the hadron calorimeter, confusion between individual particles will of course get worse. The limit here is the compactness of the detector itself. Useful energy flow measurements can be done, however; CUSB at CESR and MARK J at PETRA have done energy flow studies using apparatus that is at the same distance from the IR (or closer) and typically 100 times less-segmented than the calorimeters being considered here.

The energy resolution of the combined calorimeters for the visible energy is estimated by assuming 29% of the energy in photons and electrons, 67% in hadrons and a mean multiplicity of 20 charged particles[6]. Since about 60% of the hadrons will interact in the BGO, the resulting dE/dx is included as electromagnetic energy. The combined device resolution is ±5%; the physical distribution may be wider because of missing energy. This should be adequate for separation of the 2-γ processes and states with anomalous missing energy.

c) Muon measurement:

The precision on the muon measurement obtainable with 1.2 meters of magnetized iron, followed by drift chambers measuring the exit angle, is almost momentum-independent and in the range of 20-25%. This will allow charge identification over the whole momentum range. The total equivalent iron thickness (BGO + Fe) is 1.5 m, resulting in a punch-through probability of <1.5% for 15 GeV pions. Decay probabilities are much smaller due to the small decay volume.

4. How much physics can a compact calorimeter do at the SLC?

The three following sections specify the physics areas where the compact calorimeter will do

-- as well as general magnetic detectors or

-- better than other detectors (or where it would be unique) or

-- inadequate measurements or no measurements at all.

a) Physics that can be done as well as with other detectors

(1) Z^0 mass, width, hadronic and leptonic decay ratios

(2) $\sigma(e^+e^- \rightarrow$ hadrons) on and off the Z^0 pole: Here, the 5% rms error in the total energy measurement allows good discrimination against 2-γ processes and therefore high precision in measuring R.

(3) Jet studies: (quark-antiquark, quark-antiquark-gluon, γ-gluon-gluon):

As is characteristic of non-magnetic calorimeters, charged particles would not be spread out by the field and no detailed tracking and pattern recognition would be needed to perform jet studies. How well can one study the global parameters (sphericity, thrust, aplanarity...) that characterize the jet structure of events? Equivalently, what do the angle/energy resolutions given above imply for the resolution on the global jet parameters, compared to solenoidal detectors? The error distribution in reconstructing the jet axis (for two-jet events) does not change much using a high-quality (uranium) calorimeter rather than a conventional iron-scintillator detector[6]. A BGO device should perform in between these two cases. The following table details the comparison.

Calorimeter	dθ (em)	dE(em)	dθ (had)	dE(had)	dθ (jet)
Uranium	10mr	$10\%/\sqrt{E}$	10mr	$35\%/\sqrt{E}$	18
Iron	20mr	$20\%/\sqrt{E}$	20mr	$70\%/\sqrt{E}$	22
BGO - Fe	6mr	1%, E>1 GeV	20mr	$60\%/\sqrt{E}$	20

Energy flow analysis of multi-jet events will not be hindered by lack of individual energy-angle measurements on some of the particles. The limit on multi-jet analysis is set by the transverse spread of the jets themselves, and this is expected to be four to five times as broad as the hadron calorimeter segments. The analysis of energy flow within a jet is limited instead by the transverse spread of hadron-initiated showers in the iron calorimeter (7 cm) and its distance from the IR (75 cm). This sets the scale of the finest structure observable within a jet at about 100 mr.

(4) muon charge asymmetry. In addition to what was said in the section on detector performance, note that a $\delta p/p = 0.5\%p$ magnetic detector will give the same charge separation at 50 GeV/c; the symmetry in θ of this design would make the muon measurement more angle independent and bias-free.

(5) Muon inclusive spectra. With 1% or better pion rejection it should be relatively easy to measure muon spectra from quark semi-leptonic decays, at least outside the jet core where the lepton/hadron ratio is $\simeq 0.08$ and relatively independent of angle[6]. Over this region, representing >95% of $\Omega/4\pi$, the muon's $p_\perp$ (relative to the jet axis) will allow tagging of the parent t-quark. The momentum-independent $\delta p/p$ should be adequate to study the smooth spectrum expected.

(6) $e^\pm$ inclusive spectra. At first sight it might appear that the lack of segmentation along the particle's path would hinder the $e^\pm$/hadron resolving power of the electromagnetic calorimeter. In analogy to the muon spectra though, most of the interest in is $e^\pm$ away from the jet core and with $p(e^\pm)>2$GeV. The complementary region is

exceedingly difficult for any detector due to Dalitz pairs, γ conversions etc. For such electrons (and hadrons) note that

* A 15 GeV pion will deposit on the average 37% of its energy in 17 cm of Fe (equivalent to the electromagnetic calorimeter) while a 15 GeV $e^{\pm}$ will of course be 98% absorbed[8].

* The same pion will be entirely absorbed by the hadron calorimeter.

Although similar numbers for lower-energy hadrons are needed, it is apparent that the BGO-Fe correlation is a powerful tool for e/π separation in the absence of overlaps. The transverse shower profile information should provide at least 10 times rejection against pions with p>2GeV. Last, there are novel ways to obtain longitudinal shower development information without significantly modifying the properties of the BGO calorimeter. In summary, the combination of calorimeters should provide at least 100 times hadron rejection outside the jet core and can thus give $e^{\pm}$ spectra at the same level of muon spectra. The major drawback here is the lack of lepton charge identification.

(7) Other Calorimeter Applications.

Consider two more calorimeter applications pointed out in SLC notes:

* quark flavor tagging by missing $p_{\perp}$ [6]

* Higgs mass reconstruction by measuring the hadronic decay products[10]. The Higgs tag would be missing energy and transverse momentum in the reaction $Z^0 \rightarrow \nu\bar{\nu}H$; using an iron calorimeter for the Higgs debris, a mass resolution of 10% seems achievable.

b) Reactions Relying on Precise Electromagnetic Calorimetry:

These processes are typically rare, perhaps to the point of being unobservable, but some of them are very important; in these processes the very good energy resolution would generally enhance signal/noise.

(1) e+e- → $\gamma\ \nu\bar{\nu}$ above Z^0 pole: Here the virtually full solid angle of the electromagnetic calorimeter should help suppress beamstrahlung and e+e- → 3 γ backgrounds[9]. The good sensitivity and resolution for photons with E < 1 GeV allows the center-of-mass energy to be set just above the Z^0 pole with subsequent large increases in the signal.

(2) $Z^0 \rightarrow e^+e^-H$: If this important reaction occurs at an observable rate, it can be seen best in this calorimeter because the resolution on the missing mass to the e+e- pair is unequalled by any other detector. The error on the mass, dominated by the error on the e+,e- energy measurement, is $\delta M/M = \delta E(e+ \text{ or } e-) = 1$ to 2% for 20 GeV < M(Higgs) < 50 GeV. The remarks on e/hadron separation of the previous section apply here.

(3) Monochromatic Photons: Consider the following two processes, even though they may take place at extremely small rates:

$Z^0 \rightarrow \chi(t\text{-tbar}) + \gamma$. This would proceed through the t-tbar decay of Z^0, the two quarks then rearranging themselves according to the χ-state wave function by hard monochromatic photon emission.

e+e- → toponium states: in the a priori unlikely but amusing case that the mass of toponium is only a few GeV below the Z^0, the γ-Z^0 interferance will enhance toponium production. The advantages of a calorimeter with good resolution for low-energy γ's is obvious.

c) What cannot be done

Items such as hadron inclusive spectra, hadron identification, and lifetime measurements that require the momentum of the charged particles are obviously ruled out for this detector. Note, however, that a precision drift chamber, measuring the decay vertex of a long-lived quark, could provide lifetime information if the invariant mass of the

quark decay jet and its total energy are measured in the calorimeter system.

5. Cost

Given the uncertainties, the cost can be estimated to ± 30% as follows (in M$):

BGO at large scale production price, .75 m^3	4.5
10,000 1.25 inch by 2 inch phototubes	0.5
Read-out electronics at 100 dollars/channel	1.0
Fe Calorimeter (exclusive of muon chambers)	2.0
Readout electronics	.6
Central chambers + electronics	.5
Muon chambers + electronics	1.0
	≃ 10.0

References

1. G. Blanar et al., "Design Study for a Compact LEP Detector" presented at 1st LEP-HERA Seminar, MPI-Munich, Sept. 1980, and at 2nd Workshop on Detectors for e+e- at 100 GeV, Cornell University, Jan. 1981.

2. CDHS group, CERN-EP/80/188 (October 1980).

3. Caltech-Fermilab group, Nucl. Instr. and Meth. 130,49(1975).

4. S. Iwata, "Calorimeter", DPNU-13-80, Nagoya Univ.

5. We thank K. Shinsky for bringing this work to our attention.

6. V. Luth, SLC Workshop Note 18.

7. M. Cavalli-Sforza , CLNS 81-490.

8. M. Holder et al., Nucl Instr. and Meth. 151(1978) 69.

9. G. Barbiellini, B.Richter and J.Siegrist, SLAC-PUB 2744.

10. R. Hollebeek et al., SLC Workshop Note 27.

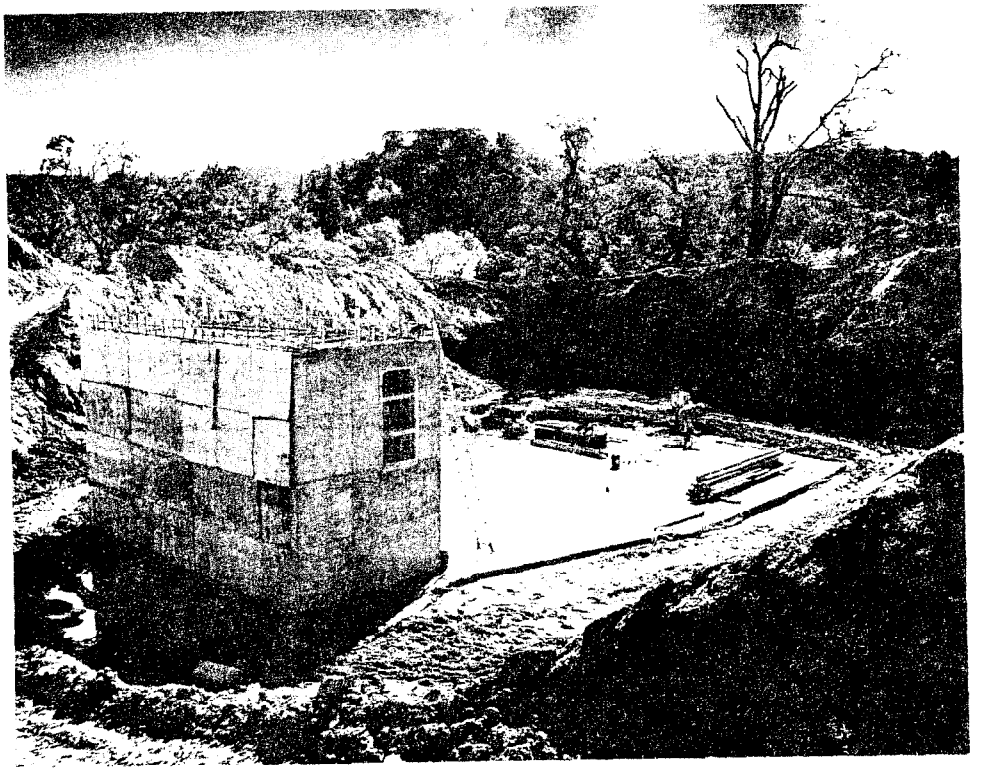

Excavation for the SLC Damping Ring project began in the spring of 1981 and was completed by the end of summer. The second photograph shows the concrete vault and access before final covering with earth in the fall.

PARTICLE IDENTIFICATION

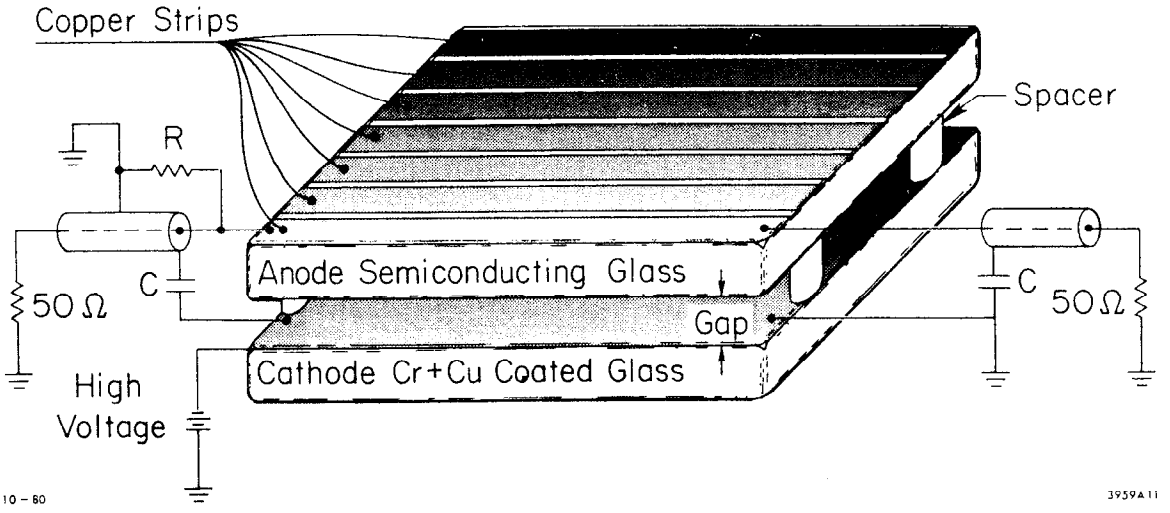

PARTICLE IDENTIFICATION

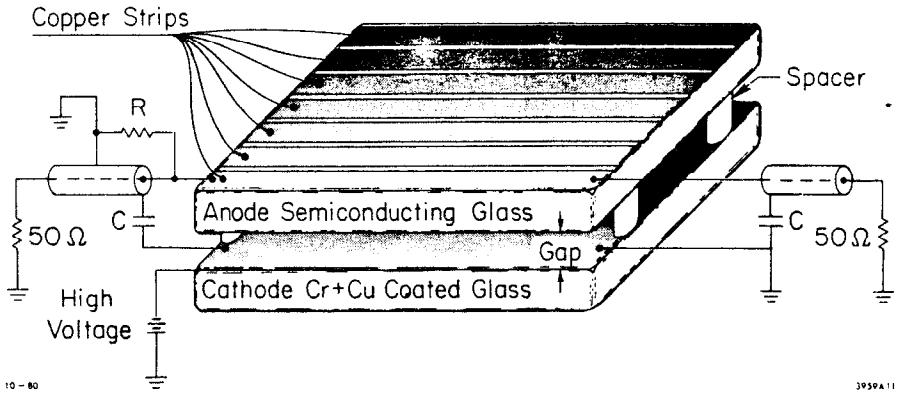

INTRODUCTION

In this report are presented the results of the SLC working group on particle identification. The report consists of four sections, each of which deals with a particular method of particle identification. These sections cover dE/dx, Čerenkov radiation, time-of-flight (TOF), and transition radiation detectors. The main emphasis of the studies has been on hadron identification and e/π separation. In general, muon identification has been left to the calorimetry subgroup.

The task of this group has been to review the various methods of particle identification, in particular as applied to the SLC environment. This was to be done without designing a real detector. Because of this restriction, the study is not complete, but we have gone as far as possible under the imposed constraints. We have presented the current state of the art in terms of detector design and provided limits on achievable resolutions and momentum ranges over which particle identification is possible. For the most part, the problems of segmentation cannot be dealt with until one can discuss actual detector designs, taking into account particular physics desires as well as additional components of a complete detector (e.g., shower counters, tracking chambers, etc.). One exception is for TOF, where the standard system of TOF scintillation counters can be reduced to a one-dimensional problem and one can discuss the question of segmentation in a semi-reasonable manner.

Finally, we are making no decision as to the best or optimum system to be used for particle identification. Again, this can only be decided within the context of a physics program and the design of a complete detector.

dE/dx

In recent years, a number of large scale detectors (see Table I) have been built to measure particle energy loss in a gas. The experimental evidence indicates that such devices can be used dependably to measure particle velocity. One advantage of this method of velocity measurement over others is that the detector that measures the energy loss can simultaneously measure the position of the particle. This not only makes efficient use of space, it also greatly reduces the confusion in associating the energy loss measurements with tracks.

A choice between the TPC approach and using wire chambers to measure dE/dx involves a large number of factors as much concerned with tracking as with particle identification. In fact, financial considerations may dictate the choice. Rather than duplicate the work of the tracking group we will limit our considerations to the accuracy with which dE/dx can be measured under various circumstances and what this translates into for identifying particles.

We have decided to use a phenomenological approach as a basis for the dE/dx predictions. The method is described in Ref. 1. The method is based on work of Walenta and Alison, although some independent input is made by Va'vra. The basic idea of this technique is to constrain the formulas for energy loss and resolution by the experimental data. This parametrization is done in terms of gas pressure, sample thickness, number of samples, the mean ionization potential, density, Z, and A of the gas medium. Because this is not a Monte Carlo calculation, one can make a fast calculation for any particular design (the computer program is available). The comparison between the program predictions and the experimental results is shown in Table I. Measurements have been made by experimenters with different particle types at different momenta. To provide a basis for comparison, the quantity $\Delta E/\sigma$ has been determined from

Table I. dE/dx Comparison with Experiments

Device	n·t·p [cm·arm]	Part.	p [GeV/c]	$\Delta E/\sigma\|_{exp}$	$\Delta E/\sigma\|_S$	$\Delta E/\sigma\|_V$
TPC(T)	192x0.4x10	π/e	0.8	11.8	16.8	14.2
ISIS(T)	60x1.6x1	π/e	0.5	8.0	12.0	10.9
CRISIS(T)	64x1.5x1	p/π	40.0	2.2	3.5	2.8
EPI	128x6.1x1	p/π	50.	5.1	6.2	4.8
JADE	48x1x4	π/e	0.45	5.0	11.3	10.0
JADE[1]	48x1x4	π/e	0.45	4.2	11.3	10.0
CLEO	117x0.733x2.4	π/e	0.45	8.3	14.7	12.7
Va'Vra I	41x1.5x1	π/e	4.0	3.2	5.0	4.2
Va'Vra II[2]	36x1.2x1	π/e	4.0	2.7	4.5	3.7
Va'Vra - 45°	36x1.7x1	π/e	4.0	3.5	4.9	4.1

Notes: 1) Analysis among large numbers of tracks in small solid angle (jet-like)

2) Full size prototype (not published yet)

3) For all calcualtions we used 90% Ar + 10% CH_4 gas.

4) $\Delta E/\sigma|_{exp}$ - Measurement

$\Delta E/\sigma|_S$ - Sternheimer estimate

$\Delta E/\sigma|_V$ - Va'vra estimate

experiment (exp), from old Sternheimer theory (S), and from the phenomenological approach mentioned above (V). ΔE is the difference in dE/dx for the two particle types. σ is the truncated mean of the distribution width obtained by disregarding the 30-50% of the samples with largest values to eliminate the Landau tail. $\Delta E/\sigma$ is therefore the number of standard deviations between different particle types.

As can be seen, the experimental values are lower than model calculations. The phenomenological approach is closer to experiment but perhaps still 20% optimistic. In what follows, we employ the phenomenological values. The predictions for possible designs that we might consider are shown in Table II and Figs. 1-3. In Fig. 4 is presented the results of calculations[2] of the expected particle separation for the TPC made using atomic energy loss models. A comparison of Figs. 3 and 4 demonstrates that the empirical model used in this note and calculations from first principles agree fairly well.

To scale from these particular examples to different designs one might use the following empirical scaling formulas:

$$\text{RESOLUTION} \simeq (\text{PRESSURE})^{-0.32}$$

$$\simeq (\text{SAMPLE THICKNESS})^{-0.32}$$

$$\simeq (\text{TOTAL NUMBER OF SAMPLES})^{-0.43}$$

$$\text{RELATIVISTIC RISE} \simeq (E_{max}/E_{min}) = 1.6 \times (\text{PRESSURE})^{-0.09}$$

These are fits to the data below 10 atm. One should use thse scaling formulas only for a crude orientation. To obtain more accurate answers one should use the above mentioned program instead. This is necessary to predict the effect of a different gas, for instance. Generally, one can argue that the gas with lower mean ionization potential improves the particle separation in the nonrelativistic region - see Fig. 2.

Table II. dE/dx Summary of Predictions

Example	n·t·p [cm·atm]	>4σ momentum limits [GeV/c]	
1 ("Minimum" effort)	40x1x1	π/e:	0.18-3.6
		π/K:	<0.5
		π/p:	<0.9
		K/p:	<0.9
		π/μ:	<0.07
2 ("TPC" effort)	200x0.4x10	π/e:	0.2-7.5
		π/K:	<0.78 and 1.5-7.5
		π/p:	<1.35 and 2.1-37.0
		K/p:	<1.6
		π/μ:	<0.2
3 ("Intermediate" effort)	100x1x1	π/e:	0.15-6.5
		π/K:	<0.62
		π/p:	<1.05 and 2.7-23.0
		K/p:	<1.15
		π/μ:	<0.12

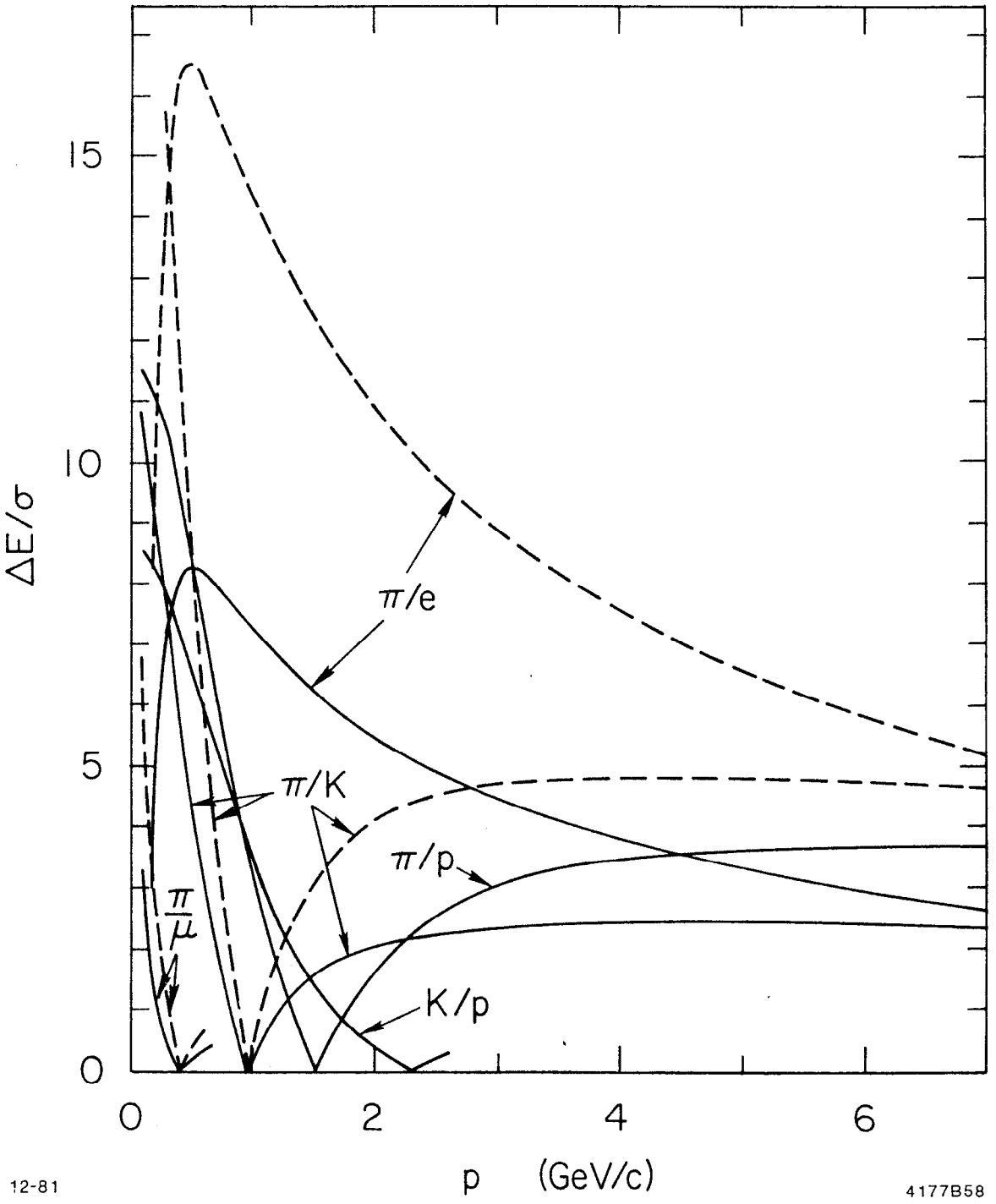

Fig. 1. Particle separation vs. momentum - dependence on number of samples. Data is for 90% Ar + 10% CH_4, 1.0 cm/sample, 1 atm., and 40 samples (solid curves) or 200 samples (dashed curves).

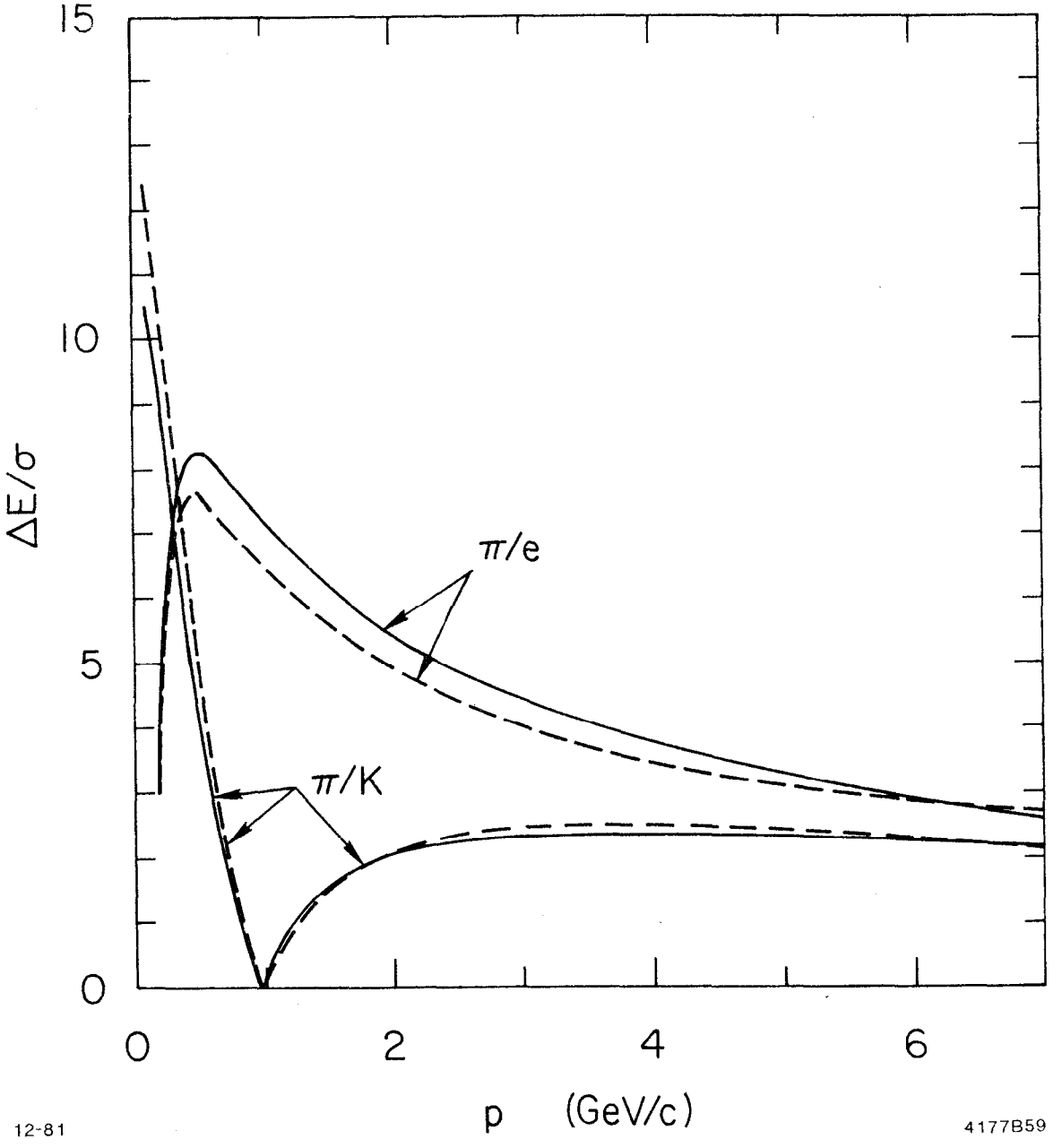

Fig. 2. Particle separation vs. momentum - dependence on gas. Data is for 1.0 cm/sample, 1 atm., 40 samples, and 90% Ar + 10% CH_4 (solid curves) or 50% Ar + 50% C_2H_6 (dashed curves).

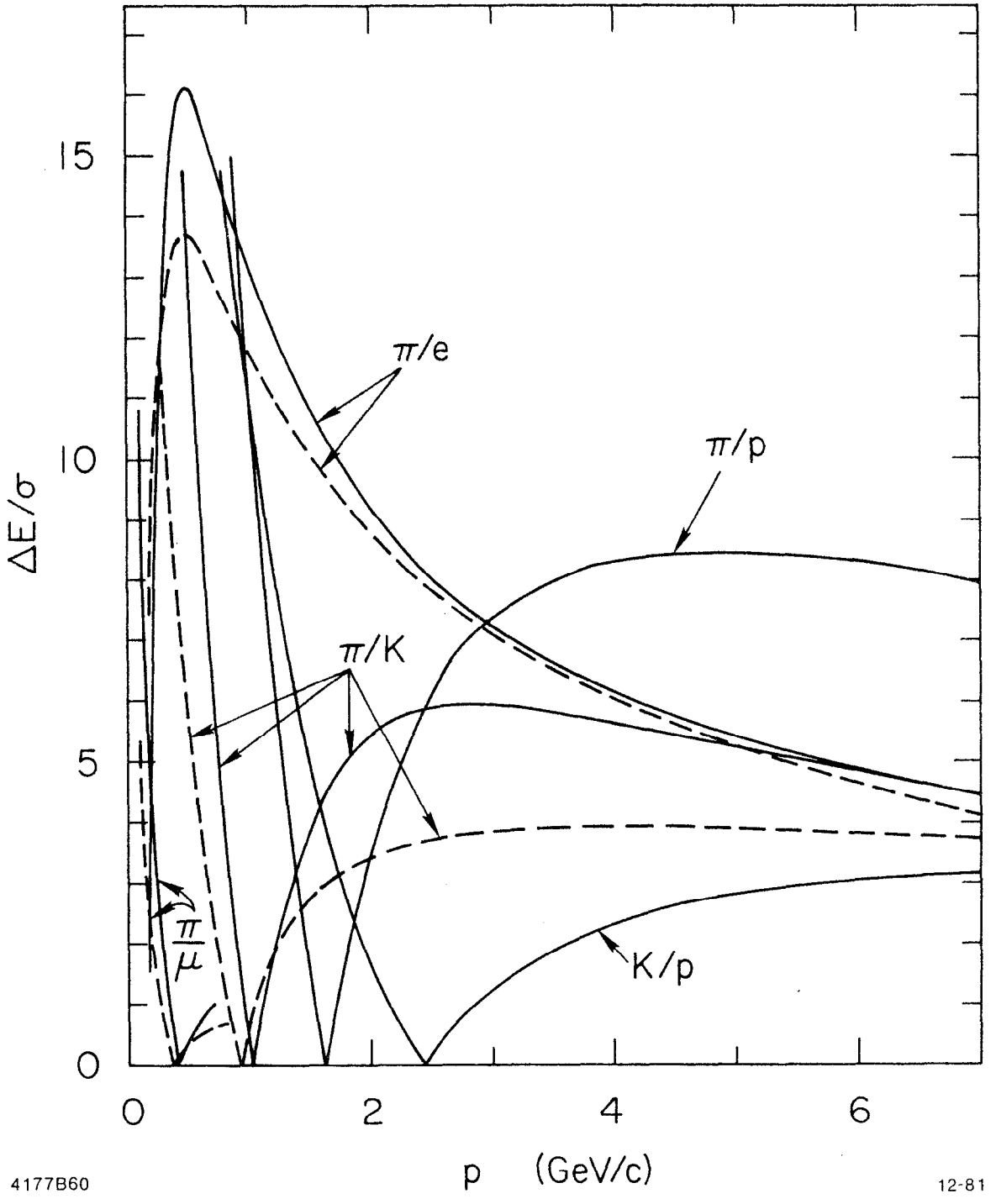

Fig. 3. Particle separation vs. momentum - dependence on presssure. Data is for 90% Ar + 10% CH_4, 0.4 cm/sample, 200 samples, and 10 atm. (solid curves) or 1 atm. (dashed curves).

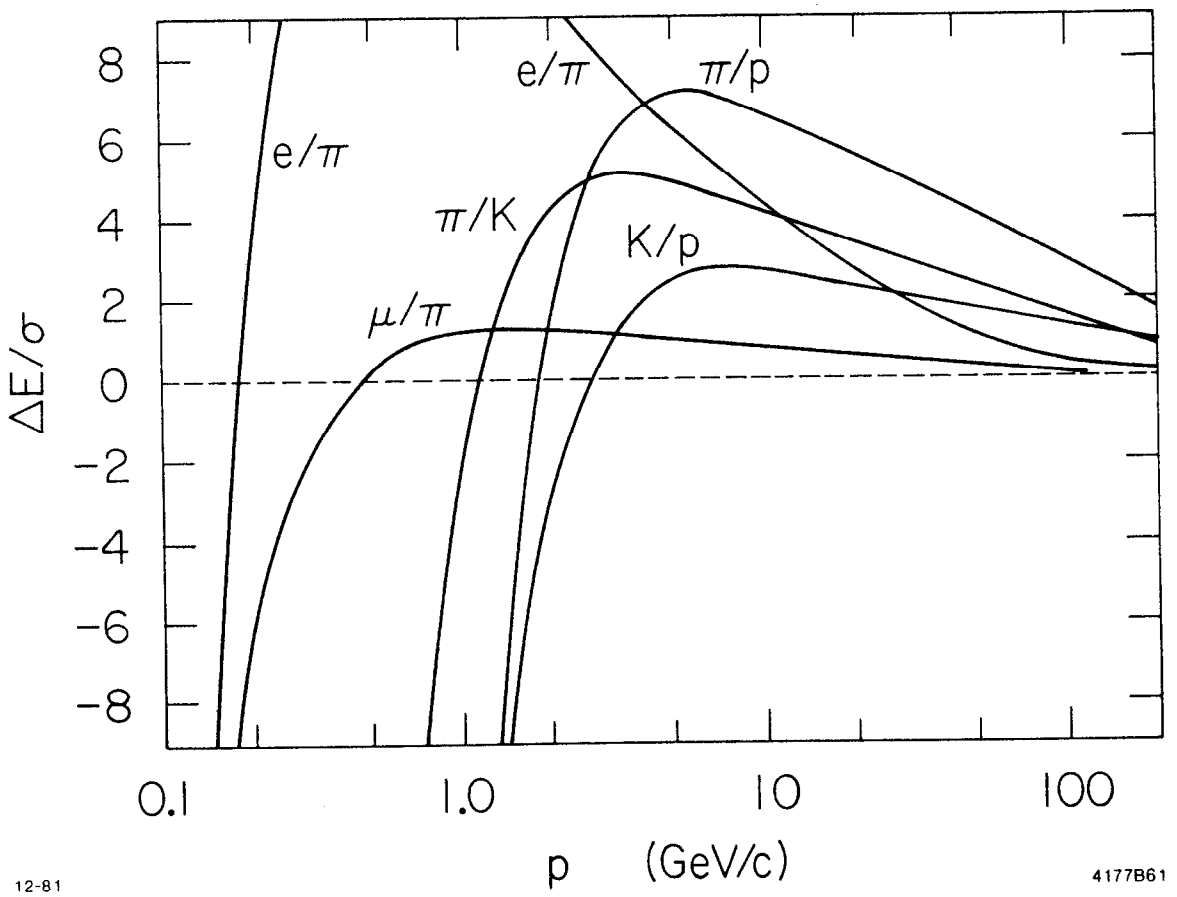

Fig. 4. Particle separation vs. momentum expected for the TPC. Data is for 80% Ar + 20% CH_4, 180 samples, and 8.5 atm.

One should limit the total gain in the chamber to $\simeq 5\times10^5$ for two reasons. First, the angular saturation corrections become more serious at higher gains (they start already at a gain of 5×10^3). Second, the ability to separate particles is reduced considerably at higher gains ($>10^5$). (A factor of 2 was measured at a gain of $\simeq 3\text{-}4\times10^5$).

The question of allowable cross-talk value is not fully settled. In the designs where one alternates the sense and the field wires, one gets typically 5-6% cross-talk from one wire to its first sense wire neighbor. The experimental evidence indicates that after the cross-talk correction has been applied the particle separation in terms of number of standard deviations improves by 4-5%, a rather small effect. In the cell design with just sense wires, one gets typically 12-17% cross-talk from one wire to its first neighbor, depending on the distance between the wires. We have done a computer simulation of the cross-talk on the data measured by J. Va'vra's full size jet chamber prototype (this chamber has 6% cross-talk). Preliminary results indicate that the effect of the cross-talk correction on the particle separation in terms of standard deviations is nonlinear and rather severe. This is presumably caused by inability to handle the large correction correctly. For 17% cross-talk we get a degradation of $\Delta E/\sigma$ by a factor of 2, for 14% cross-talk we reduced $\Delta E/\sigma$ by more than 30%, if the data is not corrected. In practice we would try, of course, to correct the data, but the question remains how successfully. A sizeable fraction of the ADC values would be negative and, therefore not measured. Also dead wires, ADC overflows, nonlinearities of large pulse heights, etc. might make correction difficult. Our preliminary conclusion is that one should not allow cross-talk to be larger than 10-12%.

In a drift chamber device the dE/dx measurement improves as the angle of the

track through the chamber increases up to about 50^0 simply because a longer ionization path is available for sampling. Beyond 50^0, a number of different effects cause the measurement accuracy to deteriorate.

Because of the overlap of the tail on one pulse with the following pulse, dE/dx information is only useful if the distance between particles is at least 1.5 to 2.0 cm at present. This is true for both TPC and drift chamber type devices. However, with better electronics and considerably more work, one could push this limitation below 1 cm.

ČERENKOV COUNTERS

In discussing Čerenkov counters, we will concentrate on the new technique of detecting light by means of photoionization of a chemical in a proportional chamber. The possibilities and limitations of Čerenkov counters employing phototubes are well known and need no review. The newer technique is much better matched to the requirements of an SLC detector because the detector for Čerenkov light will operate in a strong magnetic field without shielding and in addition allows greater flexibility in shape, size, and segmentation. After a general discussion of parameters, we will discuss threshold counters and ring-focus counters.

Typical photoionizing chemicals for a practical counter are benzene and TMAE. Since Čerenkov light is of notoriously low intensity, an important parameter is the number of detected photoelectrons per cm of Čerenkov radiation (ϕ). In terms of the Cereknov angle θ, $\phi = N_0 L \sin^2\theta$, where $\cos\theta = 1/(\beta n)$, L is the length of the radiator, n is the index of refraction of the radiator, β is the velocity of the charged particle, and N_0 depends on the photoionization efficiency, window transmission, mirror reflectivity, etc., integrated over an appropriate wavelength region. For benzene $N_0 \simeq 75$ cm^{-1}; for TMAE about the same. These values have been approximately realized in actual counters. The radiator length needed for a given counter is determined by N_0. While both chemicals have photoionization thresholds in the ultraviolet, the threshold for TMAE is at large enough wavelengths that quartz windows may be used. Benzene, with a threshold at 1350 Å, requires MgF_2 windows which are more expensive. Greater care must also be taken with mirror reflectivity at these shorter wavelengths.

The Čerenkov radiator must, of course, be transparent in the appropriate wavelength region and not scintillate. There are only a few gases which satisfy these conditions in the far ultraviolet. A mixture of argon and nitrogen is a satisfactory choice. Both have $n \simeq 1.00055$ at one atomosphere pressure in the 1250 Å region where benzene photoionizes. Such a large index is due to the fact that 1250 Å is close to the first argon excited state. The index is a factor of two smaller at 1800 Å. For a pressurized counter, this factor of two can be an important consideration. For still higher indices, liquid helium ($n = 1.027$) or liquid neon ($n = 1.10$) have been used. They introduce the usual complications of cryogenic liquids.

The proportional chambers can be made essentially 100% efficient for single photoelectrons. Thus, to get a 98% efficient threshold counter requires an average of four photoelectrons. For a ring-focusing counter, since a ring must be reconstructed, more photoelectrons are required for an efficient counter. The number of photoelectrons needed will depend on the density of tracks and the number of overlapping rings.

To define the limits of applicability of Čerenkov counters for particle identification, we assume that the allowable radiator length is 50 cm and we set a goal of 99% efficiency for fully relativistic particles. This is probably as long a radiator as is practical in an SLC detector. The index of refraction for a 50 cm long threshold counter to give the above efficiency is 1.00055. The π threshold for $n = 1.00055$ is 4.2 GeV/c so that this represents a practical upper limit for efficient electron identification in a threshold counter.

A 16 atmosphere counter using an argon-nitrogen mixture has a π threshold of 1.05 GeV/c and separates π's from K's between 1.1 and 4 GeV/c. This is close to the practical upper limit on pressure vessels of reasonable wall thickness.

The only photoionization type Čerenkov counter in operation at present is that in the HRS[3] shown in Fig. 5. 10% of the system is presently installed. When complete it will consist of 13 toruses in two layers surrounding the interaction region and subtending 3π solid angle. Each torus contains 64 segments. The 832 segments are adequate for PEP energies (3% double occupancy). The magnetic field strength and distance from the origin seriously change the segmentation needed to have a tolerable level of double occupancy. For the HRS geometry a factor of two to three times more cells would be desirable at the SLC although the present system would be usable. The additional double occupancy at high energies occurs mostly in the core of jets where the particle energies are high.

The development of a practical ring imaging detector[4] in the next year or two would provide a powerful tool for particle identification at the SLC. This device would indicate not only the presence or lack of Čerenkov light as in the conventional threshold counter, but also measure the γ of the particle well beyond threshold, extending the useful range of the radiator. Perhaps its greatest advantage in the jetty SLC environment is its potential for separating rings which are close together, even overlapping. Since the rings must be imaged by a camera-like detector, there is no cell defined as in the conventional counter. A spherical mirror images the individual photons on a detector which must have the ability to detect many simultaneous photoelectrons in two dimensions (see Fig. 6). The chief disadvantage of the device is the circular ring distortion resulting from non-radial trajectories caused by magnetic fields or decays away from the interaction region. This distortion will complicate the pattern recognition problem but also provides information on the angle of incidence to the counter.

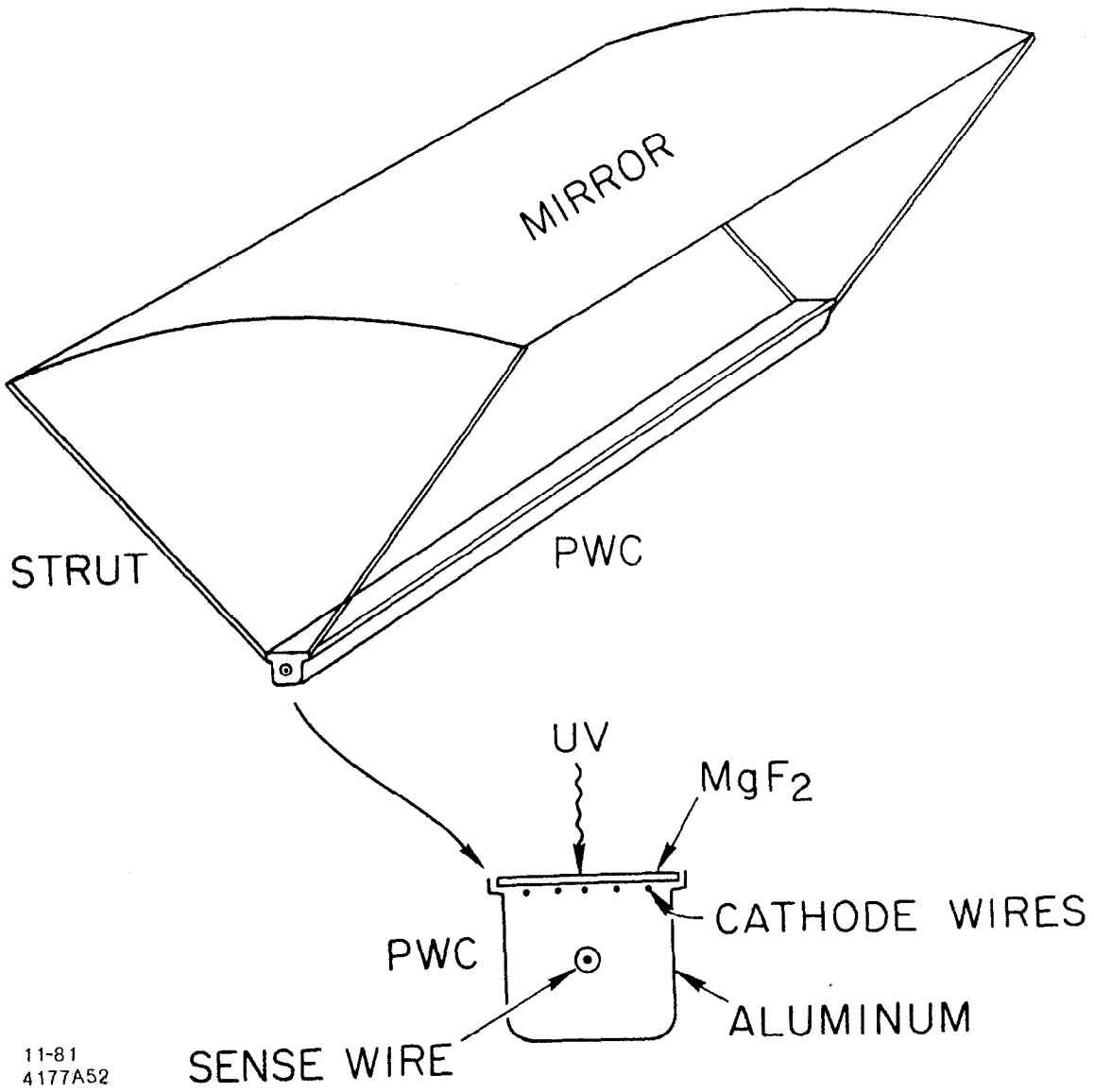

Fig. 5. Schematic of HRS Cerenkov detector.

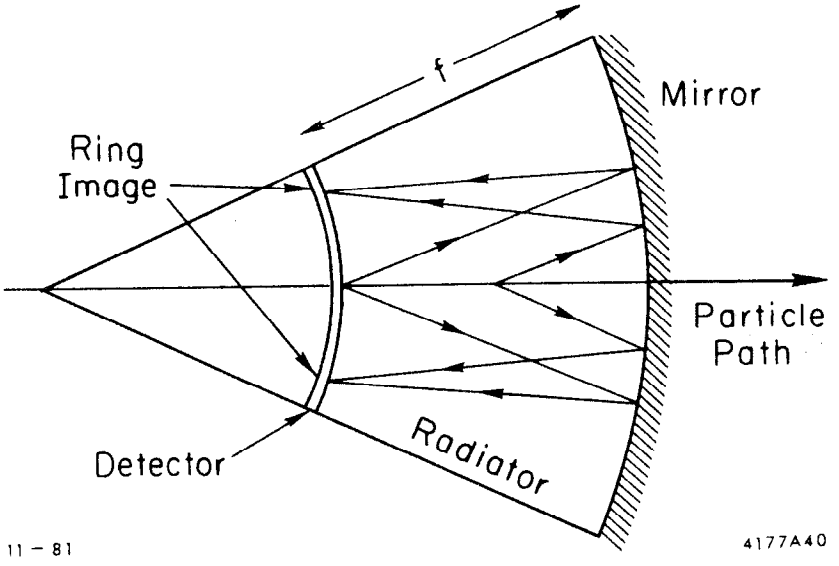

Fig. 6. Schematic of ring-imaging Cerenkov detector.

The desire to build such a powerful counter must, of course, be tempered by the non-existence of a practical device at this date. However, at least two groups are committed to proving the practicality of the technique over the next two years. Without going into the details of design, we can summarize the significant milestones which have been achieved in recent years towards building a practical device:

1. Liquid helium or neon radiator is readily available and useful because of the low dispersion (Fig. 7) at short wavelengths and useful indices (He: 1.027, Ne: 1.10) for particle identification up to 30 GeV/c.
2. Recyclable window seals of calcium fluoride, magnesium fluoride, and quartz have been made in order to allow room temperature detectors to look into the cryogenic radiators.
3. Detectors:
   a. Photoionizing gases such as TEA, TMAE, TMBI (Fig. 8) are used successfully as photon detecting agents and gaseous amplification chambers[5].
   b. The preamplification parallel plate (transparent screen) gap makes possible the efficient detection of single photoelectrons in a MWPC or a multistep parallel and amplification chamber[6].
   c. Two dimensional imaging has been done with preamplified spark-chambers with optical readout, multistep chambers with a resistive anode charge division technique, and a drift/TPC technique of drifting the unamplified photoelectron ring sideways into a preamplification gap followed by a linear MWPC where the arrival time is clocked out.

Very recent results from the CERN group[7] demonstrate significant progress towards solving the technological problems. They use a 1.4 meter argon radiator and a 20 cm imaging drift chamber filled with methane and TMAE with quartz

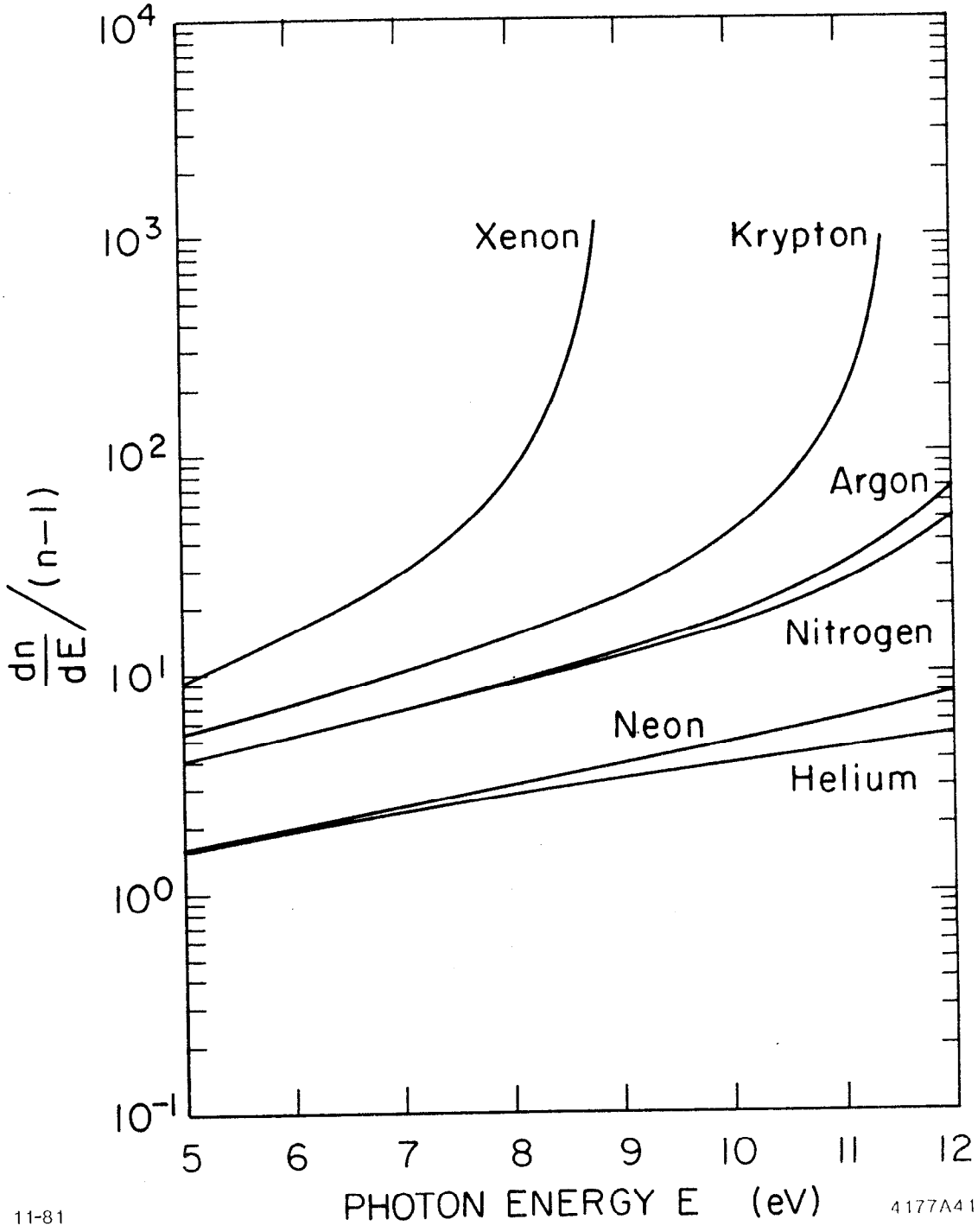

Fig. 7. Dispersion vs. photon energy for various Cerenkov gases.

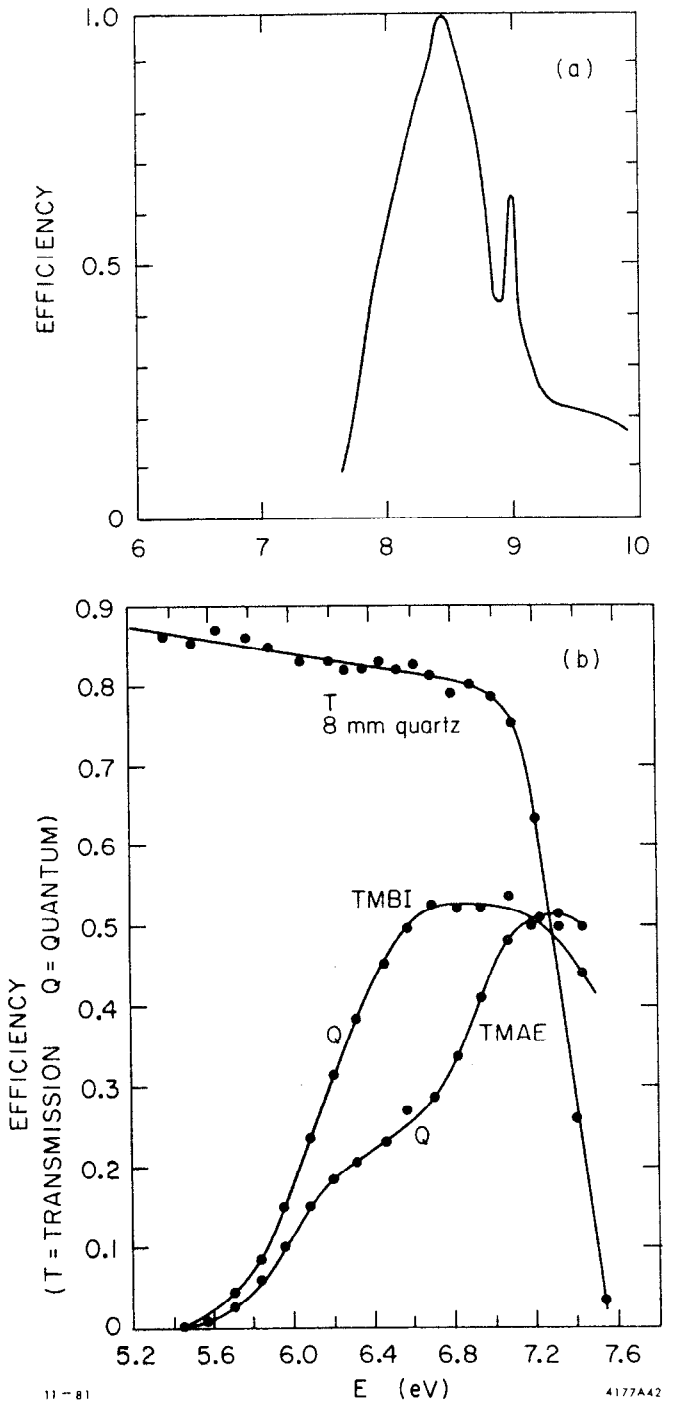

Fig. 8. Photoionization efficiency for a) TEA and b) TMBI and TMAE. Also shown is transmission efficiency for quartz window.

windows (see Fig. 9). Timing information from the wire chamber provides two-dimensional information on the ring. An example of a ring image containing ten converted photoelectrons is shown in Fig. 10. They report a value of $N_0 = 81$ cm^{-1} and expect to achieve $N_0 = 125$ cm^{-1} with technical improvements to the dirft detector. Figure 11 shows the results of a test using 6.2 GeV/c pions and electrons. A five standard deviation seperation between π's and e's is obtained. This is equivalent to pions and kaons at 22 GeV/c.

They have also made a conceptual design for a LEP detector which uses two ring imaging detectors and three radiators and no other tracking chamber. The spherically symmetric detector system is shown in Fig. 12 and is comprised of a liquid freon 14 (150^0K) radiator and detector inside the solenoid wound on an approximately spherical surface. The integrated field between the vertex point and the coil is about .2 T-m and the magnet consumes only 200 kW power. The freon radiator is placed just inside the coil and is 2 cm thick ($X = 0.036X_0$) going from a radius of 0.73 m to 0.75 m with a spherical reflecting mirror at 0.75 m radius. Superinsulation separates the liquid freon radiator from the coil. The detector for the liquid freon radiator is placed between 0.51 and 0.55 m radius corresponding to a 4 cm thick spherical drift volume filled with CH_4 + TMAE. Converted photoelectrons drift 20 cm or less along lines of constant ϕ (azimuthal angle) to a picket fence of radial PC wires placed along lines of constant θ (polar angle). A planar version of such a drift detector is shown in Fig. 9. The detectors and radiators are enclosed by spherical quartz windows 2.5 mm thick ($X = 0.02X_0$) with the cold freon radiator (150^0K) insulated from the warm detector (300^0K) by atmospheric pressure, low thermal conductivity, neon gas. The region between the beam pipe and the photon detectors (0.50 m radius) is free for installation of a tracking detector and/or a high precision vertex detector. The liquid freon has a refractive index of

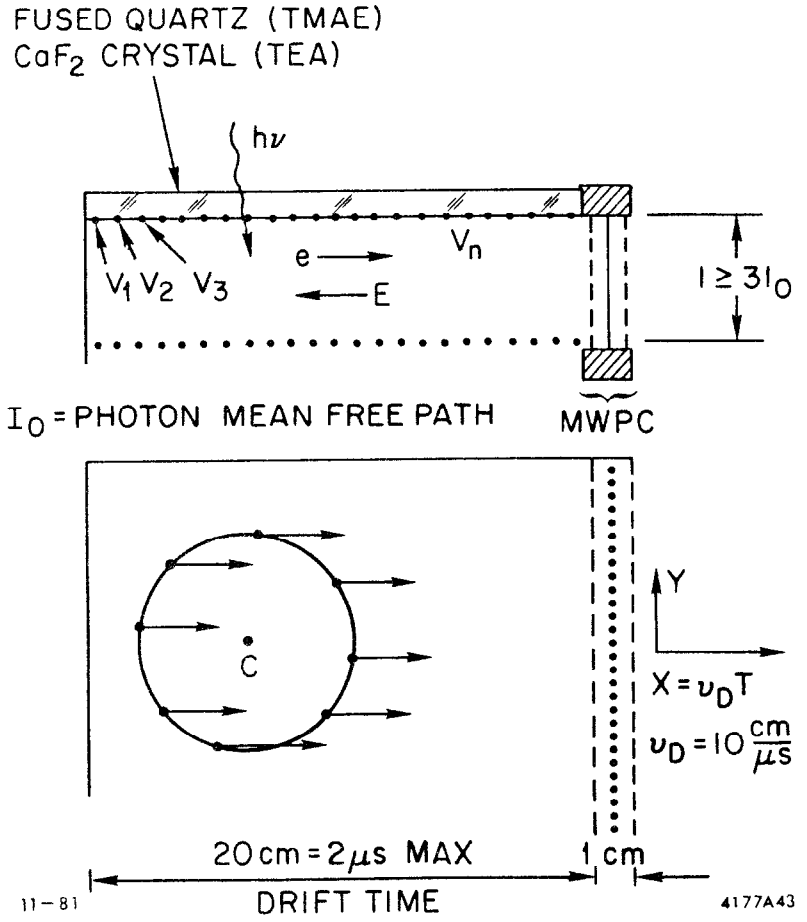

Fig. 9. Ring-imaging prototype detector.

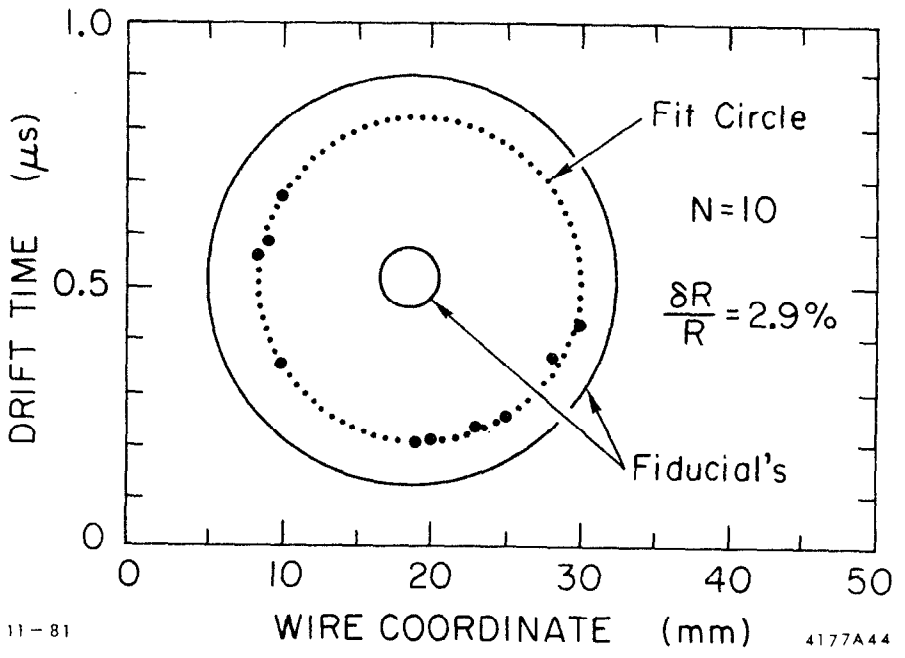

Fig. 10. Reconstructed ring image.

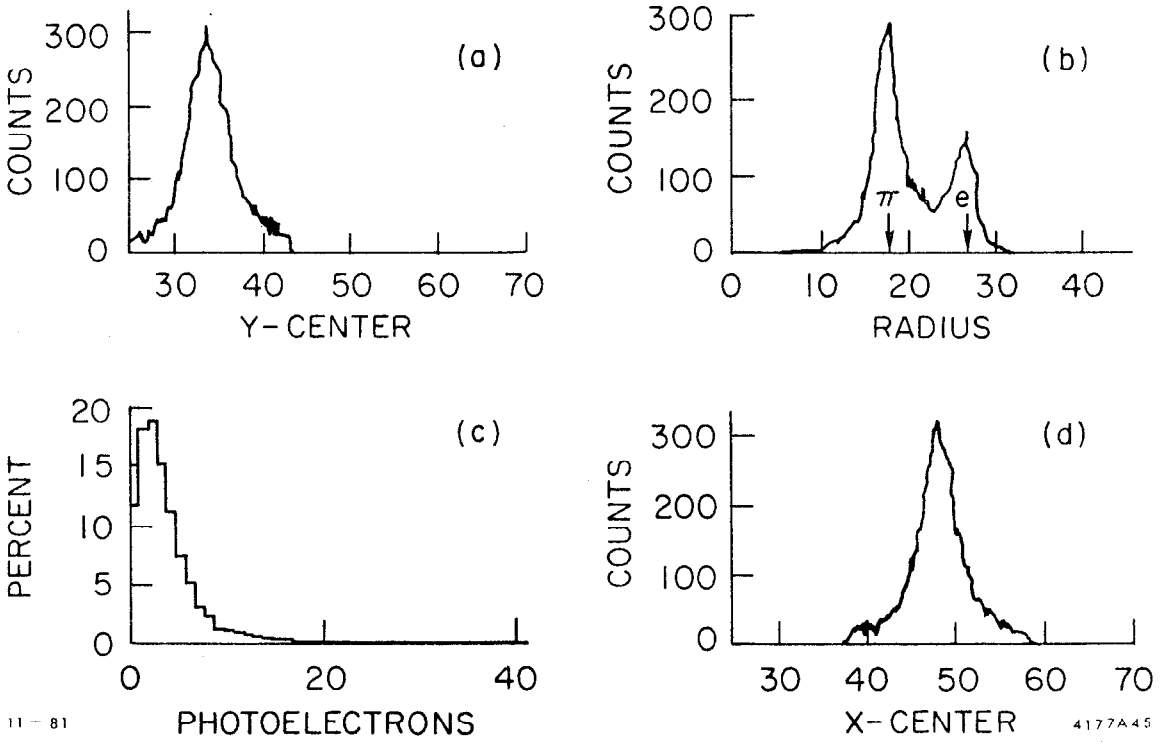

Fig. 11. Measured ring parameters for 6.2 GeV/c pions and electrons.

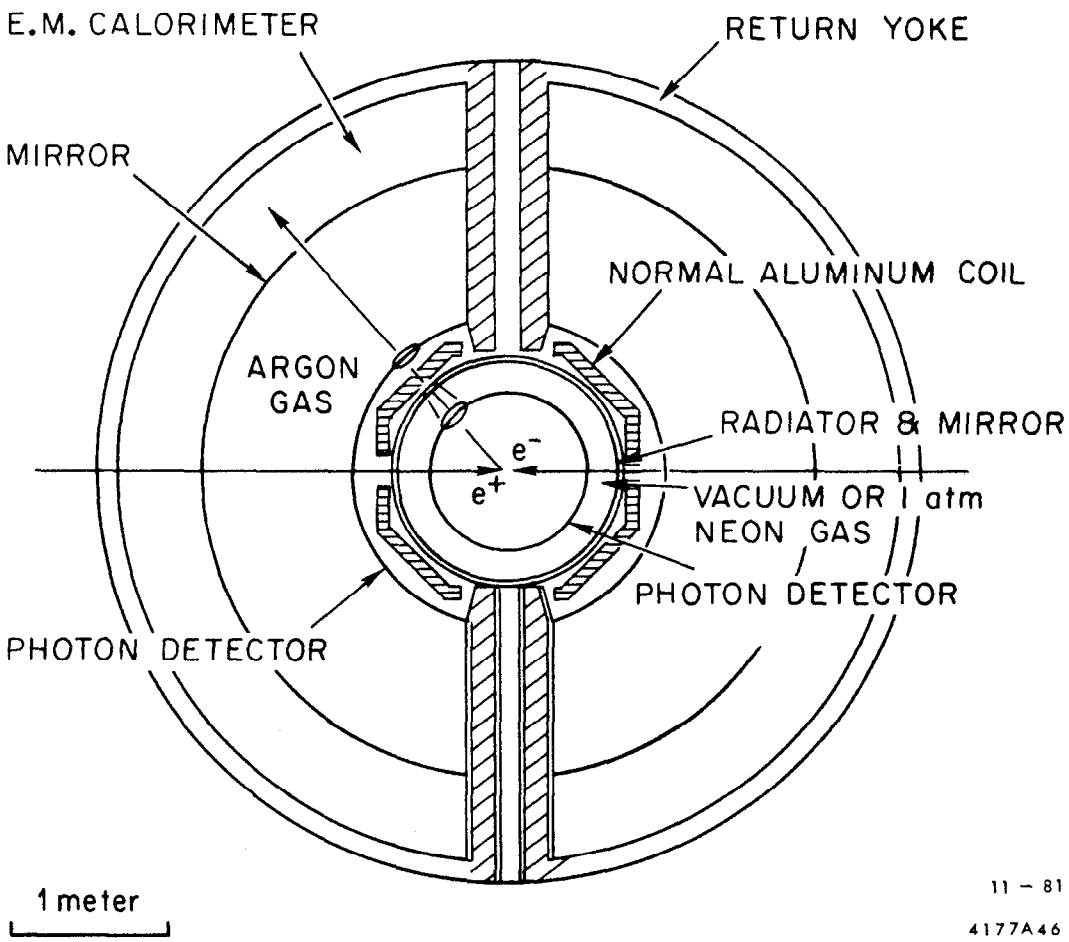

Fig. 12. Conceptual design for LEP detector.

1.15 at a photon energy of 6.75 eV and so has a threshold of $\gamma = 2$ for Čerenkov radiation. The quartz windows ($n = 1.6$) start radiating at $\gamma = 1.28$ and cut off at $\gamma = 2$ due to total internal reflection. Hence the liquid freon-quartz system is continuously sensitive to charged particles above $\gamma = 1.28$ ($p_\pi = 0.11$ GeV/c).

The number of points on the ring image from the liquid freon is about 60 ($N_0 = 125$ cm^{-1}, $L = 2$ cm) and from the two quartz windows is about 38 ($L = 0.5$ cm), so pattern recognition of the circles is possible especially if a tracking detector provides the direction of the particles as they enter the radiator. This has been established by Monte Carlo simulation of $e^+e^- \rightarrow q\bar{q}g$ jet events at $s = (50\ \text{GeV})^2$ and $s = (100\ \text{GeV})^2$.

Outside the coil is placed a one meter thick argon radiator from one meter to two meters with the detector a spherical drift detector between 0.97 m and 1.01 m with a 2.5 mm quartz window separating the argon gas from the detector. Threshold of the argon gas radiator is $\gamma = 35$ and it will produce images for a $\beta = 1$ particle with 10 points on the circle. The Čerenkov angle for the liquid radiator is 516 mr and for the gas radiator 28.3 mr and these produce images on their respective detector surfaces of 292 mr and 28.3 mr respectively.

They have calculated the precision $\Delta p/p$ with which p can be measured by the Čerenkov ring imaging method and also utilizing the B field. Combining the measurements of p and γ (from the ring image) one may calculate the mass resolution expected

$$(\Delta m/m)^2 = (\Delta p/p)^2 + 1/\beta^4\ (\Delta\gamma/\gamma)^2 \quad .$$

The number of standard deviations to separate a particle of mass m_1 from a particle of mass m_2 is

$$\sigma = |m_1 - m_2|/\Delta m$$

and this is plotted in Figs. 13 to 16 for the combinations (πK), (Kp), (πμ), (μe). The three regions labeled quartz, neon or argon indicate when a given radiator is acting as a threshold counter (i.e., a π counts but the K doesn't), hence σ is large. For the regions in between, the ring radius makes the identification to the indicated number of σ's. As can be seen from the curves, πK separation is possible to 78 GeV/c. This covers the range expected for the SLC. Note that eμ, hence even more so eπ, separation is possible by this method. Hence the study of direct lepton processes will be facilitated with this method. Note also that the number of σ's is large so that a detector which operates less well than expected still has a margin of error.

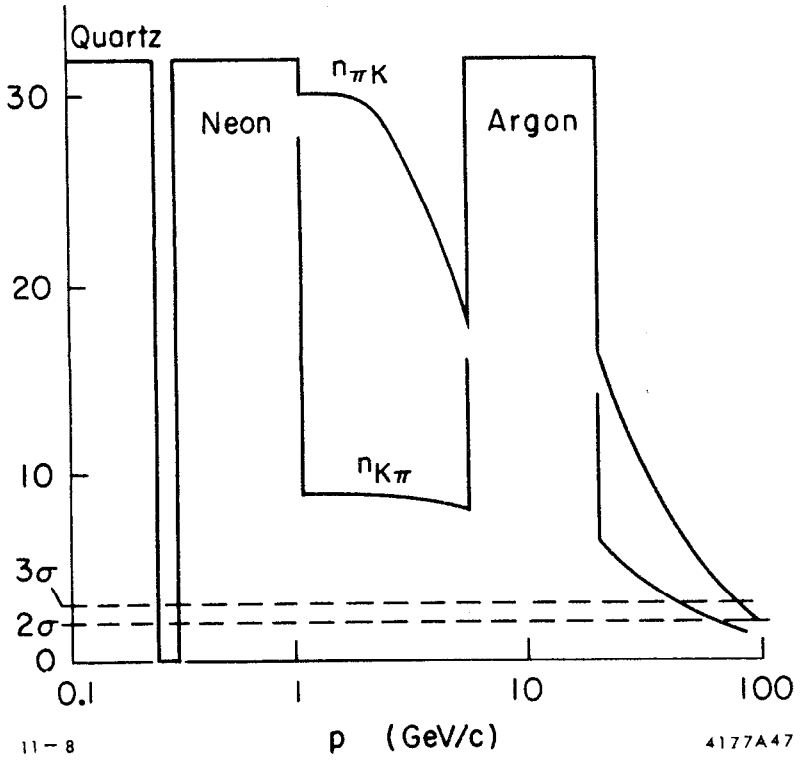

Fig. 13. π/K and K/π separation vs. momentum.

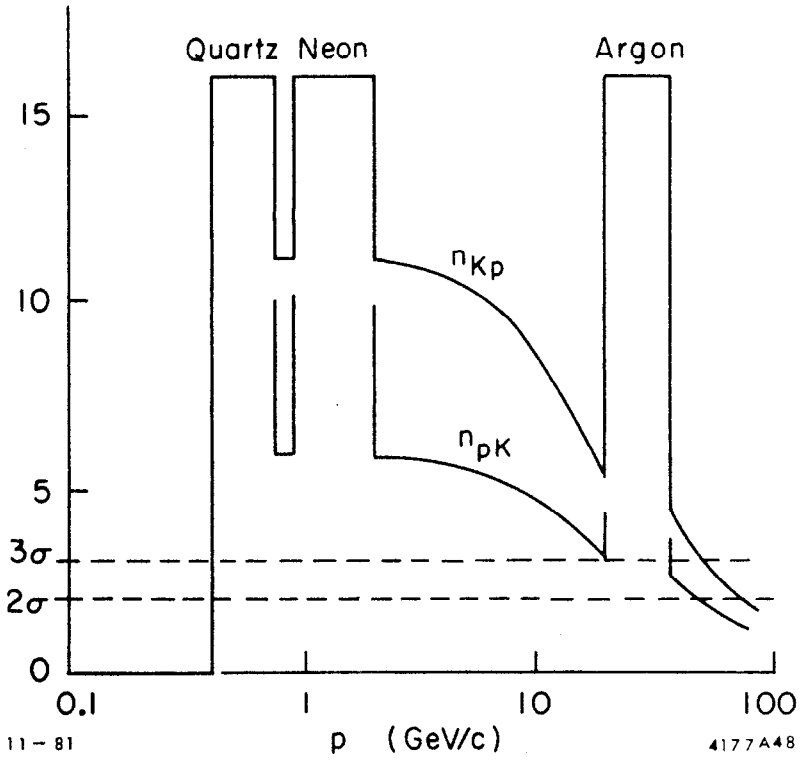

Fig. 14. K/p and p/K separation vs. momentum.

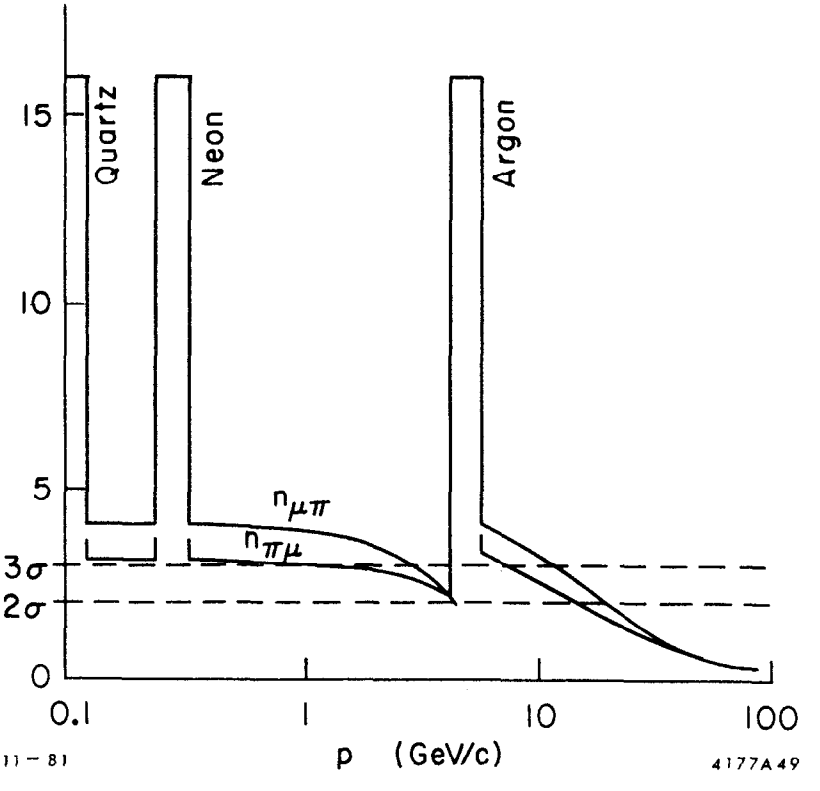

Fig. 15. μ/π and π/μ separation vs. momentum.

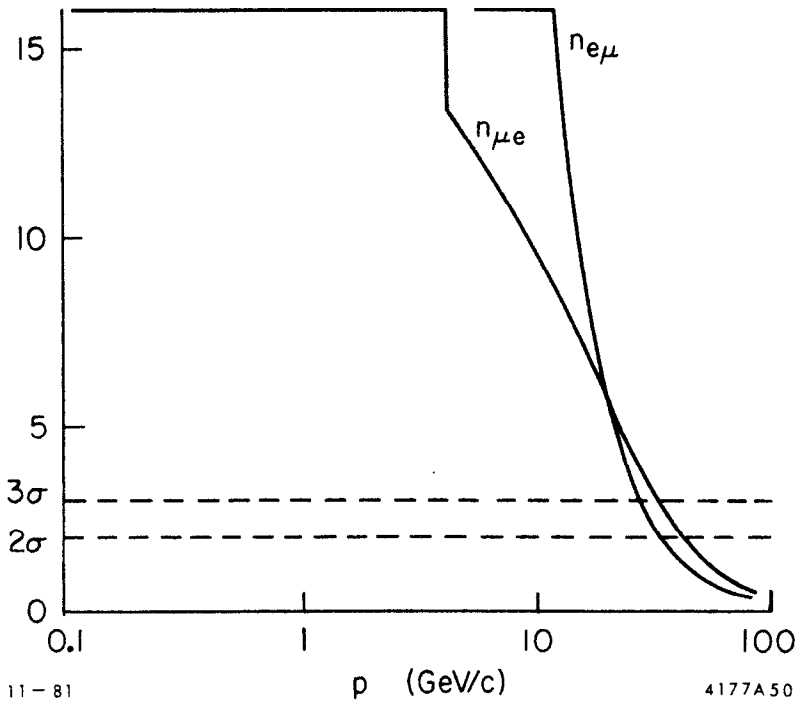

Fig. 16. e/μ and μ/e separation vs. momentum.

TIME-OF-FLIGHT

Particle identification by TOF scintillator techniques is still possible for a significant fraction of produced particles at the SLC. This is shown by the predicted kaon momentum spectrum in Fig. 17. The TOF resolutions required for 1σ and 2σ π/K separation are plotted in Fig. 18 which then gives the fraction of kaons identified, assuming perfect segmentation and acceptance. A 1.5 m radius is assumed as a standard of the detector. The resolutions achieved to date in major systems[8] are plotted in Fig. 19 and these show that a resolution σ_t approaching 100 ps is a realistic target for the next generation of TOF system.

The gains in σ_t made by these successive systems have come principally from geometry improvements which increase the photoelectron statistics at the phototube. The types of scintillator or phototubes themselves are not critical among the fast scintillators and fast 2" PMT's currently available and no breakthrough in these areas is expected in time for SLC. Similarly, light pathlength fluctuations are roughly fixed by the (3.0-3.5 m standard) length of scintillator and are well-matched to the current scintillator and PMT limitations. The only resort is then to follow the trend of Fig. 19 and further improve the geometry by using:

(1) 2" thick scintillator to produce more photons (a la Mark III).

(2) ≃3" wide scintillator and twice as many phototubes to further improve the matching to the PMT and the total photoelectron statistics.

Item (2) will, in addition, provide a necessary improvement in the ϕ segmentation for SLC physics.

An example of such a system with ≃125 counters and ≃250 PMT's is sketched in Fig. 20 where it is shown placed either just inside, or just outside, the solenoid cell. Placement in either location has various obvious advantages and

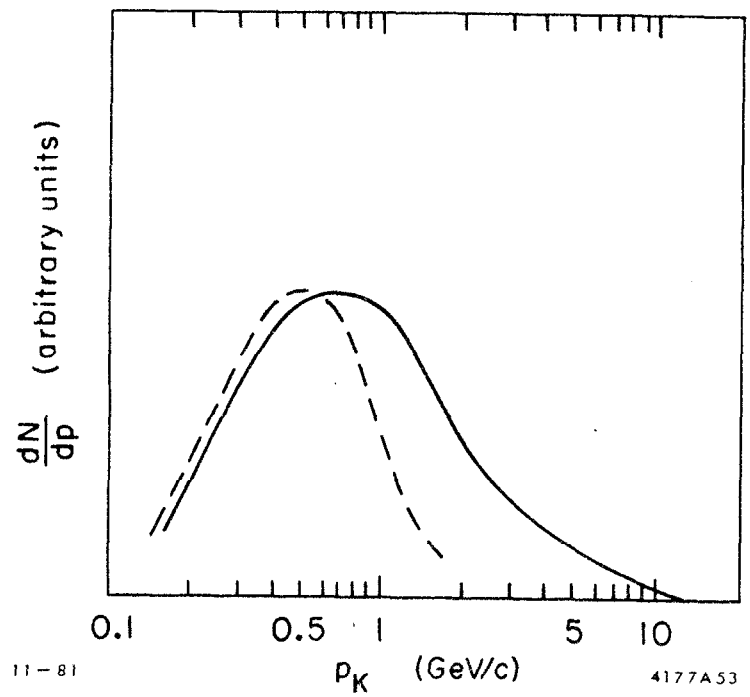

Fig. 17. Predicted kaon momentum spectrum at the SLC (solid curve) and at SPEAR (dashed curve).

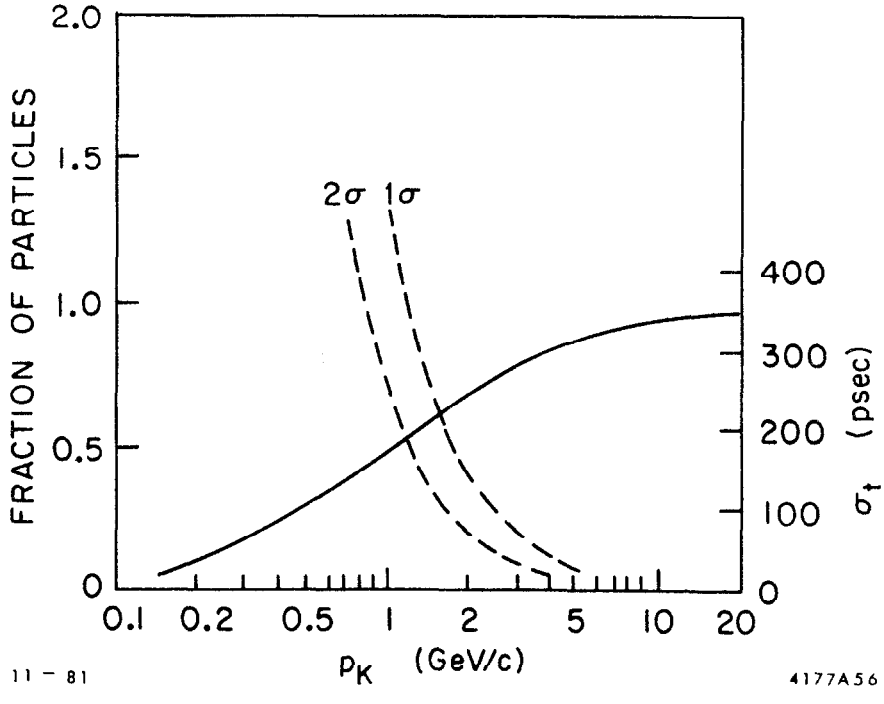

Fig. 18. 1σ and 2σ π/K separation as a function of TOF resolution and kaon identification fraction as a function of momentum.

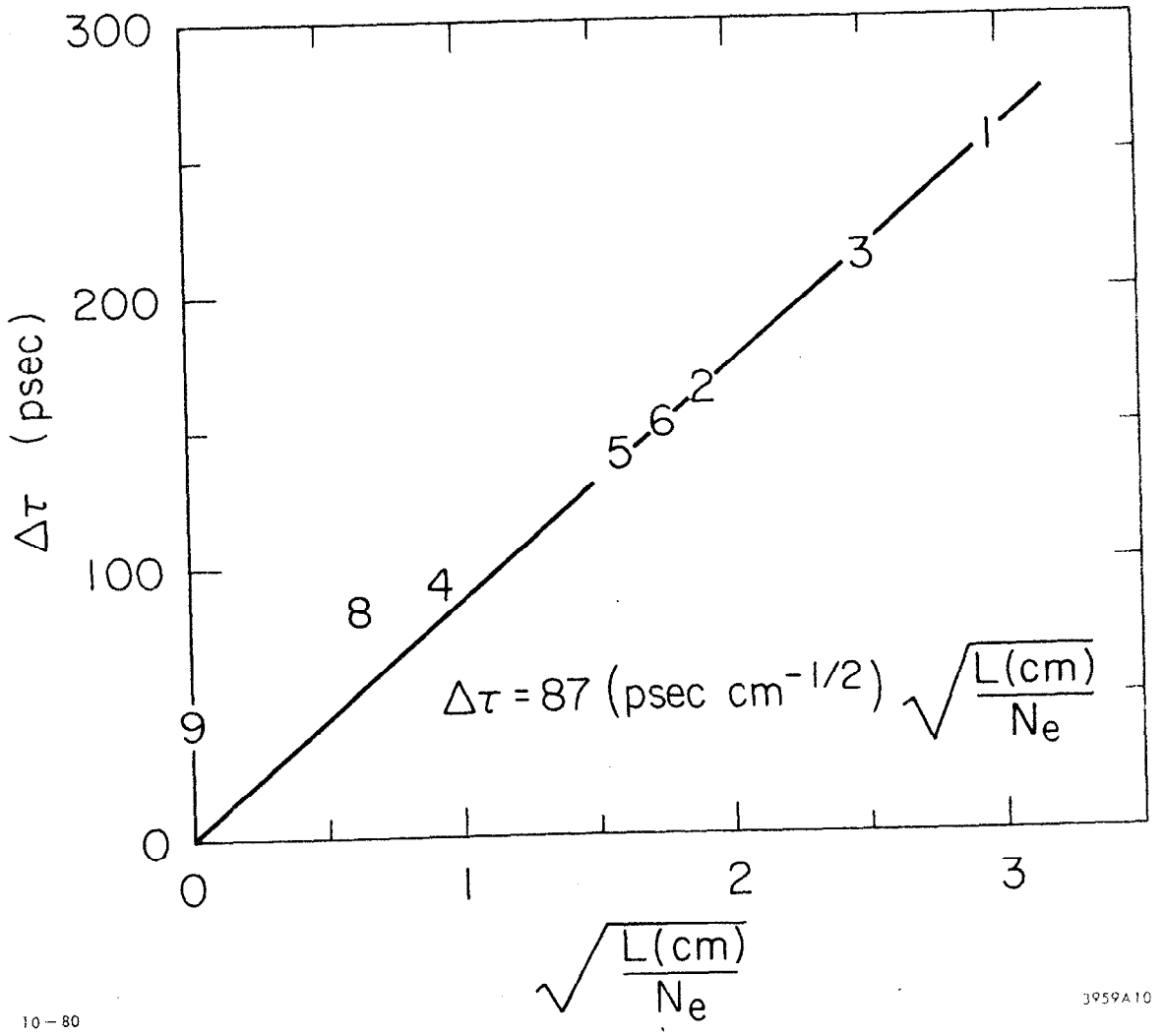

Fig. 19. TOF resolutions for working detectors as functions of $L/N_{p.e.}$

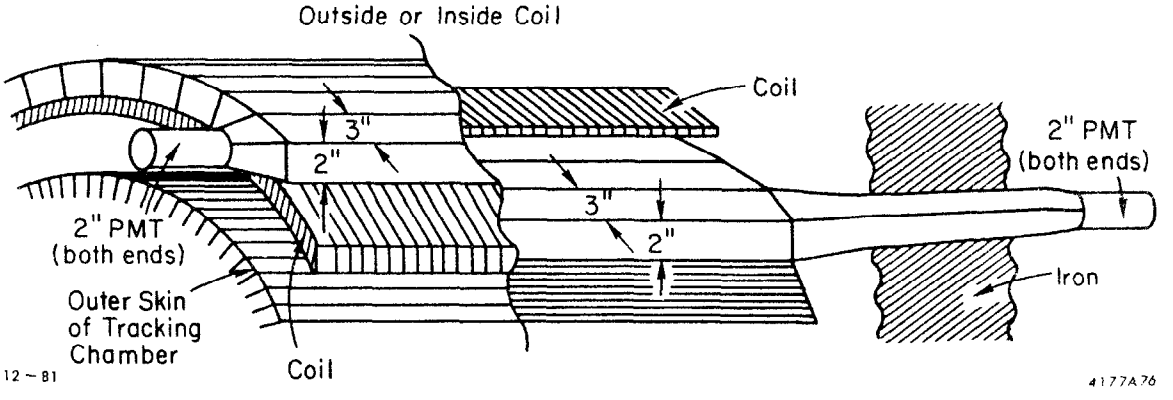

Fig. 20. Possible design for a TOF system.

problems (converted γ's) not discussed here but which must be reconciled with other choices for the detector. The long lightpipes required for placement inside the coil, however, should maintain the optimum match between the 2"x3" scintillator and 2" phototube. The possibility of a doubled TOF system which sandwiches the coil between 2 TOF layers totaling 250 counters/500 phototubes would provide a further 30% reduction in resolution but represents a larger resource commitment to identifying these lower momentum particles. The single layer 125 counter/250 tube system should give at least 200 photoelectrons and therefore TOF resolution near the desired 100 ps level. With an SLC bunchlength of 1 mm, the contribution from inherent start-time jitter is only a few picoseconds compared to 85-90 ps at SPEAR and PEP. Cost estimates can be based on the most recent MARK III system and are 300K dollars for the complete counter system.

Multihit electronics will be highly desirable to cope with the θ segmentation problem of SLC physics. Double level discriminators like the Mark II DISCO but with several TDC's for each discriminator seem straightforward. Even without fancy processing which may be possible with zero-pole techniques or some type of time-variant amplifier, such a module would provide full 2-PMT resolution for $\Delta\theta > 45°$ (and degraded 1-tube resolution for smaller separations). A ballpark estimate of multihit electronics costs at 2 inputs per single width CAMAC module are 90K dollars for the 250 tube system.

The problems of segmentation may prove difficult as evidenced by the increase in the multihit rate in going from SPEAR to PEP. To be specific, Mark II is seeing a multihit rate of 30% per track, compared to 5% at SPEAR. A simple recovery algorithm for double hits (5% at SPEAR, 25% at PEP), simply assigns the nearest phototube to the track, and is successful for 85% of the double hits at

SPEAR. This algorithm, however, recovers only 50% of the double hits at PEP because the average stray track is so much faster than at SPEAR that they "overtake" more often the signal from the desired track.

Monte Carlo simulations of the multihit rate and recovery rate for PEP (compared with real data) and the SLC at 88.6 GeV center-of-mass energy have been made for the Mark II geometry (1.5 m radius) and are shown in Table III. Note that the 125 counter system described above (but calculated here for only 96 counters) should bring the segmentation problem back to approximately the same level of severity as currently at PEP. More satisfactory results are obtained with a higher magnetic field of 15 kG, which may be desirable for other reasons. Even though 13% less tracks reach the TOF system with the 15 kG field, the segmentation is sufficiently improved to record roughly the same absolute number of tracks with single-hit counters, and fewer with irrecoverable multihit counters.

A detailed Monte Carlo study has been done of the segmentation problem for these systems using kaon detection and identification as a benchmark. Figure 21a shows the spectrum of produced kaons at 88.6 GeV according to the "standard" model. Figure 21b shows (solid line) the detection and identification efficiency as a function of momentum for these produced kaons using a simple TOF algorithm on a system with 48 counters and 5 kG magnetic field with Mark II geometry. The contamination or misidentification fraction of the reconstructed sample is also plotted (dashed line). A system TOF resolution of 100 ps is compared to present generation systems of 300 ps and also to a possible future planar spark counter system with 50 ps resolution. The TOF algorithm is simply a cut at 50% on the renormalized weight for the kaon hypothesis (see, for example, Ref. 9). Fig. 21c and 21d present similar plots but for systems with

Table III. TOF Multihit Rate

		good Single hit counters	good Double hit counters	more than 2 hit counters
PEP	M.C.	72%	21%	5%
	Data	61%	22%	6%
SLC	5kG 48ctrs	48%	27%	25%
	5kG 96ctrs	66%	23%	10%
	15kG 96ctrs	74%	21%	5%

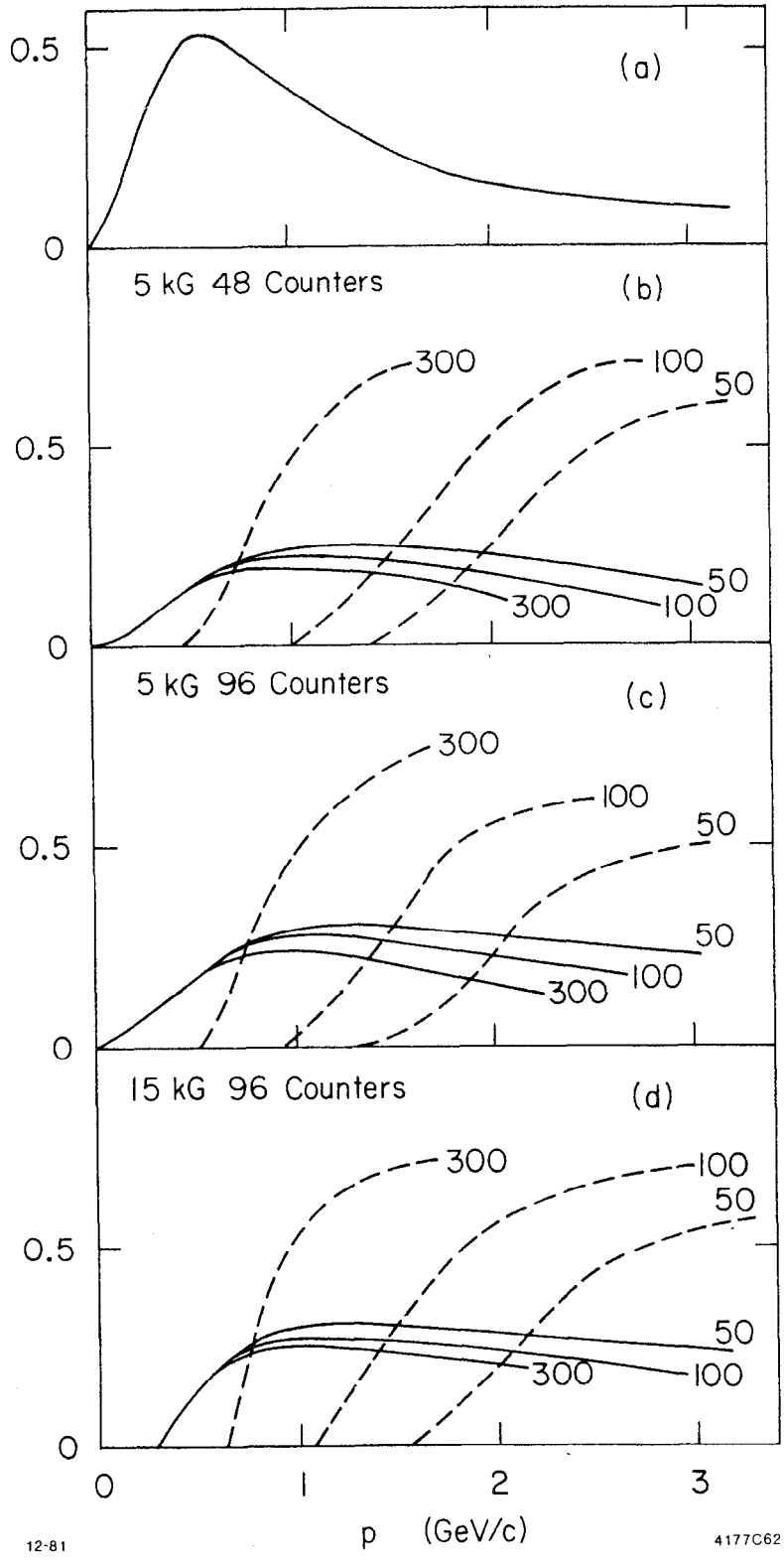

Fig. 21. a) Produced kaon momentum spectrum. Single-hit efficiency (solid curves) and contamination (dashed curves) for b) 48 counters, 5 kG; c) 96 counters, 5 kG; and d) 96 counters, 15 kG. Numbers adjacent to curves give σ_t in picoseconds.

improved segmentation of 96 counters and for 5 kG and 15 kG magnetic fields, respectively.

The dominant effect is, of course, the TOF resolution itself. Taking the momentum at which the kaon sample has 50% contamination as the benchmark limit of separability, the fraction of produced kaons in Fig. 21a which are susceptible to identification increases from .40 to .56 and then to .62 for TOF resolutions of 300, 100, and 50 ps, respectively. However, due to acceptance effects of kaon decay at low momenta and detector geometry, the fraction of produced kaons actually successfully identified is much smaller but increases significantly from .06 to .10 and then to .14 for these TOF resolutions. Increasing the segmentation (Fig. 21c) increases the relative yield of the 100 ps system by only about 10% compared to the 48 counter system. Increasing the magnetic field as well as the segmentation (Fig. 21d) gives about the same total fraction of identified kaons. These observations are a consequence of the fact that those kaons with momenta near the peak of the production spectrum in Fig. 21a ($\simeq$.56 GeV/c) tend already to be rather well separated from the core of the SLC jet. Gains from improved segmentation and higher magnetic field are apparent only in the kaon spectrum above the peak from approximately .9 to 1.8 GeV/c momentum for a 100 ps system and have a smaller effect on the total number of successfully identified kaons. In that region of momentum, the gains are approximately 20% higher yields for either of the better segmented 100 ps systems.

The conclusions of these studies using overall kaon detection as the benchmark are:

(1) TOF resolution remains, of course, the most critical variable. A 100 ps system will identify $\simeq$1.7x more kaons than a 300 ps system at the SLC

(2.5x for a 50 ps system).

(2) Improved segmentation is of value but primarily for kaons in the upper range of detection (≃ 20% more particles 1.0-1.8 GeV/c).

(3) Multihit electronics can increase yields of identified kaons by another ≃25% in this upper range of momentum.

(4) Physics judgements about the value of any TOF system discussed here must rest on the value of identifying these relatively low momentum particles not far from the peak of the produced spectrum.

The total number of identified kaons may not be, of course, the best benchmark for deciding these issues but is the only one considered here.

Spark counters (see Fig. 22) represent a significant advance over scintillation counters for time measurement (viz. 30 ps vs 120 ps), thus covering significantly more of the momentum spectrum of final state particles. Here we give some characteristics of the presently developing counters and of future counters that may be used at the SLC.

W. B. Atwood, D. Klem, A. Ogawa, Yu. Pestov and R. Sugahara have recently operated two 9 cm x 9 cm counters with 200 μm gas gap at 10 bar in IR-8 in front of the DELCO luminosity monitor. The counters opposed each other across the interaction point, and thus measured small angle Bhabha scatters. Data were recorded at single counter rates of 1-3 kHz, with a raw trigger rate of 1 Hz and a Bhabha rate of about .1 Hz. Upon PEP shut down and after a beam exposure of one billion sparks each, the counters were placed flush against each other and they collected cosmic ray triggers with a Co^{60} source employed to study the rate effect.

The counters operating at an overvoltage (ratio of operating voltage to threshold voltage) of ≃1.9 gave time resolutions of about 100 ps even though

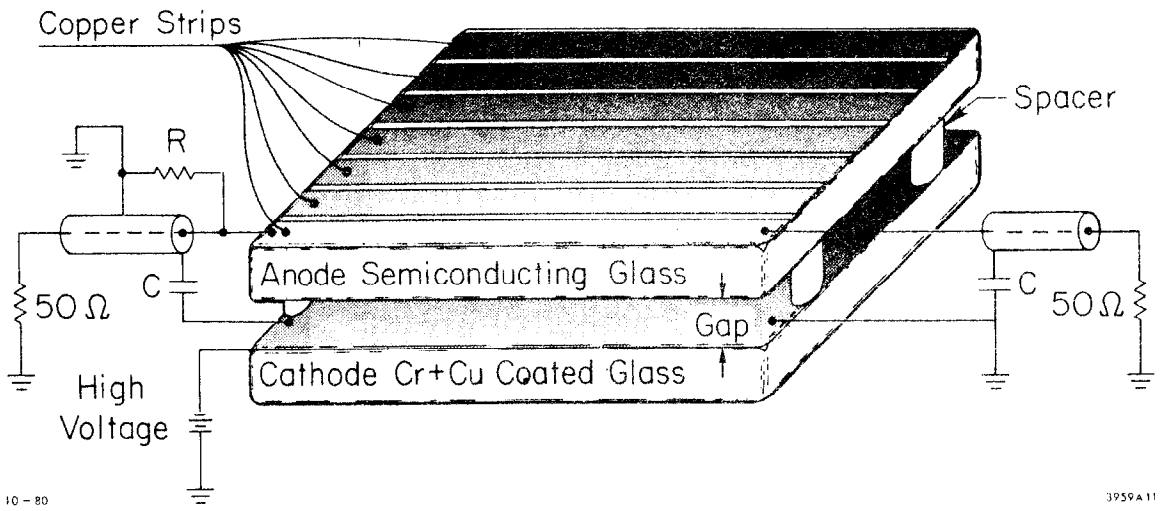

Fig. 22. Schematic of planar spark counter.

heavily swamped with beam. A definite rate effect is seen above particle fluxes of ≈6 Hz/cm^2. The time resolution at lower rates (with cosmic rays) has, however, the previously measured value of 50 ps. We figure a dead region per spark with radius commensurate with the glass thickness of 0.5 cm. The longitudinal position resolution for Bhabha events (which are highly coplanar) was 1-2 mm even at high counting rates, consistent with the TDC conversion of 50 ps/count.

Experience with counters of two different glass resistivities indicates that rate effects do change with this resistivity. Smaller glass thickness will tend to decrease both rate effects and dead area. We also experimented with different gas mixtures including neon as the noble gas and ether as a quencher, obtaining markedly better results when both were employed.

One can, in future counters, easily lower the effective time constant and dead area (by reducing the glass resistivity and thickness), to improve the rate effect by a factor of 10 and the dead area by a factor of 2. The expected beam crossing time interval of the SLC is well within the parameter of even the present test counters.

Time resolutions of ≈30 ps are readily obtained by using a smaller gas gap (100 μm) at higher pressure (20 bar), using neon and ether in the gas. Further improvements are still possible.

For SLC we envision a double bank of counters at the standard radius of 1.5 m. Counters would be 3 m long and 10 cm wide for a total of ≈180 counters. The cost of the counters themselves would be largely in the cost of the glass, which is sensitive to economies of scale. We could expect to pay about 200K dollars for this. Additional costs include pressure vessels, assembly costs, gas

systems, and high voltage. Total price would be around 400K dollars.

The electronics requirements would generally be the same as for a scintillator-PMT system with the same member of staves as our striplines. Our system has the advantage that the counter can be segmented very conveniently without interfering with its performance, for instance by employing narrow striplines. A choice of 1 cm width would lead to a 3600 TDC channel system (no multihit). Electronics cost will be therefore commensurate with that for the scintillator system, but one would probably want to have a more highly segmented system and avoid the development of multihit electronics.

At relatively modest cost and with a high degree of compatibility with other detector systems, conventional TOF scintillation techniques have the potential to identify a large fraction of the hadrons produced in standard Z^0 decays at the SLC. A 100 picosecond system seems reasonable and works over a momentum range containing 56% of the produced kaons. Although acceptance effects (decays and geometry) reduce this fraction considerably for any real system, the fraction of all particles so identified at the SLC can be maintained at about the same level now obtained at PEP.

A spark counter system may provide better time-of-flight resolution, but is still at an earlier stage of development. It is not known whether a working system can be built on the required time scale. However, such a system would operate well inside the solenoid at the expected SLC repetition rate. The system could readily be segmented as required by the jet-like events, even without the development of multihit electronics. The cost of the system would be competitive with that of a competing scintillator + PMT system even while the performance would be significantly better (viz: 30 ps time resolution, 2 mm position resolution, fine segmentation).

TRANSITION RADIATION

The detection of transition radiation as a technique to identify electrons offers several unique characteristics applicable to SLC detectors. Recent developments indicate that hadron rejection of the order of 10^{-3} may be available for 50 cm thick detectors which can simultaneously provide tracking information in high-multiplicity events. The physics emphasis of the research will necessarily decide the desirability of a transition radiation detection system (TRD) versus TOF, dE/dx, Čerenkov, or calorimetric particle identification.

Before pursuing a detailed understanding of TRD's, it is important to have in mind the general advantages:

1. TRD's provide e± identification with very low hadron contamination. Typical TRD's that have been used in experiments have obtained 10^{-1} - 10^{-2} hadron rejection. (Hadron rejection = the probability that a hadron will be falsely identified as an electron). Recent test data shows that a cluster counting readout scheme can produce hadron rejections of order 10^{-4}.
2. TRD's are quite compact. Roughly 2' thickness is required for 10^{-3} rejection versus about 4' for Čerenkov detectors. At higher electron momenta, the detector thickness is the same for TRD's, but must be longer for Čerenkov detectors.
3. TRD's use "simple" electronics. The actual detection system is a proportional wire chamber which in the original configuration was operated in a linear mode. Wires were individually latched, and also grouped together into ADC's. The cluster-counting readout will be discussed below.
4. TRD's can be used to provide an "electron" trigger within a few hundred

nanoseconds. Because these are proportional wire chamber detectors, it is relatively straightforward to form a fast trigger, which could be correlated with external systems, or tracks in other chambers.

5. TRD's have the ability to handle large numbers of simultaneous tracks without degrading their electron identification. The electron signature is typically defined on a wire by wire basis, so that the intrinsic cell size is of the order of 1 cm. This is a radical advantage when compared with typical cell sizes for gas Čerenkov counters. This advantage will become even more important when the electrons are found within jets.

As the available machine energy goes up, the probability of observing any specific final state goes down, so that increasing reliance has been placed on the detection of leptons as a clue to quark decays that are fundamentally of interest. This sort of question can be addressed by a Monte Carlo calculation, to learn how many leptons are expected, what is their momentum spectrum, and what is their spatial relationship to other charged particles. Monte Carlo simulation of all these has been done for the process $e^+e^- \rightarrow Z^0 \rightarrow$ hadrons $\rightarrow$ leptons ($e + \mu$, without γ conversions)[10]. Figures 23 and 24 show the expected number of lepton events ($\simeq$30% of Z^0 events contain at least one lepton) and their momentum distribution ($\simeq$20% of produced electrons have γ>6000). It is evident that a substantial fraction of these leptons are appropriate for a TRD system. (If lepton momentum were the only consideration, then a gas Čerenkov, which is sensitive down to $\simeq$ 100-200 MeV, would be preferable.)

Very briefly, transition radiation occurs when a relativistic particle crosses an interface between two media having different dielectric constants. At each such crossing, photons are emitted which then accompany the primary particle. This is the radiation which is detected to distinguish particles at

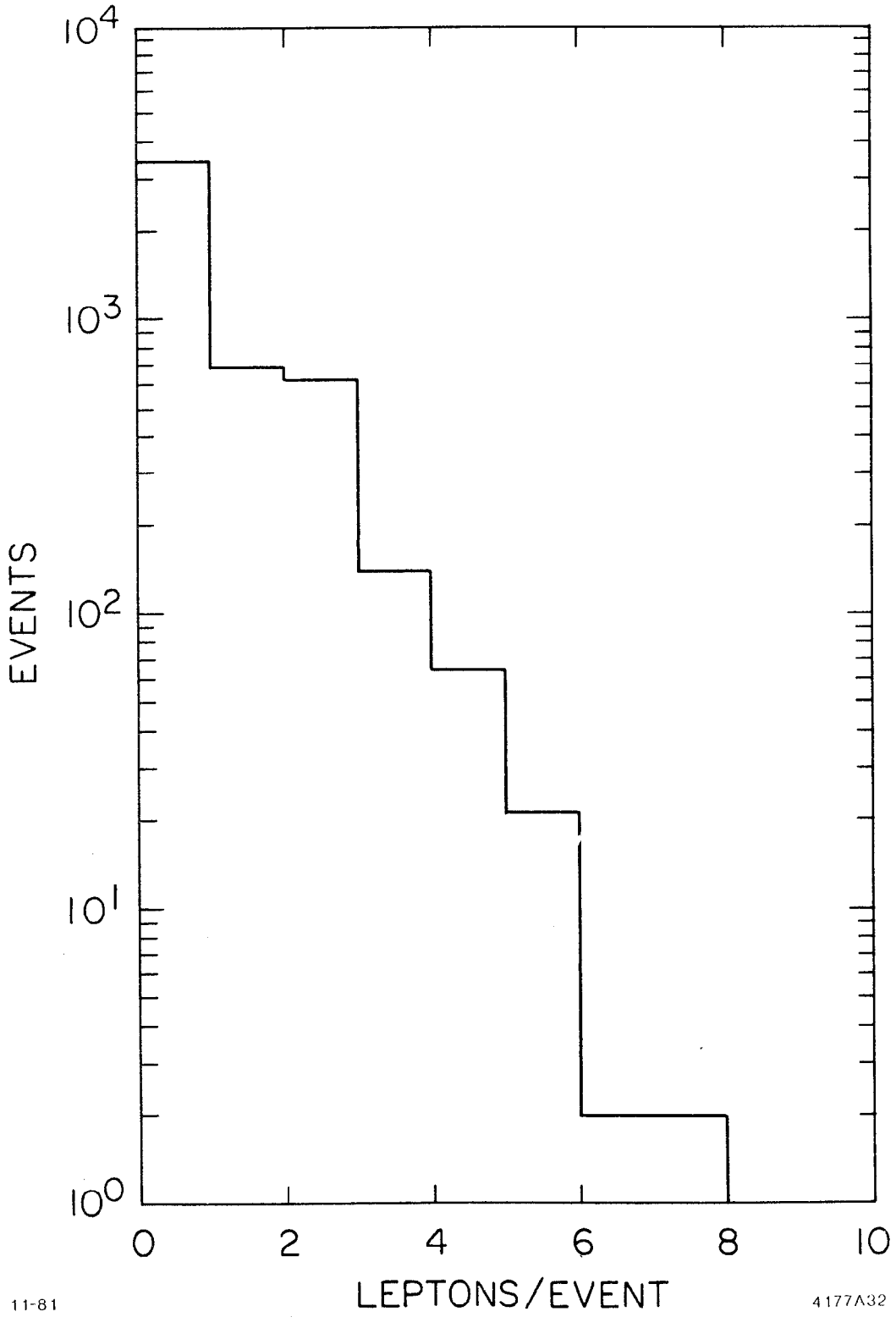

Fig. 23. The number of leptons per event from the process $e^+e^- \rightarrow Z^0 \rightarrow$ hadrons $\rightarrow$ leptons, where γ conversions are not included.

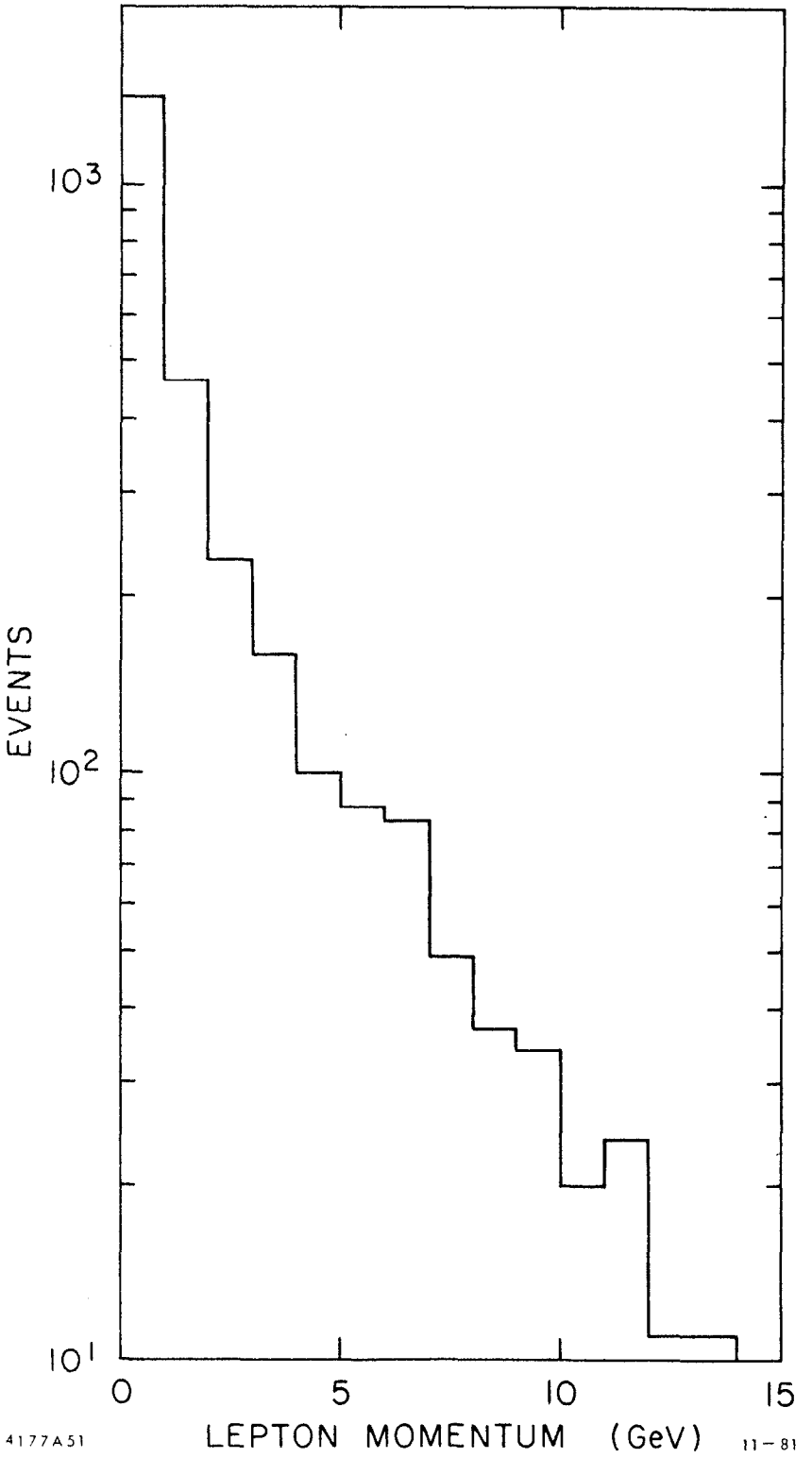

Fig. 24. The momentum spectrum of leptons from such Z^0 decays.

high γ from those at much lower γ. Practically speaking, the only particles whose γ's are high enough are electrons, since the probability of emission per transition is about α for γ's of a few thousand. The photon energy is typically $\simeq$ 10 keV, and saturates[11] for electron momenta of >4 GeV (shown in Fig. 25). The theoretical understanding of transition radiation is very detailed, and much experimental work has been done to check that the predicted phenomena are as expected. One excellent discussion appears in A. Lankford's thesis[12], as well as many further references.

The need for maximum signal strength leads to two obvious maxims: 1) Maximize the number of TR photons, i.e. use many dielectric transitions; 2) minimize absorption, i.e. use special materials for the dielectric foils (such as lithium) and special PWC gas (such as xenon-CO_2). The procedure to optimize the detector goes roughly as follows:

1. Make the difficult decision regarding what level of hadron rejection is required, for what range of lepton momentum. Increasing difficulty and cost will result from attempting to detect an insufficient number of photons as γ decreases. Practically speaking, γ>4000-6000 (i.e. P_e > 2-3 GeV) is readily available to this technology.
2. Choose the radiator foil material. Due to the simultaneous requirement of many interfaces yet low X-ray absorption, lithium foils have been selected for past experiments. Test data exist for other materials, notably mylar sheets, and recently carbon fibers.[13] These do not involve the fabrication and handling difficulties of lithium. However, their performance has not been as good.
3. At this point, the detailed theoretical model allows a computation (for a given electron momentum spectrum) that will maximize the photon yield (by minimizing interference and saturation effects) as a function of the foil

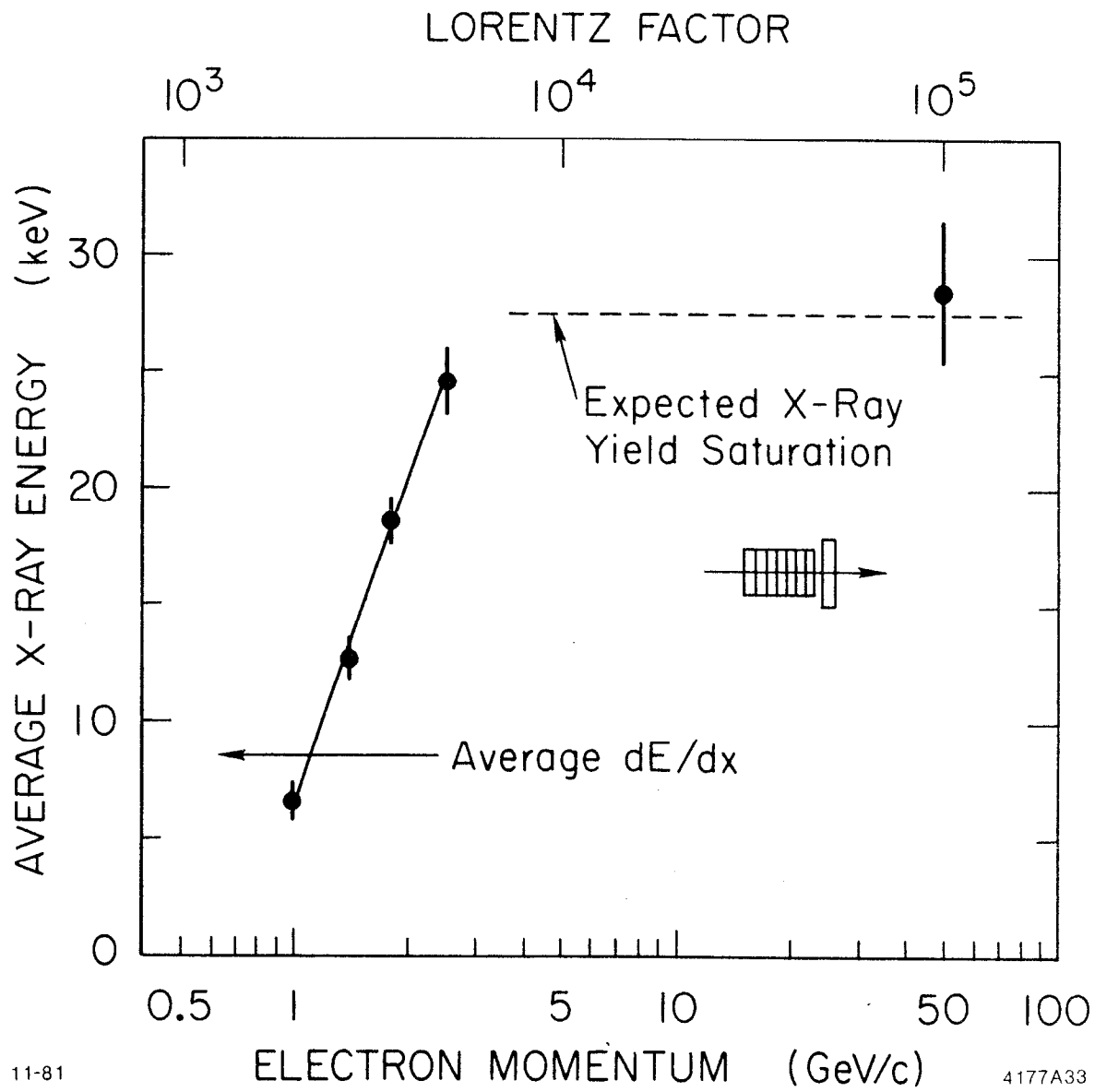

Fig. 25. Average X-Ray energy as measured in Ref. 11, showing the expected saturation at high electron energy.

thickness, interfoil gap distance, and number of foils. Typical choices for a lithium radiator system are foil thickness 10-100 μ, gap distance 100-1000 μ, # foils + gaps 500-2000.

One of the most important considerations in choosing a specific technology is its track record in actual experiments. In the case of TRD's, at least two experiments have successfully operated them, both in storage ring and fixed target applications.

In an experiment at the ISR,[12] a system of 4 octants (see Fig. 26) of TRD's were used together with liquid argon calorimeters to study vector meson production in pp collisions. This geometry is rather similar to the SLC, and demonstrates that the use of planar chambers is possible in a "cylindrical" detector. Data from these TRD's indicates that each layer was capable of ≃ 10% hadron rejection, so that the two together have a rejection of ≃ 10^{-2}. (Figs. 27 and 28). In addition, these TRD's functioned in an environment that had a high multiplicity of both charged particles and photons.

In E686 at the MPS at Brookhaven,[19] a 2 TRD system was used in conjunction with a lead scintillator electromagnetic calorimeter to study low mass e pair production in πp collisions (see Figs. 29 and 30). In this case, the electron signature from the TRD's was used in a RAM-correlated trigger to select candidate electron tracks and reject positron and γ-conversion magnetic field background. The TRD's operated directly downstream of the target, which was subjected to a $5x10^5$ sec^{-1} pion beam. The high rates necessitated special delay-line readout, but otherwise the system was conventional. The TRD + calorimeter provided 10^{-5} hadron rejection at the trigger level.

Since the time of these two experiments, further test programs have been

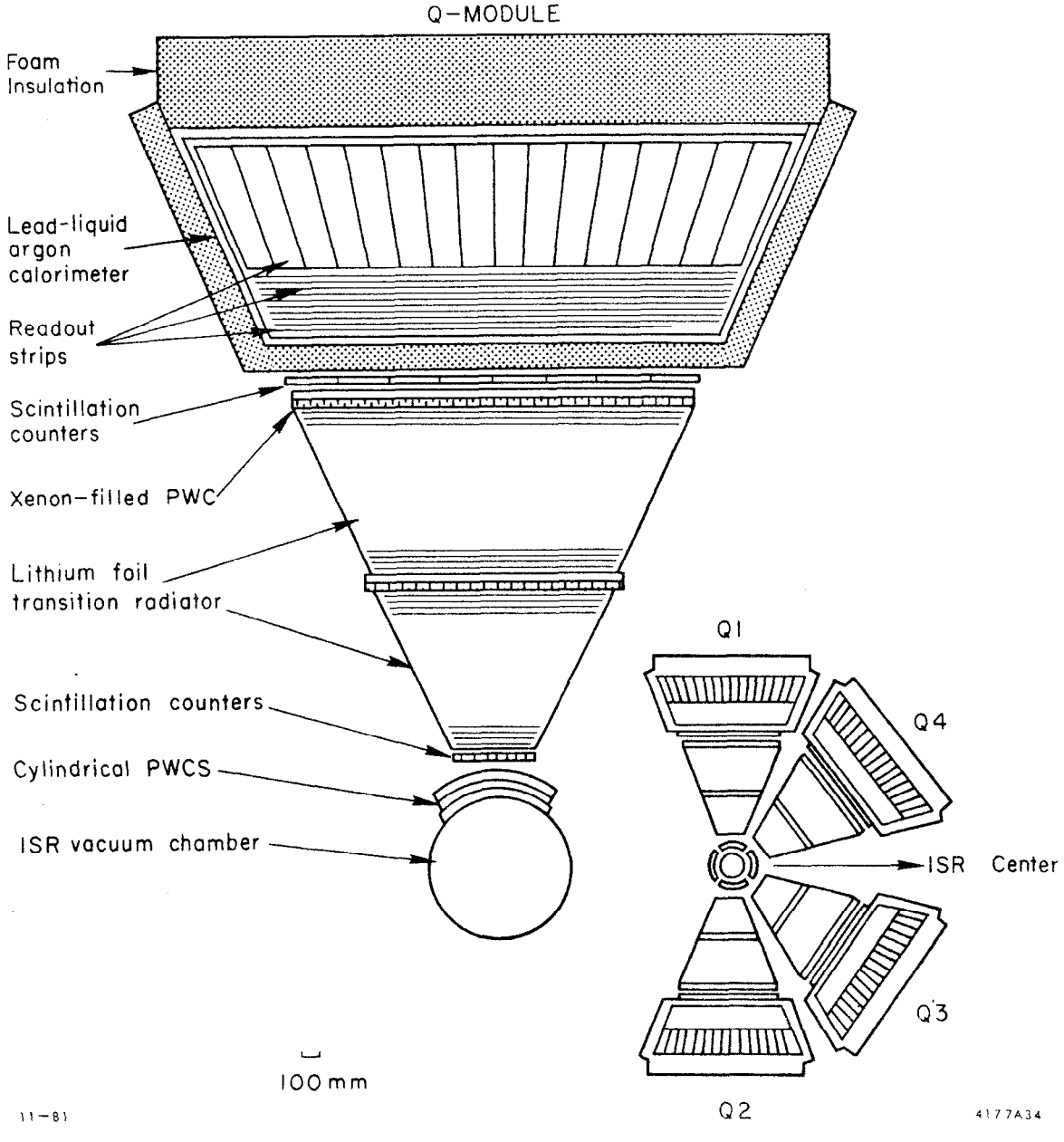

Fig. 26. Layout of the ISR detector. Above left, detail of 1 octant.

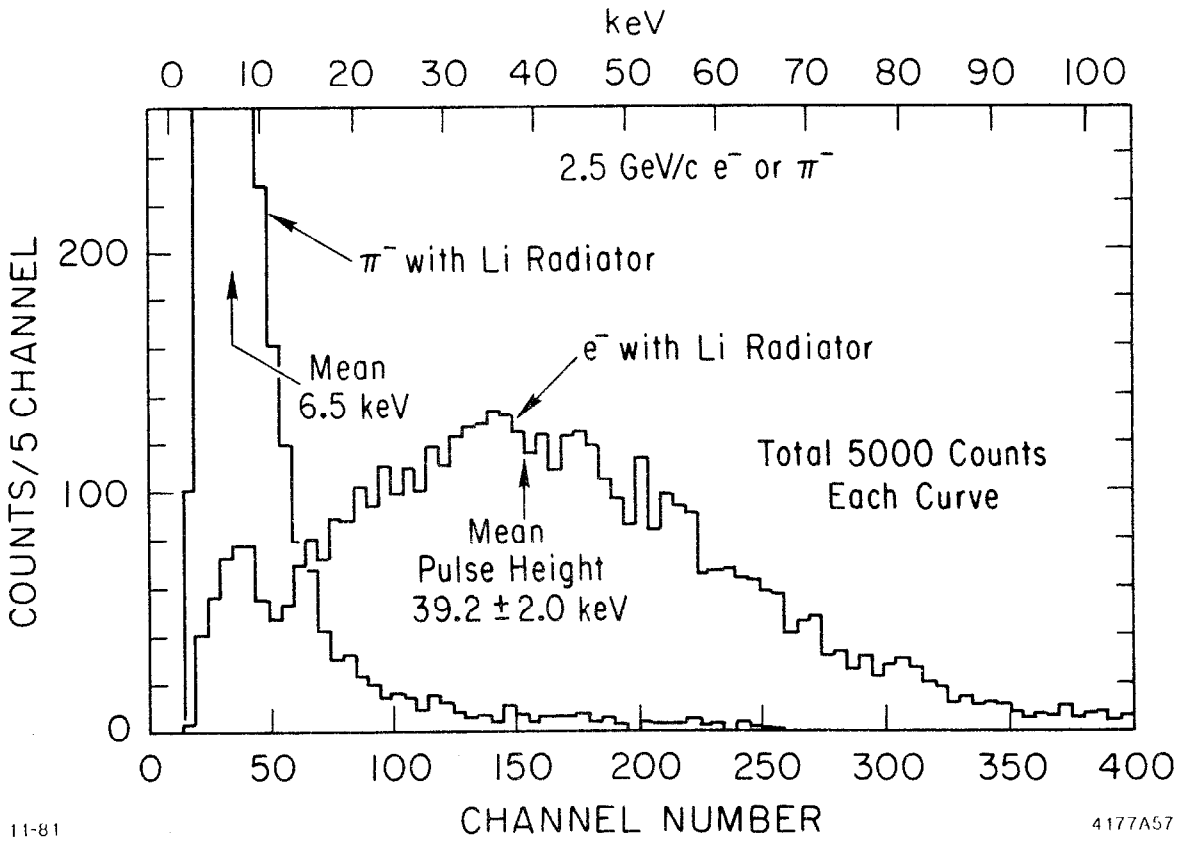

Fig. 27. Response of test version of ISR TRD modules to pions and electrons.

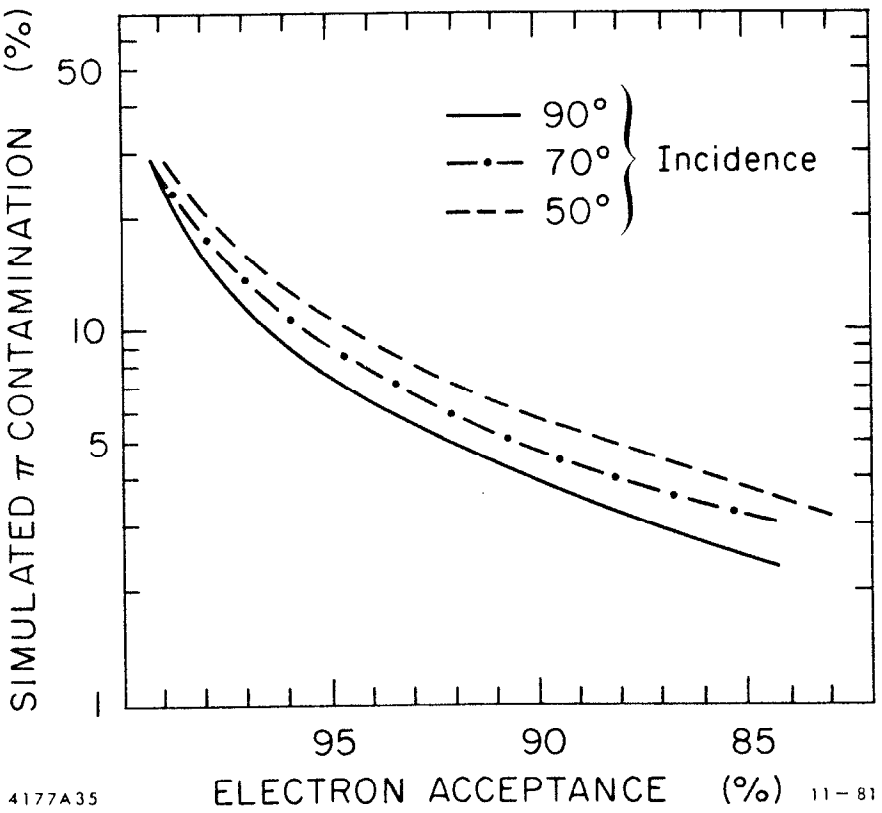

Fig. 28. Electron acceptance versus hadron rejection for a single TRD unit in the ISR detector.

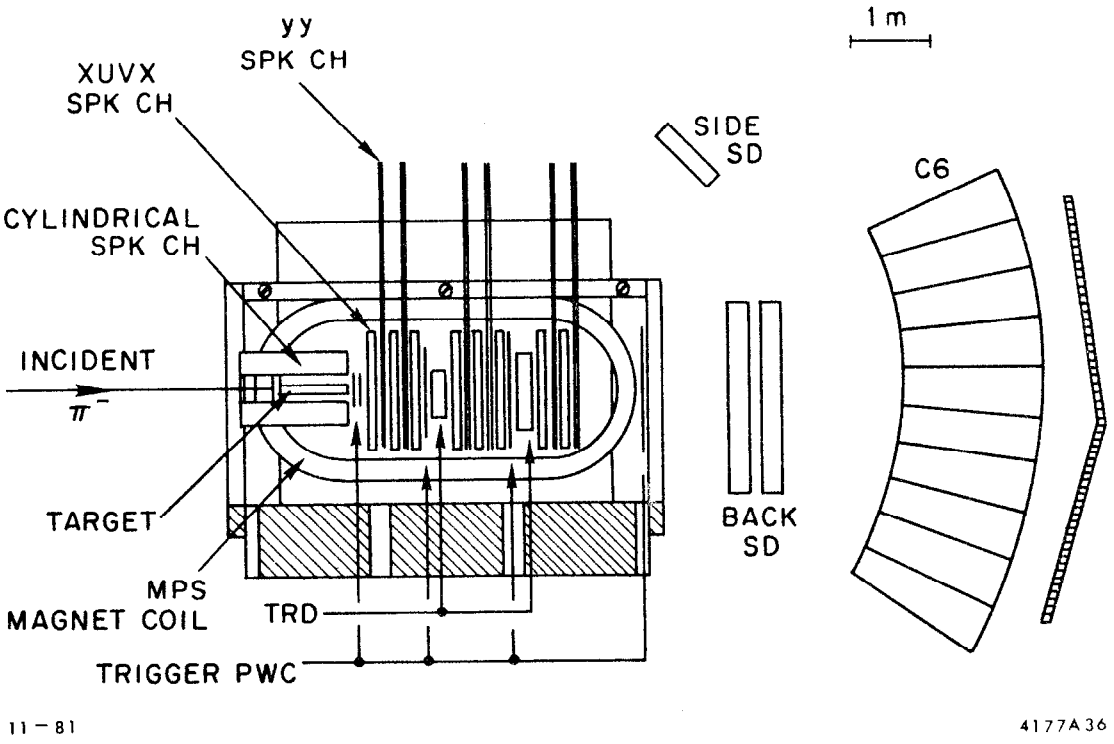

Fig. 29. Plan view of E686 apparatus at Brookhaven. TRD modules operated within dipole magnet volume at 10 kG field.

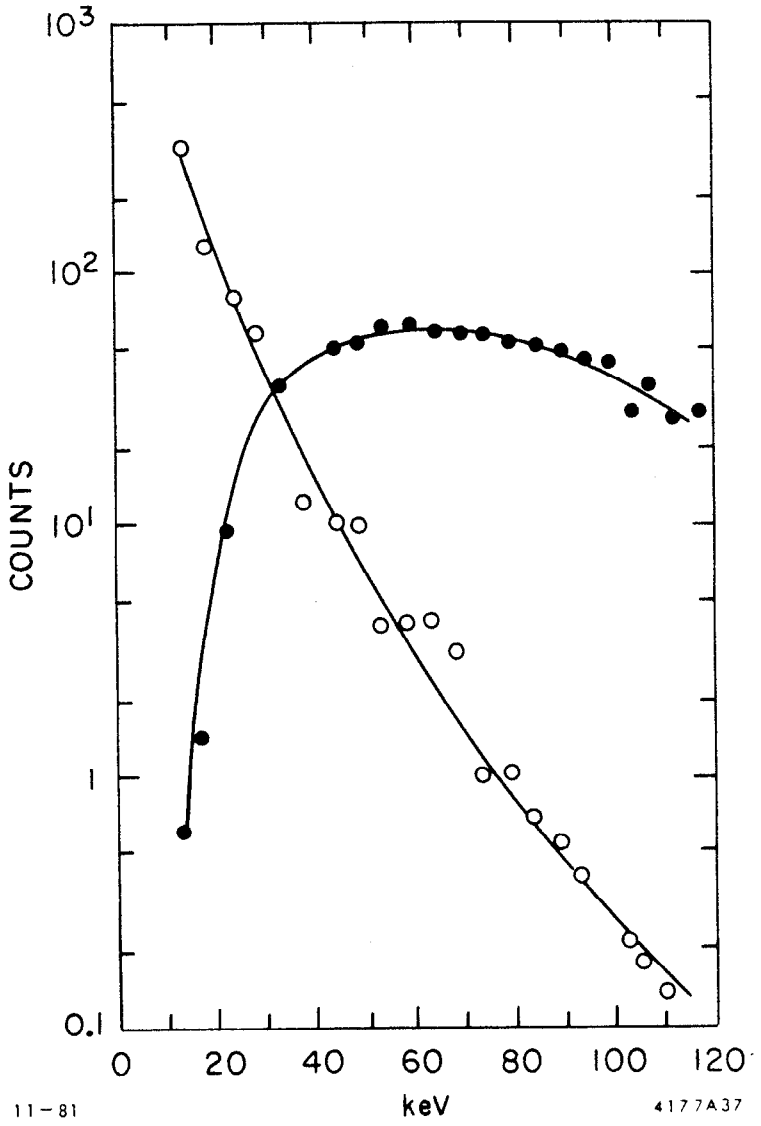

Fig. 30. Energy deposition for identified electrons and pions from K_s decays from the BNL detector.

underway[15] to utilize a measurement of the distribution of charge along the particle's track rather than simply measuring the total ionization deposition. This idea is qualitatively similar to dE/dx chambers, with the additional presence of the radiators to enhance the signal for high γ particles. This work has led to much higher hadron rejection than was previously possible with the 1 or 2 measurements of total ionization. The basic premise that generates the electron-hadron distinction is that TR has a very wide distribution of total ionization energy (but potentially many sites of deposition from many photons) whereas the background to TRD detectors, which is primarily δ-rays from hadrons, has a Poisson distribution (typically many fewer in number than from TR).

The price that is paid for the better hadron rejection is increased instrumentation. Cluster counting schemes involve many layers of PWC's + radiators, which enhance the probabilty of detecting photons before they are absorbed, but which cost in the total number of electronics channels. The punch line to the cluster counting technique is shown in Fig. 31, which demonstrates that a 70 cm-thick lithium radiator detector with 12 layers of PWC is capable of 10^{-3} pion rejection. If 10^{-2} is all that is required, then 45 cm with 8 layers will suffice. With these values as ballpark numbers, one can begin to get some rough idea of the numbers of channels required and the cost of fabrication of a total system.

Before envisioning a particular detector, some general comments are in order. Experience has shown that the dominant background for Čerenkov counters is due to some hidden photon conversion that satisfies the electron definition. Good electron identification demands that photon conversions must be minimized. Thus, any electron identification scheme must occur as near the interaction point as possible. In addition, there will be a magnetic field to deal with,

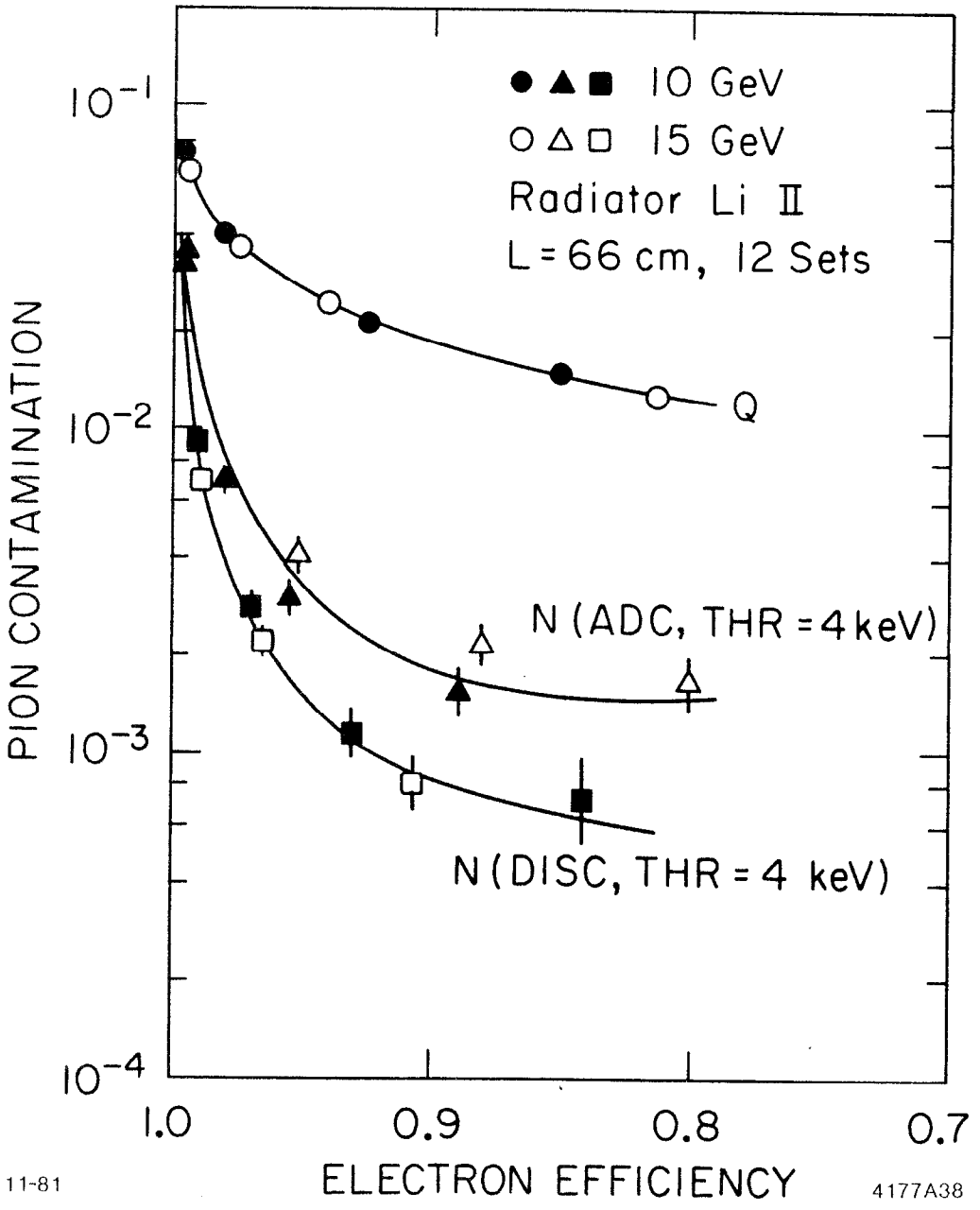

Fig. 31. Test data from Ref. 13 showing hadron rejection versus detector thickness using cluster counting electronics.

whether the geometry is solenoidal or open. Fortunately, the performance of TRD's is not degraded by operation within a magnetic field, since the ionization will occur quite close to the stiff electron track. Although the real estate near the beam pipe is highly valuable, the TRD gives two advantages in addition to particle identification: tracking information and a fast trigger. These may well be sufficient to justify assigning the region r = 10 - 80 cm to a TRD system. Furthermore, from the point of view of reducing backgrounds, it is desirable to have complementary detectors whose information can be combined, but in which one has a good rejection of backgrounds that the other is less able to reject. For example, both the above experiments used TRD's + electromagnetic calorimeters, neither of which would have been sufficient alone.

For purposes of discussion, we will sketch a possible modular detector which would be expected to provide 10^{-2} - 10^{-3} hadron rejection for $P_e > 2$ GeV/c (Fig. 32). In addition, these modules would provide tracking information in the central region of the detector, and could be used as components of the event trigger. One beauty of rectangular planar chambers is that z, ϕ, and arbitrary stereo angles are all possible. A first calculation of the number of wires in such a module gives $\simeq 10^3$ wires/octant using a rather dense (2 mm spacing on first 4 planes) grouping of wires as an assumption. Probably the electron identification would not be degraded even if the number of channels were a factor of 2 lower, so here the tradeoff comes from the need (or lack) for tracking information.

At this point it is also necessary to keep in mind a series of difficulties that this technology implies:

1. TRD's require PWC operation in a linear mode. This requires rather careful tolerances in construction, particularly in the cathode-anode spacing.

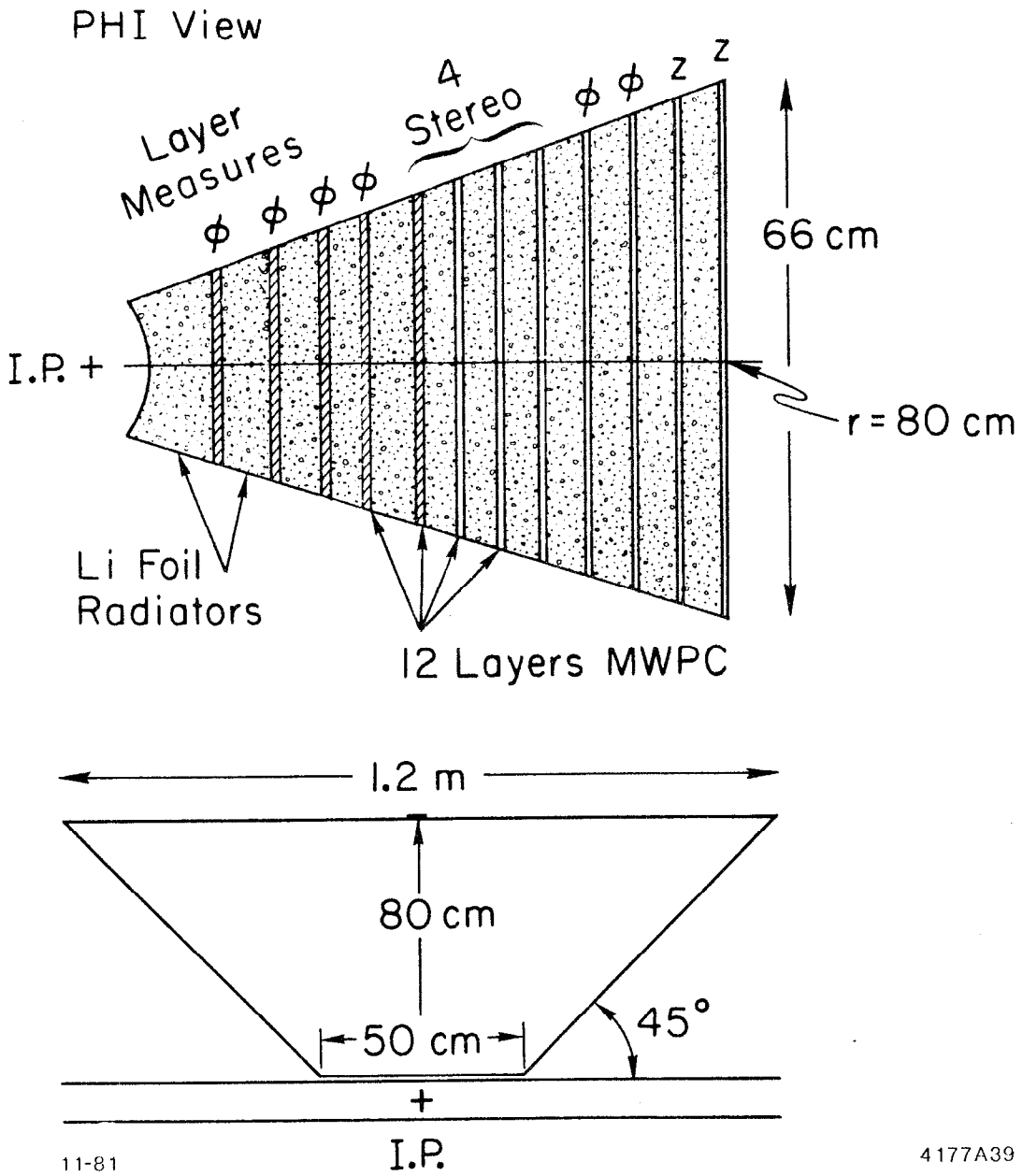

Fig. 32. Sketch of possible 12-layer octant module for cluster-counting TRD apparatus.

This is not impossible for chambers of 1 m x 1 m size. However, strong frames for such chambers occupy a significant portion of the detector volume.

2. If lithium foils are used as radiators, a sizeable effort must go toward the fabrication and packaging of radiator modules, which are coupled to the PWC's by very thin windows. The combination of fragile and volatile materials makes handling of these detectors a rather delicate operation.
3. In any wire chamber scheme, (but particularly with PWC's) there are a rather large number of electronics channels to fabricate, calibrate and operate.
4. In any modular scheme there will be blindspots created by the frames as well as unwanted sources of photon conversions.

To sum up, although electron identification remains a very high (perhaps over-riding) priority for any SLC detector, the game has gotten harder as particle multiplicities within an event have gone up. The smallish number of cells appropriate to gas Čerenkov counters problably makes their rather large volume unjustifiable. Certainly if a calorimeter is used, it will come outside the central tracking chambers, as will TOF counters. Thus any internal electron identification will be done either by dE/dx chambers or TRD's. The question of relative advantages versus disadvantages will eventually be resolved partially by history (i.e., if the TPC is not successful at PEP, then dE/dx techniques will probably not find large-scale use at the SLC), partially by physics emphasis (what fraction of the detectors' resources will be devoted to electron identification), and partially by cost (can we afford to build the detector we need?). A transition radiation detection system could certainly identify electrons in an SLC environment, and the difficulties mentioned above are by no means insurmountable.

CONCLUSIONS

We can only summarize by showing the best case numbers on particle separation for each type of system. For dE/dx, we assume a TPC-like system with 200 samples, 0.4 cm/sample, and 10 atm. For Čerenkov, a system like the proposed LEP detector is assumed. For TOF, σ_t = 50 ps over a 1.5 m flight path is assumed. For transition radiation, the parameters are not important since one will not reach the threshold for pion production of transition radiation. For particle separation in all cases, we assume 4σ separation. The relative ranges of separation for π/K and π/e separation are given in Figs. 33 and 34. Some care must be taken when using the ranges given in the figures since dE/dx separation is different in nature from Čerenkov, TOF, or transition radiation separation. For instance, in the case of π/e separation, when an electron is identified as not being a pion, depending on the momentum, it is possible that the kaon or proton probability is very high for a dE/dx system. For the other types of systems, e/K or e/p separation is always much greater than e/π separation.

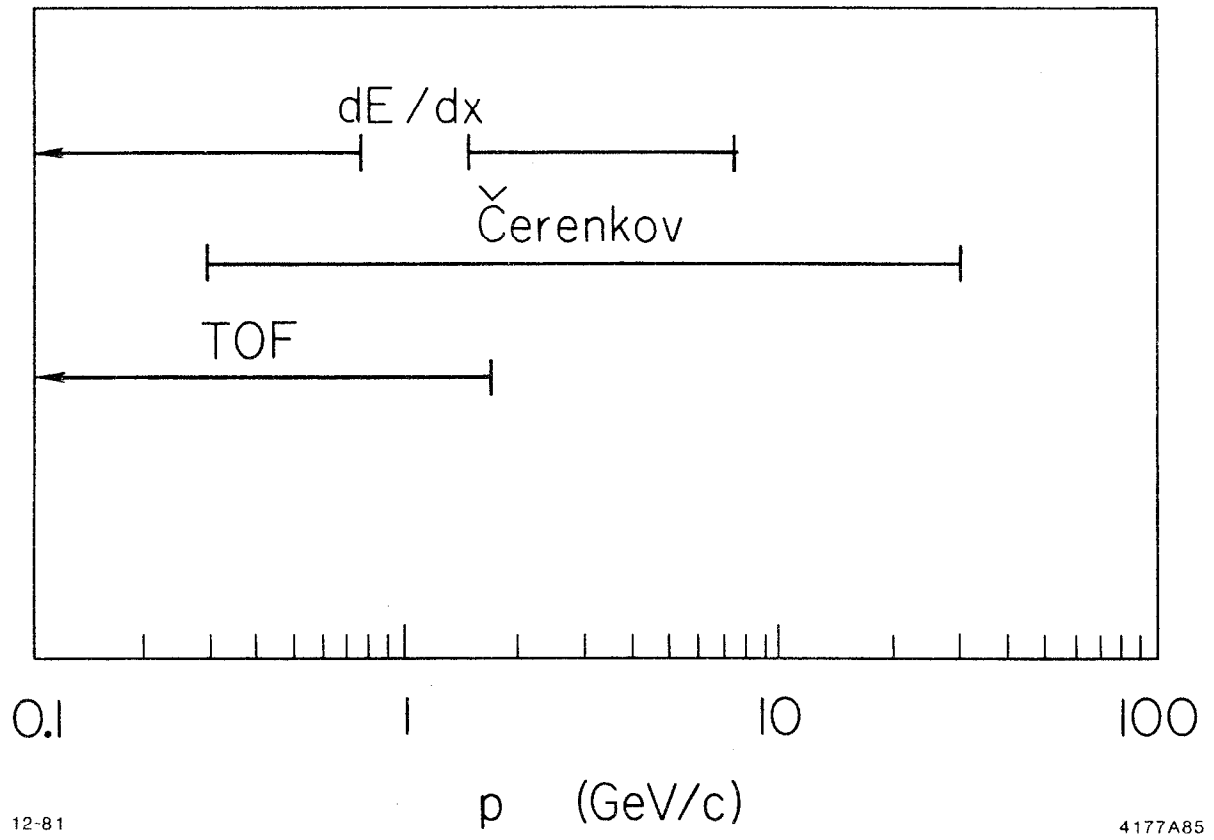

Fig. 33. Best-case π/K separation as a function of momentum.

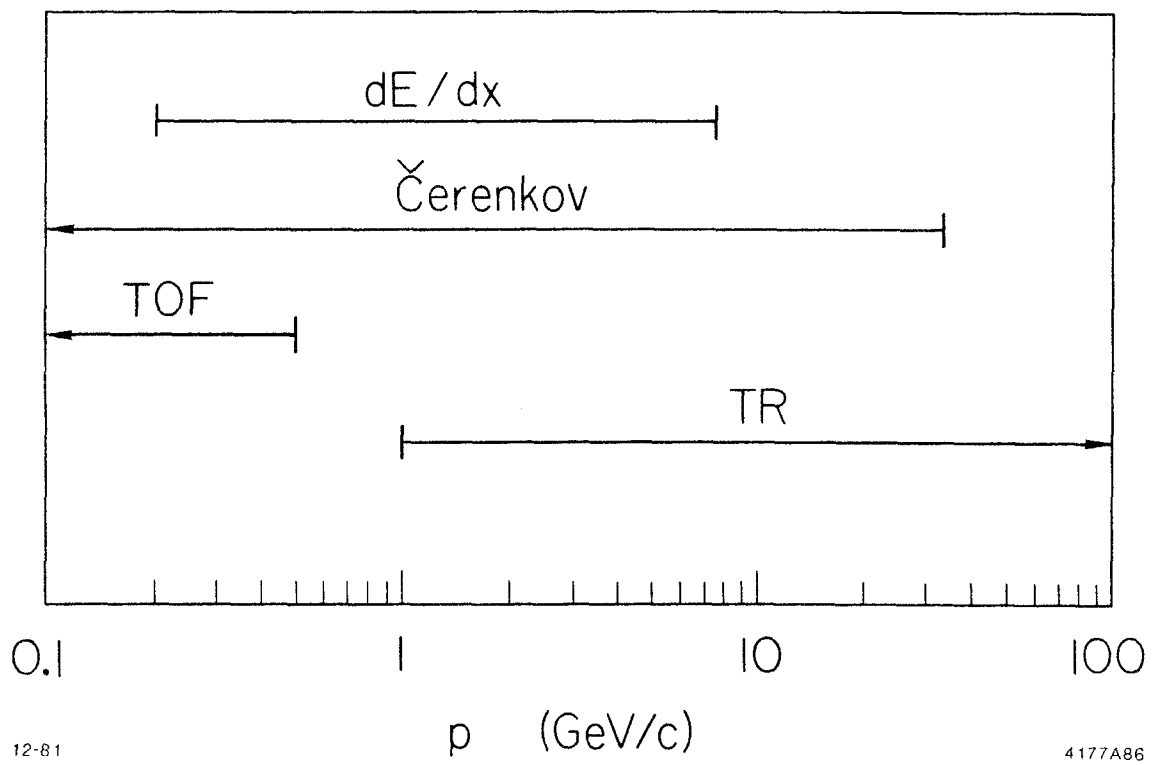

Fig. 34. Best-case π/e separation as a function of momentum.

REFERENCES

1. J. Va'vra, SLC memo #12.
2. G. Lynch, LBL-TPC-81.
3. N. Harnew and D. Meyer, Nucl. Instr. Meth. 186, 513 (1981).
4. J. Sequinot and T. Ypsilantis, Nucl. Instr. Meth. 142, 377 (1977).
5. T. Ekelof, J. Sequinot, J. Tocqueville, T. Ypsilantis, Physica Scripta 23, 371 (1981).
6. R. Gilmore, W. Lavendar, D. Leith, S. H. Williams, IEEE Trans. Nucl. Sci. NS-28, 435 (1980).
7. T. Ypsilantis, M. Urban, J. Sequinot, T. Ekelof, in Proceedings of the 1981 Isabelle Summer School, p. 973.
8. W. B. Atwood, in Proceedings of the 1980 SLAC Summer Institute, p. 287.
9. G. S. Abrams et al., Phys. Rev. Lett. 44, 10 (1980) J. M. Weiss et al., Phys. Lett. 101B, 439 (1981).
10. Data are from G. Feldman, SLC Z^0 Monte Carlo.
11. R. Bosshar et al., Nucl. Instr. Meth. 127, 141 (1975).
12. A. J. Lankford, Ph.D. Thesis, CERN-EP Internal Report 78-3 (1978).
13. C. W. Fabjan et al., Nucl Instr. Meth. 185, 119 (1981). For a review of older data, see for example S. Iwata, invited talk at the 2nd International Conference on Particle Detectors, KEK, September 1979.
14. G. Abshire et al., in Proceedings of the XX International Conference on High Energy Physics, Madison, Wisconsin, 1980, p. 158.
15. See Ref. 13 and also T. Ludlam et al., Nucl. Instr. Meth. 180, 413 (1980).

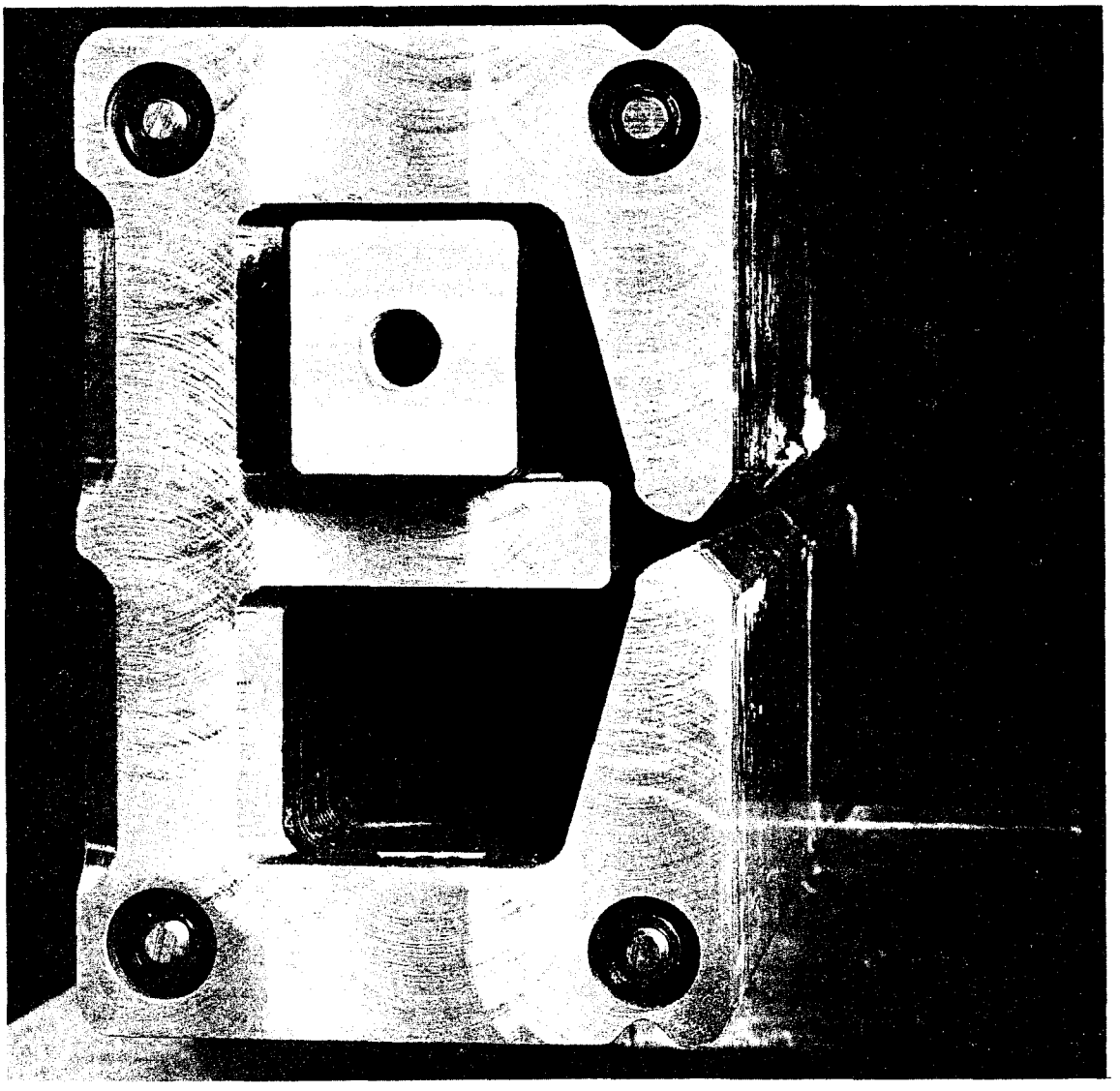

This is a prototype of one of the laminations for the collider arc magnets. These magnets, which will transport a beam of about one millimeter size, are less than one foot high and have gradients much larger than those used in circulating-beam AG machines.

ELECTRONICS & COMPUTING

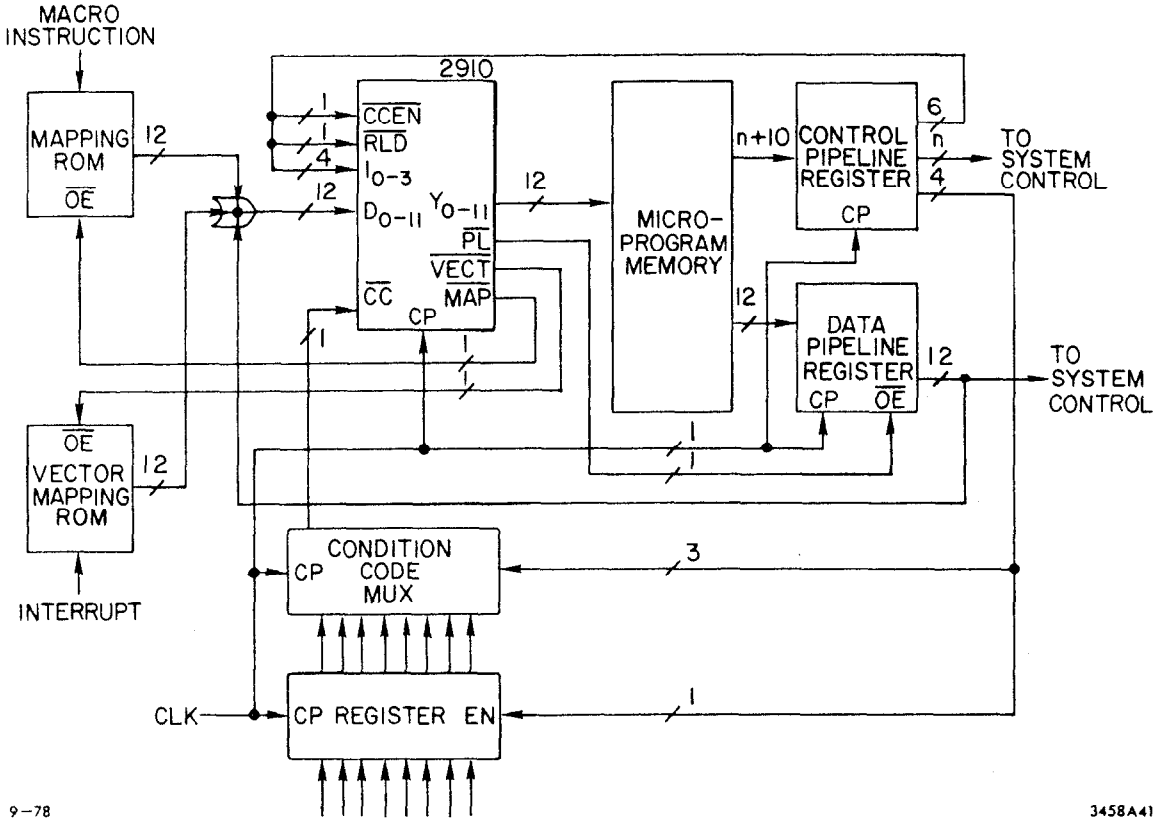

ELECTRONICS & COMPUTING

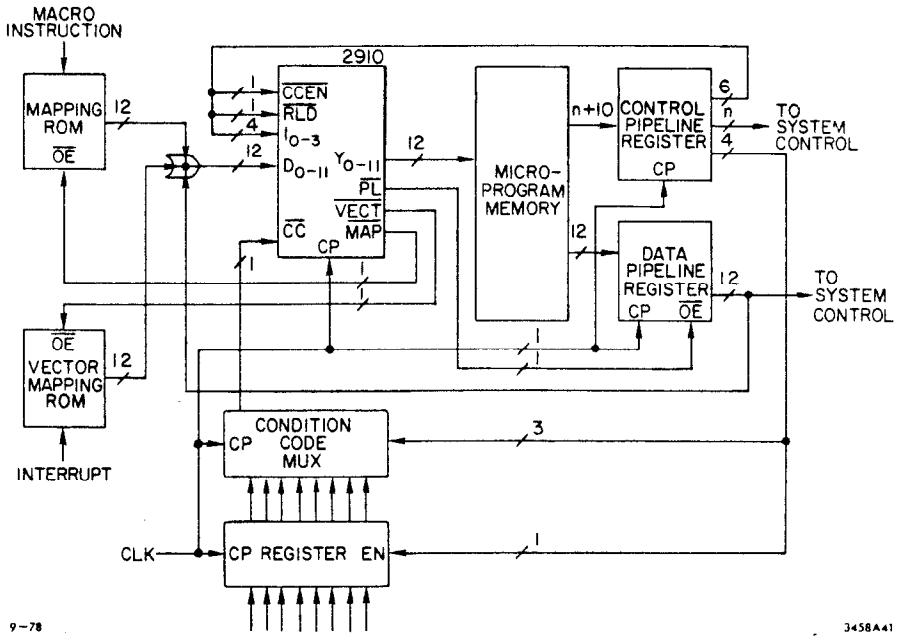

I. INTRODUCTION

This report summarizes the efforts of the Fast Electronics and Computer group to answer a set of general questions that might serve as guidelines in making architectural decisions for the instrumentation of an SLC detector. The group divided into smaller subgroups to address these questions:

(a) Will VLSI technology or custom IC's for SLC electronics offer major size or cost reductions, as compared with the present experience at the e^+e^- storage rings?

(b) Could microprocessors be employed at SLC in such a way as to greatly reduce the load of on-line data acquisition by the main on-line computer?

(c) Will the off-line computer demands of SLC require a major increase in computer power at SLAC?

(d) What types of trigger schemes can be expected to be useful at SLC, assuming the generalized detector configuration considered by the Parameters Group? Are there advantages of software triggers over hardware triggers?

(e) What new applications and/or ideas appear to be promising for fast electronics and computing, which may be reasonably expected to impact upon SLC experiments?

(f) What sort of organizational schemes seem most effective for the fast electronics of SLC detectors, taking into account the probable state-of-the-art a few years hence? Should one plan to use FASTBUS instead of CAMAC? Can a large savings in cabling costs be realized by preprocessing data on the detectors using microprocessors?

We feel that answers to these general questions, based on current and projected state-of-the-art knowledge of microcircuitry, will be of more use to the SLC project than any attempt to design electronics for an "ideal" detector. It is expected that the next phase of SLC development will consider possible modifications to existing detectors at which time these general results may be useful.

In each subgroup discussion, the unique features of SLC (e.g., beam crossing of very short duration at a very low repetition rate) were exploited. Information from other SLC working groups on rates, detector granularity, trigger modes, and acceptances expected in new detectors were used to estimate the number of channels, advantages and disadvantages of multiplexing, and efficiency of different organization schemes for preprocessing, on-line computing, and control. Although the final test of the electronics and data acquisition schemes will come when applied to a specific detector, we feel that the general conclusions from our working group will provide valuable guidelines.

Conclusions

The reports of the various subgroups follow and provide valuable information and details. However, we first list some general conclusions:

a. VLSI and Custom IC's

Although the field is changing rapidly, the present status of high-speed analog design is both difficult and expensive and offers little hope for putting large numbers of channels on a single IC. We must rely on small companies designing electronics specifically for High Energy Physics to provide special purpose digital IC's for aid in data acquisition and processing. Continuing liaison with these companies is highly desirable.

b. Microprocessors

Microprocessors can be used very effectively in specialized areas, such as controllers, fixed-instruction-set processors, and emulators (such as the 168/E used with LASS and the Hybrid Bubble Chamber). However, the effort in providing software support (e.g., compilers, cross assemblers, downloading, etc.) for microprocessors must be taken into account in deciding to make major use of microprocessors. As a rule, a microprocessor should save more than 50% of the computer time or I/O rate. It is expected that the applications of the microprocessors will be qualitatively similar to those seen at PEP. The use of micros for data preprocessing will not be a problem at SLC.

c. Computer Needs

We do not see a need to plan for any large increase in off-line computer facilities for SLC. In part this is due to the limited data rates expected from one detector operating at a time, and in part due to the expected advances in preprocessing of data during acquisition.

d. Trigger Schemes

The short crossing time of the SLC bunches makes cosmic ray backgrounds negligible. Beam-gas backgrounds will be much lower than those at PEP for reasonable SLC IR pressures. It is assumed that beam dump and beamstrahlung backgrounds will be controlled to manageable levels. Hardware triggers based on muon detection, calorimetry, showers and track-patterns have been considered and appear practical at SLC data rates. Software triggers requiring decisions at the detector are attractive from the point of view of flexibility and savings in cable costs, but it appears at present that the speed of decision-making would limit certain types of triggers. It seems likely that a hierarchical approach, using more specialized hardware to limit the rate to a software trigger processor, would be more practical than a pure software trigger. There appear to be no serious trigger problems for an SLC detector.

e. New Applications and New Ideas

Multi-hit Drift Time digitizers with 4 ns resolution or better are now possible. Bucket-brigade analog shift-registers with 1.2 MHz shift rates are available. Solid-state detectors with 10 μ resolution are now operational (silicon microstrips). Superconducting strips in conjunction with Josephson junction shift registers are being developed.

f. Organization Schemes

The optimum organization scheme seems to be a main on-line computer (e.g., VAX or equivalent) with a full complement of I/O devices, with micro's for subsidiaries as adjuncts to the VAX. The micro's would be downloaded from the VAX, interacting with only the portion of the detector to which it is connected and with the VAX. This is the scheme adopted for SLC control; detector electronics will benefit from SLC I&C development. Inexpensive high-performance micro's (such as the 168/E emulator)

should be used in situations where the VAX might become saturated. FASTBUS is a promising development but has not yet been fully tested. Thus, we suggest the need for a FASTBUS hardware and software demonstration project before detector development commences.

The Fast Electronics and Computing Work Group finds neither big problems nor major technological breakthroughs involved in SLC data acquisition and handling. Instead the unique features of the SLC beam spill and the steady advances in microprocessors (including experience in using them) point to substantial economies in per-channel costs in instrumenting SLC. Liaison with the solid-state electronics industry, particularly with small firms specializing in HEP equipment, should be maintained to encourage development of circuitry of interest to SLC.

II. VERY LARGE SCALE INTEGRATION AND CUSTOM IC'S

Initial attempts were made to execute some of the basic designs of drift chamber electronics in a single integrated circuit. The functions considered were low noise amplifiers, discriminators, time-to-amplitude converters and analog sample-and-hold systems (e.g., TAC's and SHAM's). These efforts encountered the following major difficulties:

(1) SSI or MSI designs can mix materials technologies to advantage. For example, n-MOS, p-MOS or c-MOS switches can be used for applications requiring low leakage and linearity, while bipolar technology can emphasize speed capabilities. The use of a single IC implies a commitment to one technology.

(2) The MOS materials can be used to fabricate transistors (FET's) with noise figures less than 1 $nV/\sqrt{Hz}$ using SSI. However, as the transistor IC area is reduced in LSI, this noise performance is degraded by orders of magnitude.

(3) The low duty factor of SLC is ideal for using low cost capacitively coupled electronics, but it is difficult to fabricate large capacitors on IC's. Typical IC capacitors are 100 pf or less.

(4) The packaging of LSI IC's is a severe limitation which is often overlooked by the novice. It is considered a major problem by VLSI designers.

   (a) The number of pins available on the package limits the number of channels possible in multichannel designs. Attempts to reduce the requirement of one output pin per channel by the use of internal multiplexers and ADC's usually fail by requiring one or more pins per channel for memory capacitors.

   (b) The permissable power dissipation in a single chip is a severe problem. The speed of the MOS technology is overtaking that of bipolar, but the power dissipations are similar at similar speeds.

(5) The costs of a custom IC design in bipolar technology equals or exceeds $100 K. Semi-custom designs are available at or above $10 K.

Conclusions

(1) Low speed (1-5 MHz) digital designs are common, and semi-custom digital gate arrays with speeds up to 100 MHz are available. Special purpose digital IC's to aid in data acquisition or processing are feasible.

(2) High speed analog design is difficult and expensive, and offers little hope for putting large numbers of channels on a single IC. The cost and expertise required are such that we do not feel SLAC will develop its own analog custom IC's. Therefore we must depend on the small companies designing electronics specifically for High Energy Physics and also the large companies where designs in general use have application to high energy physics, such as ADC's or low noise amplifiers. As an example of commercially available IC's similar to those required for SLC, EFCIS has developed an 8-channel PWC readout on a single IC with speeds only 2.5 times slower than present MSI designs. Another company is developing a 25 MHz CCD of 128 bits, 8-channels on an IC. The anticipated cost of this IC is $50.

(3) Semi-custom IC's for analog applications are a possibility for relatively low frequency electronics such as an amplifier-integrator for a hodoscope with a large number of channels. We are still investigating this possibility.

(4) Since this field is changing rapidly, continued monitoring of industrial developments is necessary.

III. MICRO'S AND PREPROCESSING

The Micro's and Preprocessing subgroup has studied the state-of-the-art in microprocessors and what we may expect at a time that a detector would be built for SLC. Microprocessors employ technology which is one of the fastest moving in the industry. This fact coupled with the lack of specific requirements on preprocessing which would come from the other subgroups and SLC groups has led us to not attempt to make explicit choices on which micro's to use, but rather to make an estimate on what would be available in the near future and what capabilities we might be able to expect.

The subgroup also felt that one should be very careful about the use of micro's. They are generally very inexpensive so there is a tendency to use them in many areas where they do something good for the detector. However, it is not always clear if the net gain in using them is worth the effort to implement them. Since they are in fact small programmable computers, the support system for them, in terms of manpower supplying compilers, cross-assemblers, downloaders, operating systems, etc., may become quite substantial. So the subgroup has followed the guideline that unless a microprocessor is going to do something significant, like save more than 50% of the computer time or I/O rates, then it is probably not worth doing it.

We have divided our discussion into the following categories:

A. Controllers: Front-end processors, in the style of the BADC currently in use at PEP.

B. Fixed Instruction Set Processors: Chip or board level microprocessors, generally in MOS technology, in the style of the INTEL 8086 which will be used for SLC Instrumentation and Control.

C. Emulators: High performance number crunchers, generally in Bipolar Technology, in the style of the 168/E in use with LASS and the Hybrid Bubble Chamber.

A. Controller

By "Controllers" we mean specialized processors usually located in a path where the data flows from the front-end electronics towards the host data acquisition computer. One example is the BADC which is currently in use in a number of PEP detectors and also in the fixed target program at SLAC. Their use has demonstrated that it is well worthwhile to use a microprocessor for this application. Since there is some confusion about the work that these processors do, it is probably useful to describe here the possibilities.

1. Zero Suppression

The processor can compare the data in each channel against a table in order to decide which channels have data and which have noise or only pedestal value. Thus only the data from channels with valid data are transmitted towards the data acquisition computer. This greatly reduces the volume of data that need be transmitted and hence makes the data transfer time much shorter. It also eliminates the need for the pedestals of each channel to be adjusted to be below a common threshold value, thus probably reducing the cost of the front-end electronics and the time it takes to install them.

2. Time Multiplexing

The processor allows one to time-multiplex the data into a single expensive resource. For example rather than having an ADC on each channel, one can have a sample-and-hold circuit on each channel with a single ADC for a large number of channels. The processor would control the multiplexing of the analog sample-and-hold circuits to the ADC. This scheme has the disadvantage of taking a longer time to digitize the data, but this is probably not a problem at SLC because of the long time between beam crossings. The advantage of this scheme is that the cost of the front-end electronics is reduced by not having an ADC for each channel.

3. Data Formatting

The processor can generate a block of data in buffer memory formatted for easy reading by the data acquisition computer. That is, it can give

the data points with tags indicating to which channel the data corresponds. The tags can be in terms of chamber, layer, wire rather than crate, module, channel. Another example is to give the address tags of the first wire followed by the data for a number of consecutive wires, thus reducing the data flow to the host.

4. Data Correction

The processor can correct the raw data following an algorithm such as a quadratic correction if the processor has some arithmetic capabilities. One can even convert the data to physics units such as nsec or MeV. Some groups prefer not to correct their data, pointing out that the CPU time saved is not significant and that they may not fully understand their calibrations until months after the data are taken. If data correction can be done, however, the large number of constants associated with the correction procedure need not be in the memory of the data processing computer.

5. Trigger Assist

While reading out the channels under its control, the processor can calculate certain sums that may later be used for a downstream trigger processor. In this application the processor is limited only to the data it can see, but whatever it can do for a trigger it gets done in parallel over all the controllers, thus saving a trigger processor time that might be needed.

6. Calibration Assist

During a calibration procedure, such as charge injection to the front-end amplifier, many sums must be made. When the processor can do these sums itself, then again a huge amount of data need not be transferred to the host computer, thereby speeding up the calibration procedure. One needs, however, a method of transferring these sums to the host computer.

7. Local Monitoring

The channel by channel histogramming can be done by the local processor. Additional programming effort must be made to have a histogramming package that can run on the processors, and a method of displaying the results on a terminal must be provided. The CPU time saved is again

not significant but the memory space saved may be worthwhile. Histograms that depend on cuts on the events which depend on other parts of the detector could be difficult because each processor only sees its local data.

The time constraint at SLC is to complete the digitization of an event before the next beam crossing, unless there is a hardware trigger which causes a readout in less than one crossing in 50, for example. This means that a fast bipolar processor is required to do some combination of the above possibilities and this processor is generally a microprogrammable bit slice design. They may include a hardware multiply chip which can do a 16×16 bit multiply in under 200 nsec if data correction is required. Bipolar specialized controller circuits such as the Signetics 8X300 or the AMD 29116 are ideal for this application in many respects, especially the bit shuffling involved in formatting, but unfortunately they are poor in arithmetic capabilities.

Microprogramming involves one level more difficulty than assembly programming. A FORTRAN compiler is not likely for this kind of processor. However, most of the work that these processors need to do are well defined fixed programs so that the effort of a few "experts" in microprogramming in the group is reasonable considering the benefits derived from it.

B. Fixed-Instruction Set Microprocessor

There are many fixed-instruction set microprocessors available on the market and it is a very competitive and fast moving area in the industry. They are available as 8 bit, I6 bit, and even so-called 32 bit, in either chip level or board level. Their speed is not very impressive compared to a VAX or an IBM mainframe and if they do any floating point calculations, their speed is even slower. Generally software support for these processors lag behind the introduction of the hardware, which can cause us problems if we want to use the most modern processor. They are, however, very inexpensive and can handle a large amount of memory. Eventually a realtime executive monitor becomes available which can run on the processor.

An 8086 with 8087 floating point chip system is being developed for the SLC I&C. By the time the detector construction should begin the system should have sufficient software support to make it easily usable for the experimenters. That is, it will have a FORTRAN cross-compiler and a realtime debugger.

The kind of applications which are best suited for this kind of processor is probably where time is not a critical factor, such as in the monitoring of gas and high voltage systems. They may also be used as computers during the initial testing of the detector subsystems. The integration of such microcomputers into the detector readout system is a subject discussed by the organization subgroup.

In the future we can expect processors of this kind to be introduced with capabilities of large mini-computers. We must be careful, however, to avoid being fooled by the claims of the manufacturers. A case in point is the recently introduced iAPX432 from Intel. They say that it is a "micromainframe" with an operating system "in silicon," and other features which allow running on a very high level modern language. On close examination, however, we discover that its performance is not likely to be much different than a 16 bit microprocessor with floating point chip. This is because the chip only has a 16-bit wide data path to its internal processing section and its so-called high level language features introduce a large overhead in making memory accesses. The 16 bit Motorola 68000 processor has 16 32 bit registers internally, yet the iAPX432 has only one 16 bit register which means that it will always be limited in performance by its memory speed. Its instruction set which is designed for high level languages is so complex that is probably impossible to read a memory dump. The full software support will probably lag the hardware by 2 years. Nevertheless, when such processor becomes mature, they will offer us a better processor for the kinds of monitoring tasks described above.

C. High Performance Emulators

A high performance emulator is a bipolar microprocessor which runs, in some manner, the same instruction set as a commercial computer. The 168/E, for example, emulates the IBM 360/370 series computers by translation of the IBM machine instructions into microinstructions. Then execution on the microprocessor produces identical results as when the original code was executed on the much larger IBM machine. Performance of 1/2 to 1/3 (depending on the code) of that of the 370/168 have been achieved for a cost of only $6000. The reason the performance/cost ratio is so much better than a real computer is that the emulator is effectively a bare CPU without the I/O capabilities of a real computer. The pre-translation also leads to greatly improved performance without the cost and complexity of sophisticated circuit design.

The great advantage in using an emulator, besides its performance/cost ratio, is that almost any code that runs on the large mainframe can run on the emulator. Thus code can be developed on the user friendly large mainframe, with all of its debugging, histogramming, graphics, and other software and hardware resources. The programmers need not interfere with the other work going on at the interaction region computer while debugging code for the emulator.

One disadvantage of the emulator is its lack of I/O. Thus they are generally incorporated into a system as a slave processor to some real computer. On the other hand, it is much easier to design efficient interfaces between the data acquisition system and the emulator than a real computer. The experience of the SLAC Hybrid Bubble Chamber group is a good example. There a CAMAC module spies on the data transfers on the DATAWAY and makes a copy of the data in the memory of the 168/E processor. The processor is then quickly started to run a complex trigger algorithm. CAMAC PWC digitizer modules have even been rebuilt as 168/E modules so the digitized data appears as memory to the processor, thus reducing the time to transfer the data to the processor to zero.

The processor is the size of a CAMAC chassis and has a high initial cost ($4000) if compared to fixed instruction set processors. It is therefore only practical when its performance is needed.

Group EB at SLAC is starting a collaboration with CERN to make an improved version the emulator which has been dubbed the 3081/E. It will have the performance of an IBM 370/168 with 2^{31} bits of address space. The processor should be available in about two years.

Conclusion

We have studied the various kinds of microprocessors and feel we understand where they can best be used. The future will bring improved performance versions of what we are using today. Nothing dramatically different has been introduced by the industry since the time the PEP detectors were designed, hence we expect that SLC detector(s) will be qualitatively the same as PEP detectors. Of course a dramatically new idea may occur which uses today's style components, but at least the use of micro's for preprocessing at SLC will probably not be a problem.

IV. INVESTIGATION OF COMPUTER NEEDS

It appears that provision of adequate conventional computing will not be particularly difficult for any of the detector designs most commonly talked about. Data and trigger rates are inherently limited at SLC, and in any case computing requirements are experimentally loosely (and not even necessarily positively) correlated with such rates. If this assertion that the essential conventional computing requirements for any reasonable physics objective can be relatively easily satisfied is true, then one can focus on providing for these needs in an economical and effective way as possible.

The existing on-line and off-line computing systems are capable of expansion should this prove necessary. SLAC's central off-line facility is based on IBM's 3081 mainframe, in a "bottom-of-the-line" configuration. By virtue of its basic architecture it is capable of expansion by at least a factor two in capacity, so that it would have the power of, say, ten 370/168's.

Currently most on-line data acquisition computers at SLAC are DEC VAX computers, 32-bit virtual-memory multiprogramming machines originally procured when PEP experiments were started. A VAX-11/780 model has roughly one-quarter the capacity of an IBM 370/168. In a couple of years one can expect VAX systems 3-4 times more powerful for roughly the same price. A number of other manufacturers have also aggressively entered this arena, so that choice of another vendor may be appropriate by the time work starts on SLC detectors. Since hardware capabilities continue to go up, and the costs of acquiring them continue to go down, one can focus on the (larger) cost of application development, i.e., how easy is it to interface, develop, and debug a particular piece of software or hardware. These questions should be addressed not only when moving from one mainframe vendor to another, but also when one considers moving an application to custom-built special-purpose hardware as well.

Finally, at some point SLAC should reevaluate its policies regarding the provision of off-line computing for outside users. These were developed in the days when experiments were shorter and simpler,

collaborations smaller, and there was a clearer distinction between on-line and off-line analysis. Physics is rather more complex now and one might anticipate not only administrative changes but also technical ones (such as providing more satisfactory remote access to SLAC computers, for example).

V. TRIGGER SCHEMES

When considering trigger schemes for SLC two features standout:

(1) The instantaneous luminosity is extremely high, although the number of particles in a bunch $\lesssim$ the number in a PEP bunch, and the event rate expected is substantial (~1/sec at the z_o peak).

(2) There is a long time between pulses.

We show that as a result of (1) triggering for canonical type detectors is easy, in the sense that it should be straightforward to reduce the ratio of false triggers to real events to a value << 1. Consequently, discussion of dead times, tape-writing limitations, etc., fall outside of the purview of this group.

The second feature could be used to construct complex hierarchical triggers in hardware, software or a combination thereof. However, in the light of the previous comment this does not appear to be necessary. It is none the less important as it makes possible an elegant solution to triggering difficulties posed by calorimeters with a large number of channels.

A. Characterization of Events

We consider four classes of events.

- High multiplicity, including at least one electromagnetically showering particle.
- Events which consist of 1 or more γ's (+ neutrons)
- Low multiplicity charged tracks only.
  - — Muons
  - — Electrons
  - — Hadrons
  - — Combinations

  We note that these tracks will be energetic.
- Fully neutral, non-showering, hadron events. (All-neutrino events were not considered.)

B. Detectors

We assume that all detectors will have electromagnetic shower detector capability and a muon detector. We consider in addition three other options.

a. Tracking chambers.

b. Hadron calorimeter.

c. Both of the above.

We do not assume the detector will have scintillation counters. Should a radically different detector be used, obviously the trigger would have to be re-examined.

C. Trigger Types

As we shall see in the next section, the background rates are expected to be very low and a loose trigger can be employed. A satisfactory trigger which would be adequate for all proposed experiments* and which would place very few restrictions on unforeseen surprises could be made from $\geq$ 1 GeV of e.m. energy, or $\gtrsim$ 1 charged track with $\gtrsim$ 1 GeV/c or 1 GeV of energy in the hadron calorimeter. The calorimetric triggers could easily be changed to require some $p_\perp$ constraint by weighting segments appropriately.

D. Backgrounds

a. Beam-gas. The ratio of beam-gas at SLC/beam-gas at PEP

$$\approx \frac{(\#\text{ in bunch} \times \#\text{ of crossings/sec} \times \text{pressure})_{SLC}}{(\#\text{ in bunch} \times \#\text{ of crossings/sec} \times \text{pressure})_{PEP}}$$

$$\approx \frac{5 \times 10^{10} \times 180}{10^{11} \times 5 \times 10^{5}} \left(\frac{P_{SLC}}{P_{PEP}}\right) \sim 10^{-4} \left(\frac{P_{SLC}}{P_{PEP}}\right) \ll 1 \ .$$

* All-neutral events do not fall under the designation of proposed experiments and are obviously only triggerable given a detector with option b.

b. Cosmic rays. Assuming a gate width of 1 μsec 180 times/sec it is easy to see that none of the proposed triggers will have any serious cosmic-ray background.

c. Stray particles into detectors from synchrotron radiation, beamstrahlung, beam dump: We expect ~10-100 γ's ranging from keV to tens of MeV into the detector† per crossing. Once again it is clear that none of the triggers will be affected by these backgrounds. Slow neutrons from the dump can be well shielded and should pose no problem.

E. Proposed Trigger Schemes

A Mark II type tracking trigger would certainly be adequate for the tracking chamber. Calculations show that this type of trigger can handle many large backgrounds of soft tracks, particularly if a minimum momentum of 1 GeV/c is required.

Calorimeters with a large number of channels pose a serious triggering problem when the decision to accept an event must be reached in a time scale of microseconds, even if the trigger is only based on a simple threshold. The signal from each channel must be split and a linear analog sum performed. Aside from the expense there is very limited flexibility and a poor signal/noise ratio which necessitates the use of high thresholds and/or a requirement of high local energy deposition.

In the SLC environment if we assume that BADC's, or variants, thereof, will be used to read the data, the noise and flexibility problems can be neatly circumvented by reading every event into the BADC's, and then summing or performing more complex tasks digitally either in hardware or firmware. There is some cost involved if the number of channels assignable to a BADC is limited by the permissable read-in time of 5 msec. If a trigger which did not involve the use of BADC's were devised, then a read-in time of, say 15 msecs, would introduce negligible deadtime. The precise numbers will depend on the BADC's available and the multiplexing scheme (if any). However, it seems clear that the added cost will be a

† Hans Sens, private communication.

small fraction of the cost/channel (probably less than the cost of the analog system) and the advantages in reliability and cleanliness of the trigger clearly indicate that this approach should be followed.

There is, of course, the additional advantage inherent in this approach, namely flexibility. In the event of unexpected backgrounds, for example, or for monitoring purposes, the non-null BADC data can be processed by hardware (which can be modified without digging into the large data acquisition system) to look for clumping, etc., and by firmware or even by software as discussed in the next section.

F. Software Triggers

While we do not advocate a software trigger at this point, we feel it should be discussed, as the unique beam time structure does make the use of software in the trigger plausible. Such a trigger permits the most flexibility. For example, it is possible to modify drift chamber trigger parameters contingent on the electromagnetic calorimeter information.

Specifically, each event would be read into a buffer memory. Transfers from several detector subsections would take place in parallel. The event in its entirety would then be transferred to one of a few dedicated microprocessors such as the 3081/E (the new improved 168/E).† There the event would be examined until it was decided either to discard it or to write it on tape. The system could be FASTBUS from detector readout through to the dedicated microprocessor. Since the entire event is transferred, the system is a true pipeline. The only timing requirement is that the transfer from detector to BADC, from BADC to buffer memory, and from buffer memory to microprocessor be each done in under 5.5 msec. The requirement for the microprocessors is that the average number of SLC crossings needed for readin and processing be less than the number of processors. It is estimated that using FASTBUS it is possible to read 80 K bytes in 4 msec so that a software trigger is not implausible.

---

† This step could be subjected to a lower order hardware or firmware decision.

In addition to providing maximum flexibility in the trigger definition, other advantages discussed in connection with the digital calorimetric trigger are further enhanced by a software trigger:

- A potential savings in cabling compared to a purely analog sum trigger. The data paths for a software trigger must already exist for the data acquisition, calibration, and monitoring.
- All devices can be handled in a similar manner. There are no device or crate boundaries.
- Certain detector monitors may require data from every beam crossing in order to accumulate statistically significant data in a reasonable time. This is very easy if all the data is available to a microprocessor before being selected by a trigger.

The major short-coming is speed of decision making for certain types of triggers. Standard processors cannot, for example, come close to matching the Mark II track finding module in speed.

G. Calorimetric Trigger

The calorimetric triggers can be setup as hierarchical triggers. If an early stage can reduce the event rate enough, then the more sophisticated stages can take longer than 5 msec. A likely hierarchy would be:

a. Simple word count of non-null ADC's.
b. Keep total energy deposited without regard to location.
c. Calculate energy deposited in each segment and require two or more segments to exceed threshold.
d. Make energy clusters and find energetic tracks.

The CPU time (on a 370/168) for these for Mark II liquid argon data is:

a: 0.08 msec
a+b: 0.33 msec
a+b+c: 1.30 msec (getting module and strip numbers one by one)
a+b+c+d: not known yet.

The lower levels may be done by hardware or firmware instead of software. If a BADC (or extension thereof) could calculate local sums of energy deposited segment by segment, the time for (a+b) would be about 0.12 msec and for (a+b+c) about 0.20 msec. Also an intelligent device

at the buffer memory mentioned above could read these local sums and combine them. Full readout could be done only if sufficient energy was deposited.

H. Tracking Chamber Trigger

Emulating a Mark II track finding module is out of the question.

A promising alternative is to note that this trigger is only needed for low multiplicity charged track events with no electrons or photons. There will always be at least one stiff track in these events. Charged hadrons will leave some signal in the electromagnetic calorimeter and these can be used to define narrow roads through the tracking chamber which would be searched for a sufficient number of hits. We expect that this can be done very rapidly. Finding a stiff track for triggering is much less difficult than finding all tracks for measurement.

A word of caution is in order. At the present time the background rates make it appear that sophisticated triggering is not required to reduce the event rate to acceptable levels. Further, the point has been made in this section that the flexibility offered by a software trigger would enable one to tighten the triggers if necessary with barely a break in stride during a run. However, we note that if there is a substantial amount of soft background which needs complex algorithms to achieve acceptable trigger rates, then the software solution may be the least acceptable. The reason is that there will then be a larger non-null word count which would cause the time taken to read data to increase linearly with the word count, and the time to execute algorithms to rise at least this fast. Thus, these are precisely the conditions which necessitate clever hardware changes.

I. Calibration Triggers

These fall into three classes.

1. Those initiated by computer.
2. Those initiated by a beam crossing.
3. Those which are asynchronous, e.g., cosmics or radioactive sources.

Types 1 and 2 should not pose any unusual problems but type 3 may cause some difficulties in the absence of scintillator. In particular, if one used a muon trigger, the time would be too rough for precision calibration of drift chambers. We note Mark III does not use cosmics for anything but the most gross tests on their drift chamber. They propose to calibrate at the ψ. Since there is probably no ψ at SLC energies, it may be necessary to align the chambers with a laser or x-ray source and fit the single start time parameter using real data.

Conclusions

1. The trigger rate does not appear to pose a problem.
2. The time structure of the beam enables the problems associated with calorimeters with a large number of channels to be handled digitaily in a simple manner.
3. The possibility of using software in the trigger exists, but the possibility needs to be examined: (i) if it offers a real advantage in the actual detector proposed, and (ii) if it could handle the highest backgrounds which could be foreseen.
4. Some thought needs to go into calibration triggers.

VI. APPLICATIONS, NEW IDEAS, AND MATCHING OF ELECTRONIC CAPABILITIES TO DETECTORS

A. Multihit Drift Time Digitizer

Present day technology could achieve 3 to 4 ns resolution (least count) equivalent to an rms spatial resolution of 44 to 58 μ. Unlike analog solutions to the multihit problem there is no cost penalty for greater hit depth for the proposed digital method and the multihit capability is virtually unlimited. Extrapolating the trend of IC development, one may expect faster components that will simplify the circuits, thus allowing a higher density. Multiplexing of signals in conjunction with wire "scrambling" should provide a means of reducing the number of active digitizer channels. In a sparse system this should be easily accomplished with a minimal risk of losing wire identity. Moreover, a double multiplexing scheme using complementary "scrambling" should further minimize this problem.

B. Bucket-Brigade Analog Shift-Registers

These are suited for measurements of analog quantities e.g., sampling of analog signals. A staggered clock is required driving many devices to obtain samples over a useful time interval. The shift register has 32 bits organized as parallel-in/serial-out. Readout, subsequent to sampling, is limited to the maximum shift rate of 2 MHz with an extended rate of 5 MHz, max, albeit at a degraded performance.

The device was tested in 3 modes:

Mode 1. The sensitivity is 4 pC full-scale, when the charge is deposited on the interior capacitor. Full scale modulation at the output of ≃3 V peak-to-peak is achieved together with a signal/noise of 3000.

Mode 2. In this mode amplitude sampling is achieved since the signal is deposited on a very small storage capacitor. The dynamic range is limited to ≈8 bits at a signal/noise of 300. Rapid sequences of sampling are possible as the BBD's can be cleared in about 50 ns by strobing in a reference signal.

Mode 3. With a fast FET-input multiplexing circuit added ahead of the BBD's it is possible to achieve the full dynamic range of ≈11 bits together with fast sampling. A 500 MHz signal processor is planned using 8 BBD's of 32 parallel inputs and 64 switches at 2 ns intervals for a total sampling time of $8 \times 32 \times 2$ ns = 512 ns. Bucket brigades have not exhibited spectacular rates of new developments. One should keep an eye on these devices in the hope that both the shift rate and the number of buckets will increase in the future. Also more than one manufacturer should be available to avoid the problems associated with single sourcing.

C. Superconducting Strips in Conjunction with Josephson Junction Shift-Registers

The energy deposited by the passage of a particle makes the strip locally normally conducting. The signal is applied to a parallel-in/serial-out Josephson junction shift register.

1. Advantages

The detector can be of small radius; with 10 μ strips and 20 kG field, and a radius of 15 cm, the device would match the resolution of the SLAC Mark II detector.

2. Problems

The technology is not fully developed yet. There will be a dependence on IBM for devices. It looks like an elegant possibility at some distant time.

VII. ORGANIZATION SCHEMES

The organization subgroup is studying to what extent new technology in the form of microprocessors and local networks could be used with new detector, with two basic objectives: (1) simplifying the job of checking out and calibrating several pieces of the detector independently and simultaneously, but with the goal of easy integration into a complete detector; and (2) allowing for the possibility that a major on-line task such as tracking or display could be off-loaded to a powerful micro to ease the load on the main computer. In addition, we are trying to determine the suitability of FASTBUS.

We have been influenced by the SLC/Linac control system and are considering seriously what aspects may be useful. One element that we completely agree with, and strongly recommend for anyone planning to employ separate CPU's is the following: The micro should be used only as an adjunct to a large computer (referred to as a VAX for simplicity) which will have software facilities for generating code, the majority of which should be in a high level language, linking with a library of utilities, downloading to the micro, and symbolic debugging. Note that this implies that the micro need only talk to the portion of the apparatus to which it is connected, and to the VAX; it has no need for the terminal, printer or mass storage. This is the scheme adopted for SLC control in which a VAX communicates to multiple 8086/8087 micros over a CATV network, but the philosophy makes the user interface largely independent of the nature of the micro or the network.

The SLC control scheme will be ready for use by others shortly, with software and hardware already developed. It is thus an obvious choice for elements of a detector requiring monitoring and control, such as gas and high voltage systems.

Most detectors divide naturally into subsystems which are usually developed, constructed, and checked out independently and even separately. During this phase one has need for a computer interfaced to the device, which should have most of the elements of the eventual on-line systems: diagnostics, debugging, calibration, display, and data logging. Clearly

it would be useful if such software could be simply incorporated into the on-line system when the detector is assembled, and if special exercising and debugging code could still be used to diagnose problems afterward. This implies that if a micro is used for the checkout, then it should have an associated mini or main frame for downloading code generated by a cross compiler, and that the detector integration be reversible in the sense that the independent pieces can still be run (i.e., triggered) independently. An open question here is whether a micro used during the checkout should keep some data acquisition and monitoring tasks, or whether these should all be given to the VAX. Certainly such a system makes it easier in principle to make a gradual transition from the initial state in which different parts of the detector are being independently checked out, through an intermediate state where one might want to set up a common trigger for several pieces (i.e., use cosmics and a central tracker to study a shower detector), to the final configuration in which all parts operate on a common trigger, and data from all is logged.

Another area in which cheap high performance micros (like the 168/E) could be useful is if the on-line computer becomes saturated. In any case, major tasks of on-line code such as event display and track finding could be off-loaded from the acquisition system without much trouble if the code were designed with this eventuality in mind. This has led to the concept of multiple independent CPU's, each capable of using the same high level language and each using the same copy of source code and all with access to the raw data.

FASTBUS - The formal definition of the FASTBUS instrumentation system is nearly completed. Since it is designed to allow a distributed data acquisition network in a much more flexible manner than possible with CAMAC, we are examining it for suitability. One impression is that one pays heavily for flexibility with complexity. But it certainly has the advantage of potentially unifying all elements of the data acquisition system in one network with a standard protocol, and allowing the flexibility discussed above. To be considered seriously for a detector, we feel that a demonstration of a working system, with both software and hardware, should precede the start of serious detector design.

TWO DETECTOR MANAGEMENT

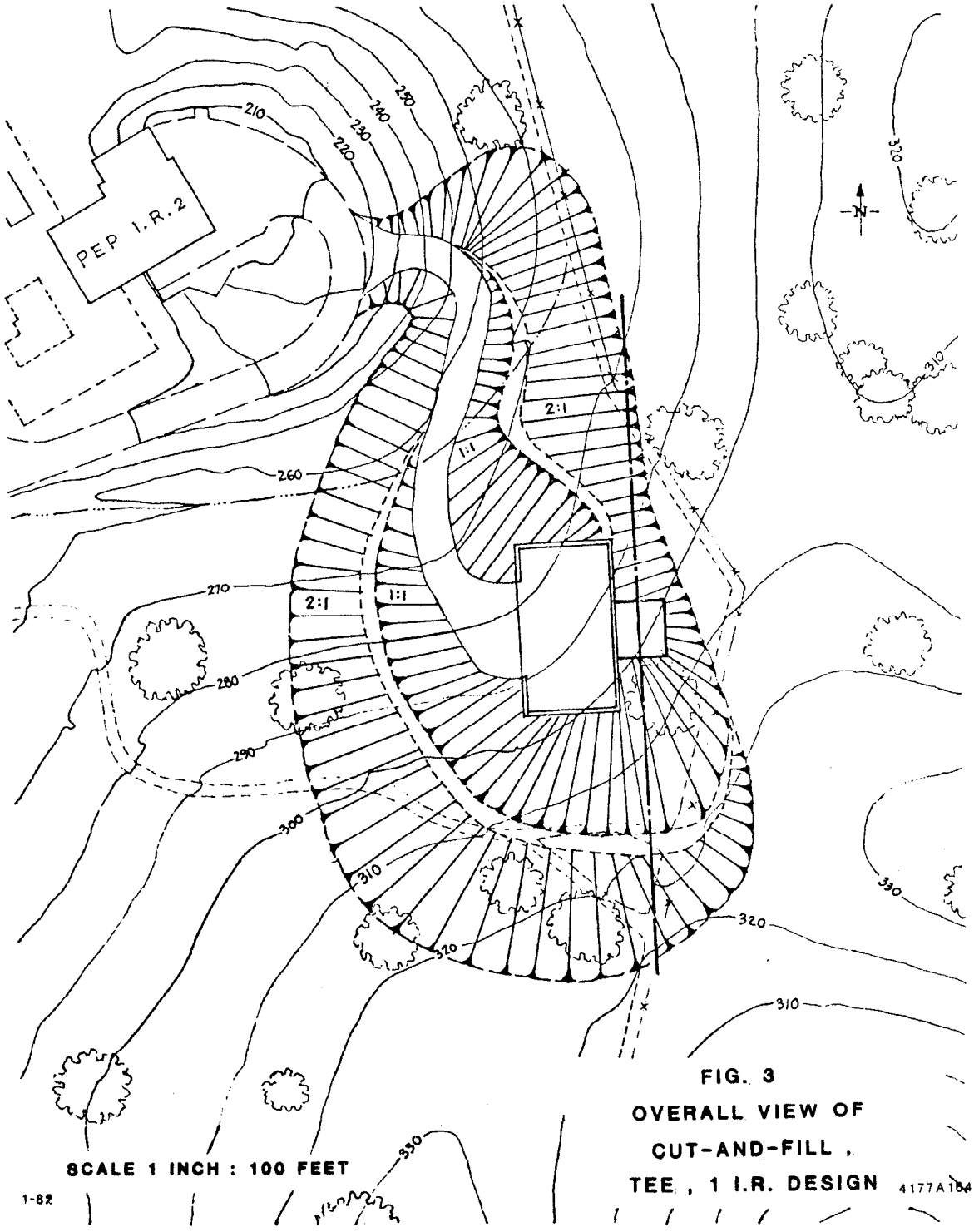

FIG. 3
OVERALL VIEW OF
CUT-AND-FILL ,
TEE , 1 I.R. DESIGN

4177A164

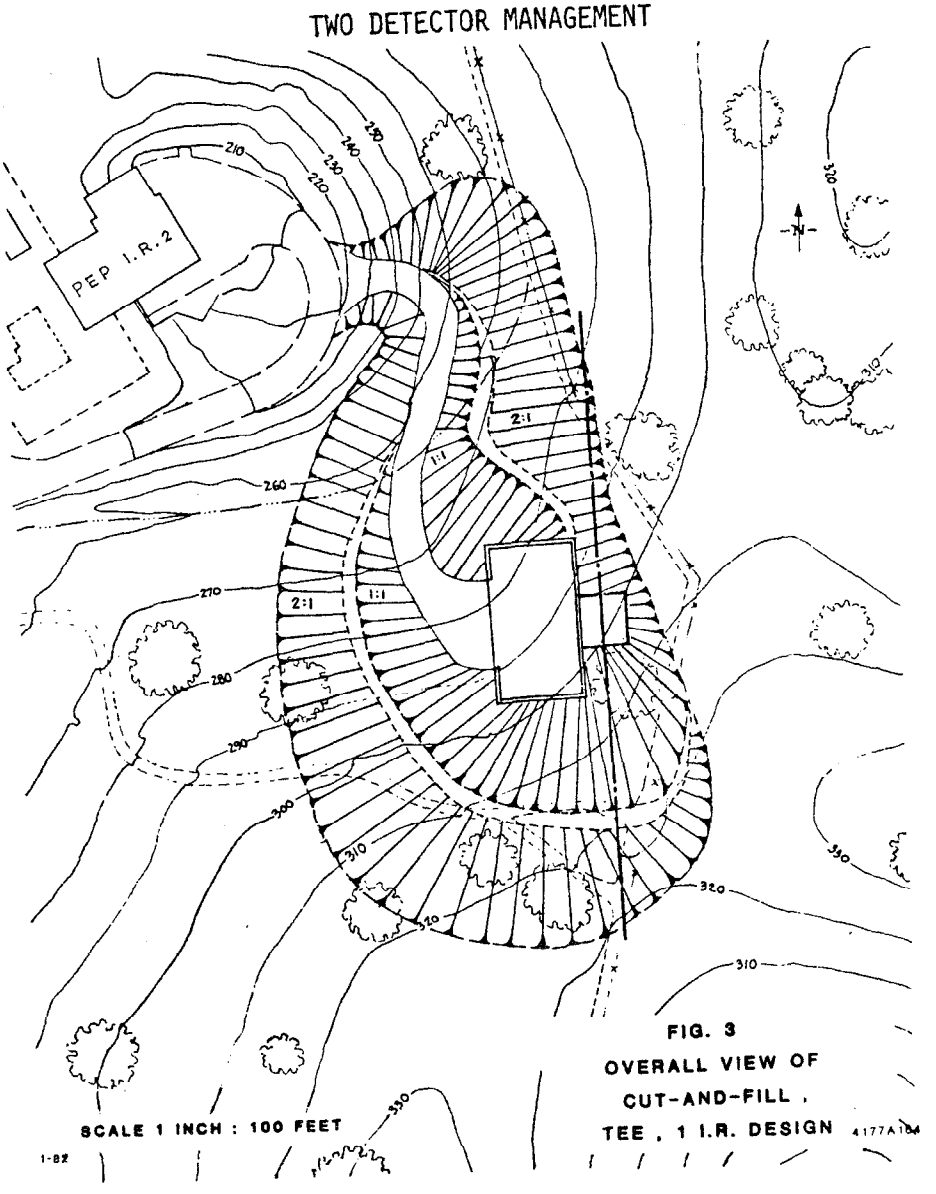

FIG. 3
OVERALL VIEW OF
CUT-AND-FILL .
TEE , 1 I.R. DESIGN

1. INTRODUCTION

This report summarizes the considerations of the Two Detector Management Subgroup of the SLC Workshop. The work, carried out from May through November of 1981, concerned the overall design of the interaction hall, or halls, and of the associated detector staging areas. Our goal, as indicated by the Subgroup name, was to explore designs in which two detectors could operate most efficiently at the SLC.

One requirement of the SLC experimental areas, which was not previously encountered at colliding beams facilities, is that maximum use must be made of the available beam time since data are collected by only one detector at a time. Therefore, a variety of different concepts have been reviewed with the goal of achieving the best use of the colliding beams at minimum cost within the framework of the technical requirements of the SLC.

As a guide to the interaction region and staging area sizes, and to the support and service facilities required for detector operation, studies were made of colliding beam detectors both existing and planned. The study included e^+e^-, pp, and $\bar{p}p$ detectors. These studies covered: (a) size considerations, including the space required for access to detector components and for opening the detector; (b) the weight of detector components which determines the crane capacity; and (c) special detector requirements such as the need for cryogenic support facilities. In these studies the subgroup also examined the options of the use of an existing detector from SLAC or other accelerators, or the construction of a new detector or detectors. Section 2 summarizes these studies.

Section 3 of this report gives an overview of the designs which have been examined, and their technical constraints. An important issue in these considerations was the comparison of the one interaction region (1IR) concept versus the two interaction region (2IR) concept. In the 1IR concept the SLC has one interaction point, Fig. 1a; and the experimental area is designed to facilitate exchange of the detectors at that interaction point. In the 2IR concept the SLC has two interaction points, Fig. 1b; there is a detector at each point, and the beams can be steered to collide at either point.

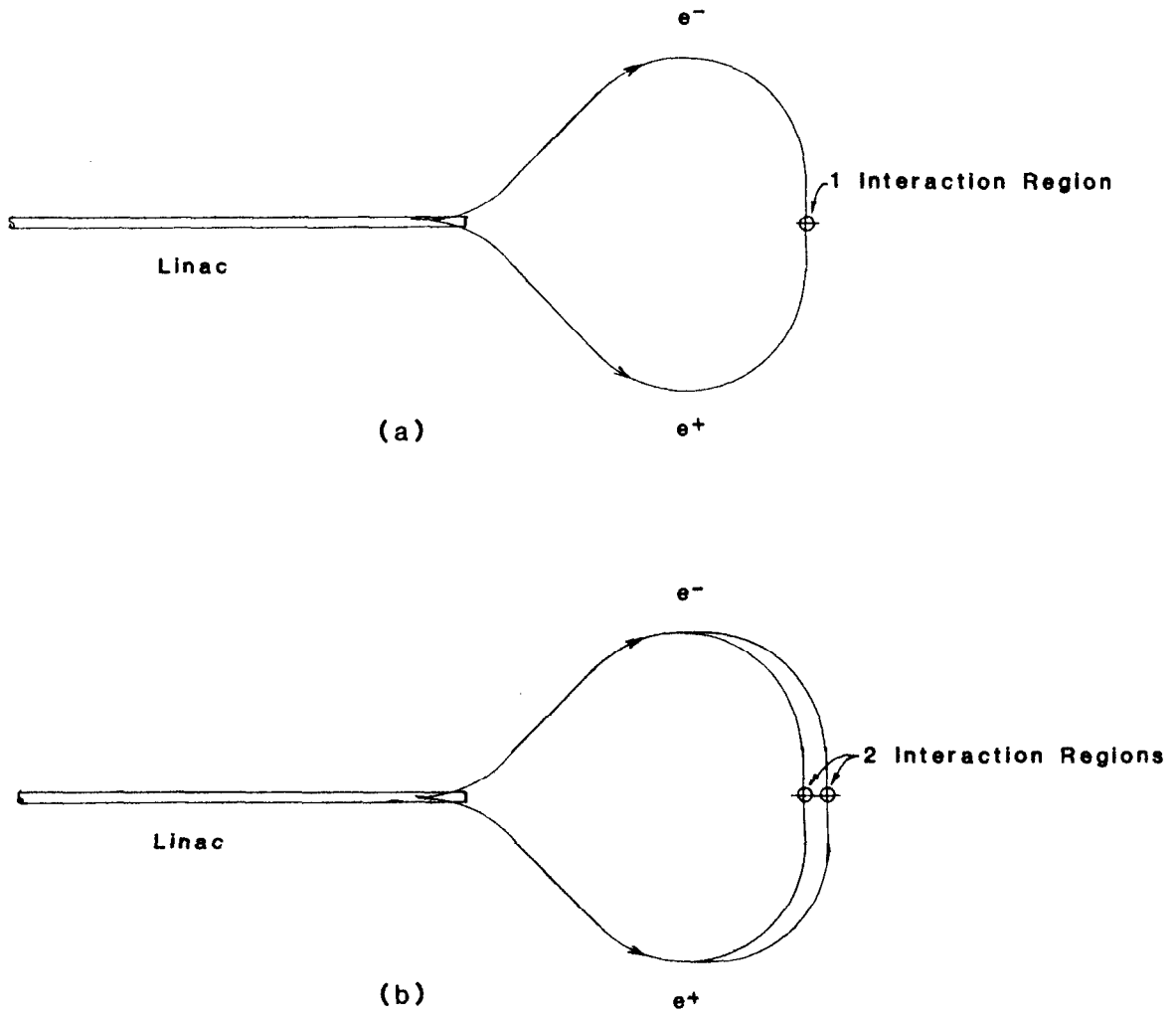

FIG. 1 SCHEMATIC DRAWING OF

1-82 (a) 1 I.R. and (b) 2 I.R. CONCEPTS 4177A162

The 1IR designs are discussed in Sec. 4, where three versions are presented. In the case of the 2IR concept, four different designs are described in Sec. 5. In either concept rapid switching between detectors is desirable in order to make more efficient use of available beams during the installation or replacement of experiments. The 2IR scheme makes switchover times of a few hours to a few days quite feasible, though the ideal of pulse-to-pulse switching looks impractical. We have found that construction costs of the experimental area for the 1IR and 2IR solutions are likely to be roughly equal. The 2IR design obviously implies extra costs because of (a) the additional final focus and beam dump system; (b) the additional arc tunnels required; (c) the additional beam magnets, vacuum systems, and control systems in these arcs; and (d) the beam switching systems. There is also concern that construction of the more complex 2IR scheme may introduce some delay in turn-on of the SLC.

In Section 6, these design concepts presented in earlier sections are discussed with respect to their relative merits. The arguments are concerned mainly with cost, utility, and turn-on scenarios for the 1IR and 2IR schemes. A summary of this discussion along with the Subgroup recommendation for a 2IR scheme is presented at the end of Sec. 6.

2. DETECTOR SIZES AND OTHER PARAMETERS

Table I summarizes the parameters of three classes of colliding beam detectors: PEP and PETRA detectors, other existing detectors, and proposed detectors. Using these parameters, the Subgroup arrived at a minimum floor size for the interaction region vault. The vault is that part of the experimental area which contains the beam interaction point (IP), the final beam focusing system, and the detector.
The walls and ceiling of the vault must provide the primary radiation shielding, hence minimizing costs requires minimizing the vault size.

The vault floor area must be larger than the detector size given by the z and x of Table I for two reasons:

(i) Detector repair usually requires retraction of end caps, or splitting apart of the detector either along or perpendicular to the beam line. This can require up to an additional ±3m in the x or z directions.

(ii) Detector checkout and maintenance requires access to all sides of the detector. The need for this space will increase if more electronics aremounted on detectors in the future.

These considerations led to the following sizes for the vault floor

Rectangular:	16 m along beam by 14 m transverse
Circular:	21 m diameter

These sizes would probably not accommodate the two largest detectors in Table I, the LEP "large" and the VLD.

A beam height of 5 m above the floor was selected as compatible with all the detectors in Table I.

Turning next to the two questions concerning detector weight:

(i) Total weight: In all the 1IR designs, a detector must be moved into or out of the vault as a unit; hence the total weight is important. Most detectors, as shown by Table I, weigh less than 2000 metric tons; therefore the capability of moving up to 2000 tons must be designed into the experimental areas.

TABLE I. DETECTOR PARAMETERS

Name	Status	Length along beams z (m)	Width x (m)	Total Height (m)	Beam* Height (m)	Crane Height Required (m)	Total Weight (tons)	Largest Piece Weight (tons)	Magnetic Field (T)	Uses Cryogenic Fluids
HRS	Operating	10	10	10	4	15	2000	100	1.6	yes
MAC	Operating	8.6	8.6	8	4	10.5	350	~120	0.55	no
MARK II	Operating	7.4	9.5	8	4	10.5	1800		0.5	yes
TPC	Checkout	7.0	7.4	9	4	10.5	1000		1.5	yes
CELLO	Operating	8	6	6	~4		1400	~125	1.5	yes
TASSO	Operating	6.2	11	7.4	~4	9.5	1000	30	0.5	no
UA1	Checkout	12	12	9	4.5		1500	75	0.7	no
Typical "small" LEP detector	Proposed	10	11	10	4				?	?
Typical "large" LEP detector	Proposed	10	18	10	5	12	2000		?	?
CESR II calorimetric	Proposed	5.2	4.4	4.4			~300			
CESR II magnetic	Proposed	7.5	7.5	7.5			~2000			
Small field detector	Proposed	7	8	8	4				0.3-0.5	yes
Very large detector	Proposed	14	11	10	5	15	~4000		1.0	yes

*For operating detectors this is beam height being used, for others it is beam height required.

(ii) Weight of heaviest component: Assembly of some of the detectors listed in Table I requires a crane capable of lifting 100 to 125 metric tons with a minimum crane height of 15 m. However the assembly of these unusually heavy parts could be done with a portable crane in special cases. Then a permanent 50 ton crane should be sufficient in the final assembly area.

To conclude this section we note that a number of existing and proposed detectors use cryogenic fluids such as liquid helium or liquid argon. The plumbing associated with these cryogenic requirements could place additional constraints on the staging of the detector but this question has not been studied in detail in this report.

3. OVERVIEW OF DESIGN CONSIDERATIONS

a. Location and Terrain

Fig. 2 shows the proposed location of the interaction point or points on the SLAC site. The location is about 100 m east of PEP's IR2. The ground slopes upwards towards the east. An access road for moving detectors or major detector components must come from the west to minimize cost. The average ground elevation at this location is about 90 m.

Information obtained from seismic techniques and test borings in the north arc tunnel and IR region indicates a rather poor ground structure near the surface. As a result, the beam line elevation has been decreased substantially from earlier designs. The problem lies with the Santa Clara Formation of rock, which is sufficiently weak material that construction of the tunnel becomes very difficult. By lowering the tunnel of the north arc, it can be situated below this formation, reducing costs. Thus geological constraints on the arc tunnel depths put the interaction point elevation at 60 to 70 m. (In the design drawings included with this report an elevation of 63 m is used.) Hence that point is now as much as 30 m below the present ground level. This depth has exercised a powerful constraint on the design and construction method options for the experimental area.

b. Construction Methods

Two general construction methods have been considered so far by the SLC engineers.

(i) Cut-and-Fill Method: The area is excavated to about the depth of the vault floor. The vault, assembly area buildings, counting houses, and earth retaining walls are then constructed. Finally some of the earth is put back. The depth and the weakness of the ground at the proposed location leads to a need for extensive retaining walls and gentle slopes. This method would be used for those designs where the access roads lead directly to the floors of the vault and staging areas. Examples are the 1IR tee design, Sec. 4a and the 1IR roll-in design, Sec. 4c.

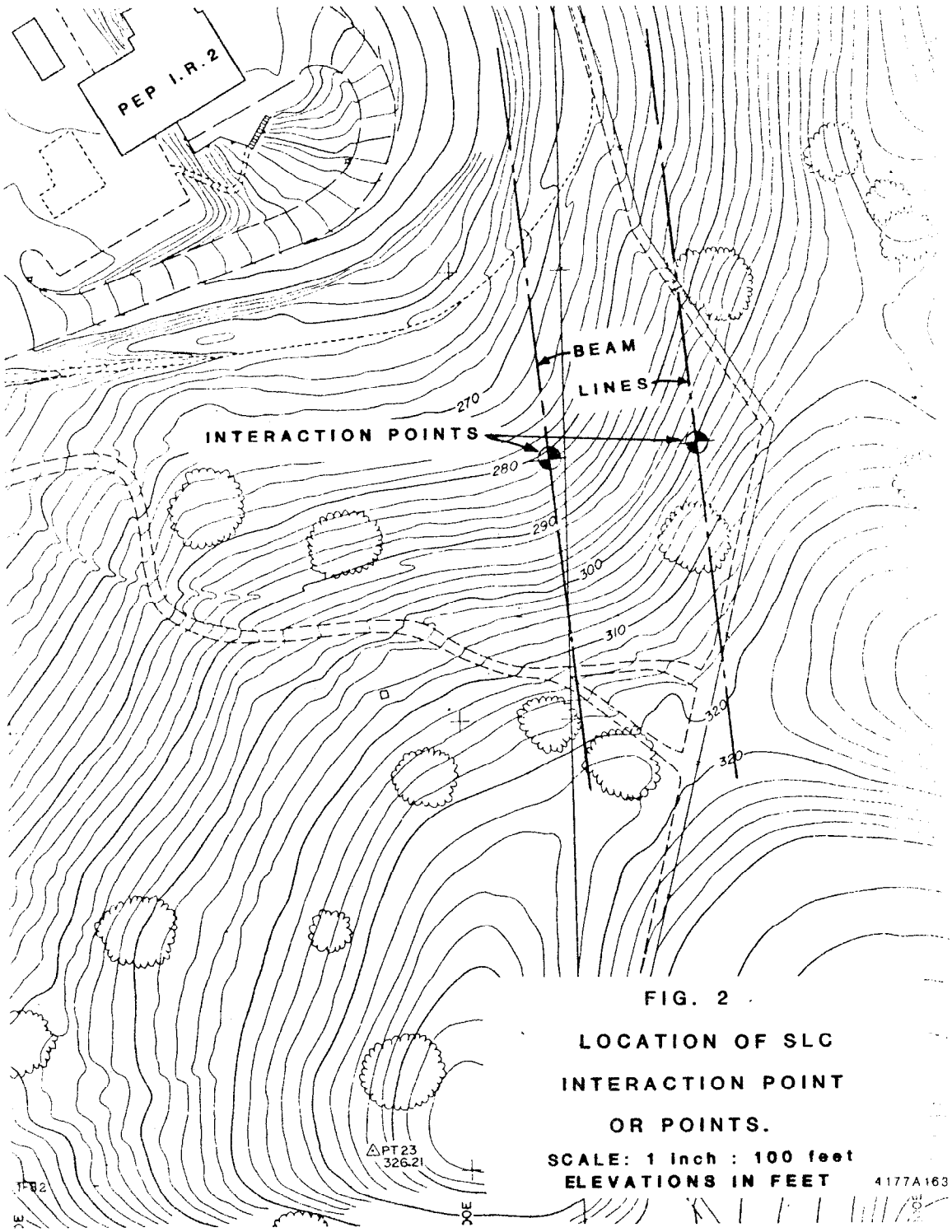

FIG. 2

LOCATION OF SLC

INTERACTION POINT

OR POINTS.

SCALE: 1 Inch : 100 feet

ELEVATIONS IN FEET

4177A163

(ii) Below-Ground Method: The alternative method is to keep the access roads, some of the counting houses, and perhaps part of the staging area nearly at ground level. The beam vault or vaults, and perhaps part of the staging area would then be about 30 m below ground. They would be constructed by digging large circular pits. The pits might be contiguous or might be connected by halls dug underground. Examples are the 1IR push-pull design, Sec. 4b, and the 2IR designs of Secs. 5b(ii), 5c, and 5d. In these schemes the detectors are assembled and checked out on the floor of the pits, or in a staging area adjacent to the pits.

c. Vault and Staging Area Size

The function of the vault and its size has been discussed in Sec. 2. The staging area has several functions: it provides space for detector construction; it provides space for detector check-out on cosmic rays; and it provides space to store a detector when it is off the beam line. An ideal staging area requires about 20 m x 20 m per detector. However in the below-ground designs such a large area is too expensive; and in these designs a portion of a 21 m diameter, circular area is used.

d. Detector Transport

In the 1IR designs it is highly desirable that within a period of several weeks or less: one detector is moved out of the vault, a second detector operating in check-out mode in a staging area is moved into the vault, and that second detector is put into operating condition in the vault. This has been achieved in the PETRA interaction region which contains the PLUTO and CELLO detectors. Even in the 2IR design it is desirable that one of the detectors can be moved quickly out of its vault, to allow accelerator physics studies at the interaction point.

e. Counting Houses and Electronic Trailers

We do not know what type of detectors will be used at the SLC, hence our counting house criteria must remain general. We estimate that each detector requires a counting house totaling about 300 m^2 in floor area. The experimental area designs presented in this report are too preliminary to justify exact specification of their location and size. However in each design we have made sure that there is sufficient room for counting houses, and for shielding of those houses from radiation.

Our primary concern was that the SLC must be able to use existing detectors, perhaps upgraded. Most existing detectors have electronic trailers, often called LEACH's, which contain fast electronics and sometimes other detector servicing equipment. Some of the trailers are quite extensive, the floor area being of the order of 100 m^2. Many of the designs presented in this report can handle trailers of this size, but some only have room for much smaller trailers.

In the below-ground designs, Secs. 4d, 5c, and 5d, it is still an open question as to the best place to put the counting houses. Should they be close to their detectors, perhaps in an auxiliary pit dug for that purpose? Or should they be partly or entirely on the surface?

f. Radiation Shielding

Initial studies have been done (T. Jenkins and J.L.Harris, Collider Note No.:130) on the shielding required for the interaction region. Two different sets of criteria were used; one set for a worst case accident; the other set for the annual dose limit. The worst case accident assumes that the full beam power targets in the interaction region with a dose rate of less than 25 R/hr. This worst case accident was the most stringent criteria. It requires that at least 1 m of concrete be used to shield the interaction point, assuming that the shield walls are at least 7 m from the interaction point. The designs presented in this report meet that requirement. A nominal thickness of 2 m is used in the figures.

4. ONE INTERACTION REGION DESIGNS

The Subgroup studied a variety of concepts for a one interaction region experimental area. It selected the three designs presented here as the most promising and as representing different approaches to the 1IR design.

a. Cut-And-Fill, Tee, 1IR Design

This design, Figs. 3 and 4, is derived from the experimental area design used in the SLC Conceptual Design Report (CDR). The staging areas and counting houses for both detectors are on the west side of the interaction region vault. The west side is used because the ground elevation is lower than on the east side, allowing less excavation for the wall and access road. Following the design philosophy used in the CDR each detector is moved into or out of the vault with all its electronic cables intact, and with its cryogenic components cold. Hence a detector can be checked out in the staging area on cosmic rays, and then moved into the vault almost ready for physics operation. The construction method is cut-and-fill. The maximum depth of cut is approximately 30 m; and the vertical:horizontal slope of the remaining earth walls would be about 1:2. Hence a large amount of earth must be removed, of which about 40% is used as backfill. The design details follow:

(i) Vault: The vault is 16 m along the beam line. The width is 7 m to one side of the line and 10 m to the other side, allowing for a large asymmetric detector. The vault has its own 15 ton crane.

(ii) Staging Area Building: The staging area is 44 m wide by 17 m deep, providing enough room for the assembly of two detectors. The building has thick walls which also serve as earth retaining walls. Inside is a 50 ton or larger crane.

(iii) Counting Houses and Electronic Trailers: Each counting house has three floors plus a usable roof area. The area per floor is at least 7 m x 10 m. There is room in the staging area building for small electronic trailers, about 100 m^2 or less in floor area.

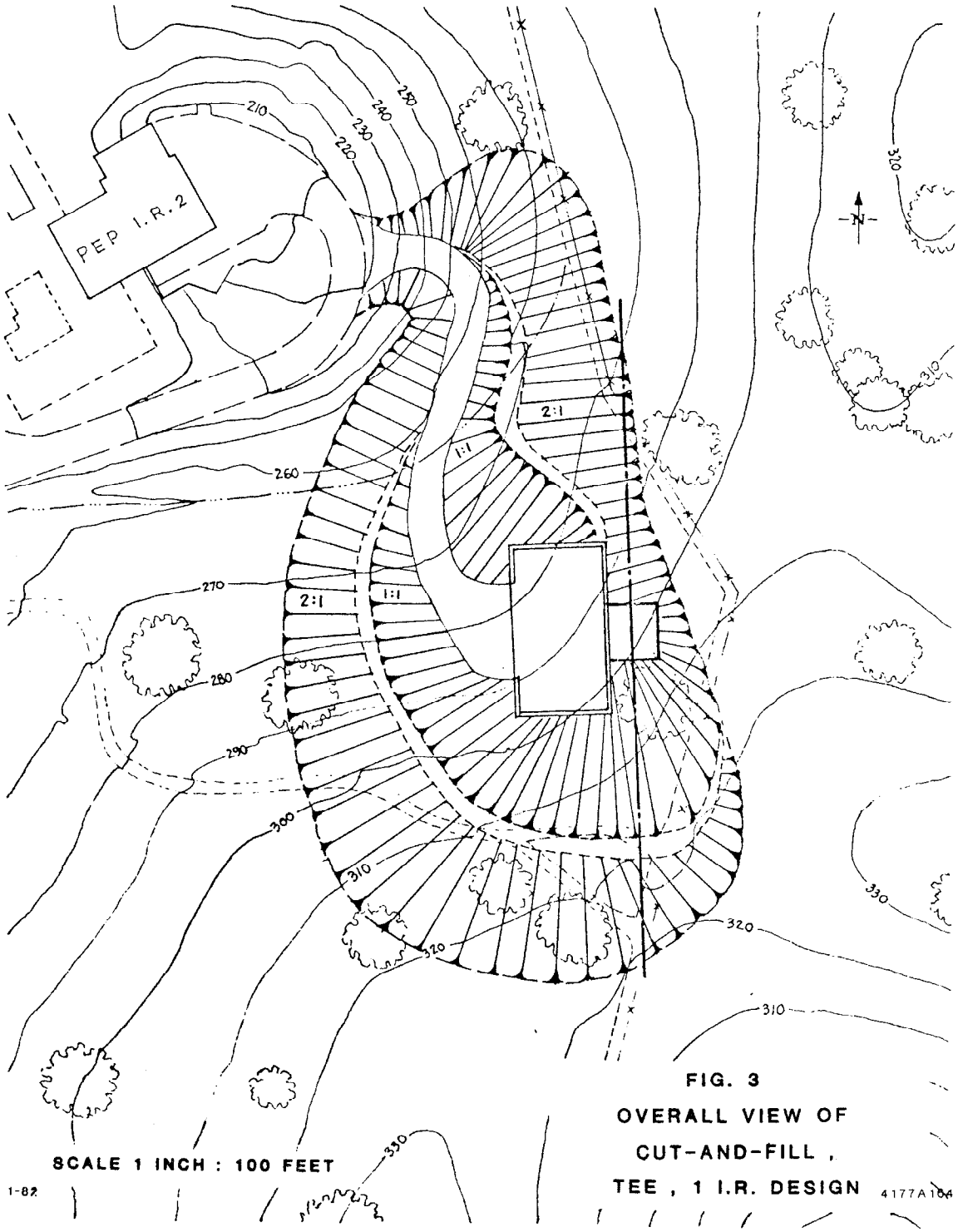

FIG. 3
OVERALL VIEW OF
CUT-AND-FILL ,
TEE , 1 I.R. DESIGN

4177A164

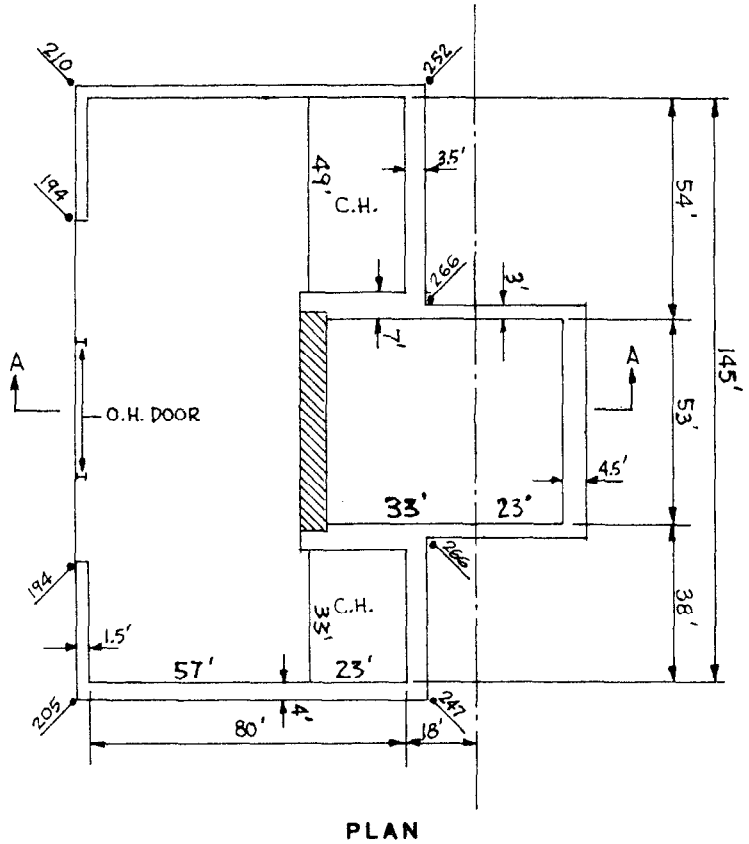

PLAN

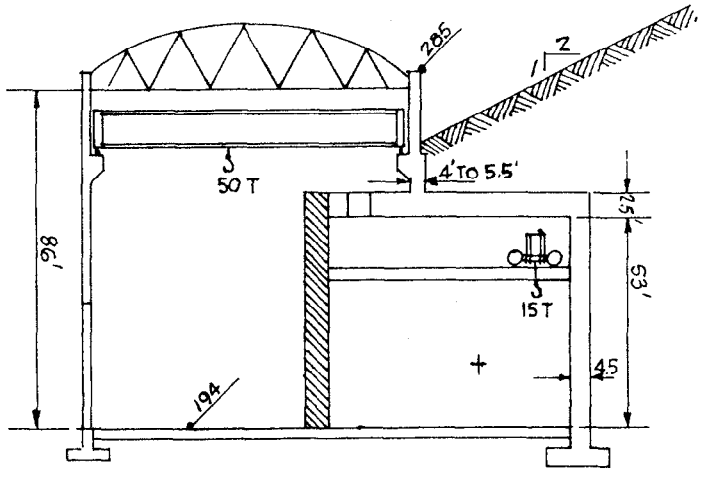

SECTION A-A

SCALE 1" = 40'

xxx = FIN. GRADE

FIG. 4 DETAILS OF CUT-AND-FILL , TEE , 1 I.R. DESIGN

1-82 4177A165

b. Remote Staging Area, Roll-In 1IR Design

This design Fig. 5 has one IR vault constructed by the cut-and-fill technique with an adjacent assembly area and counting house. The IR is at about the same elevation as IR2 at PEP and a substantial road runs between them.

This SLC IR is not very different from IR8 at PEP. The assembly area would be separated from the collision region by a shielding curtain and wall. A 50 ton capacity overhead crane would service the assembly - IR area. A 3 story counting house is located just outside the assembly area. The road outside the assembly area has a spur to allow one detector to be parked, allowing for the passage of a second detector in and out of the SLC IR area.

This IR scheme does not allow for changing detectors on a few days time scale, but instead would allow for changes on the few weeks to few months scale (ideally during summer shut downs). Its location next to IR2 at PEP makes checkout of a new detector at PEP easy. The subsequent move from IR2 to the SLC is less difficult than, for example, the Mark II move from SPEAR to IR12 at PEP. If a reasonable data running period at the SLC turns out to be three or more months the change-out time and PEP check out period could be quite reasonable.

c. Below-Ground, Push-Pull, 1IR Design

We looked at two ways to build a push-pull 1IR experimental area: by cut-and-fill or by deep-pit excavation. A preliminary examination of the cut-and-fill method indicated it would be more expensive due to the cost of excavating for the east assembly area and its access road. Therefore, the most promising push-pull 1IR design appears to be that using the below-ground construction method Fig. 6. The two assembly areas and one vault are constructed by digging three overlapping circular pits, each about 21 m in diameter. The pits extend down about 20 m below an access floor which has been excavated to a 78 m elevation.

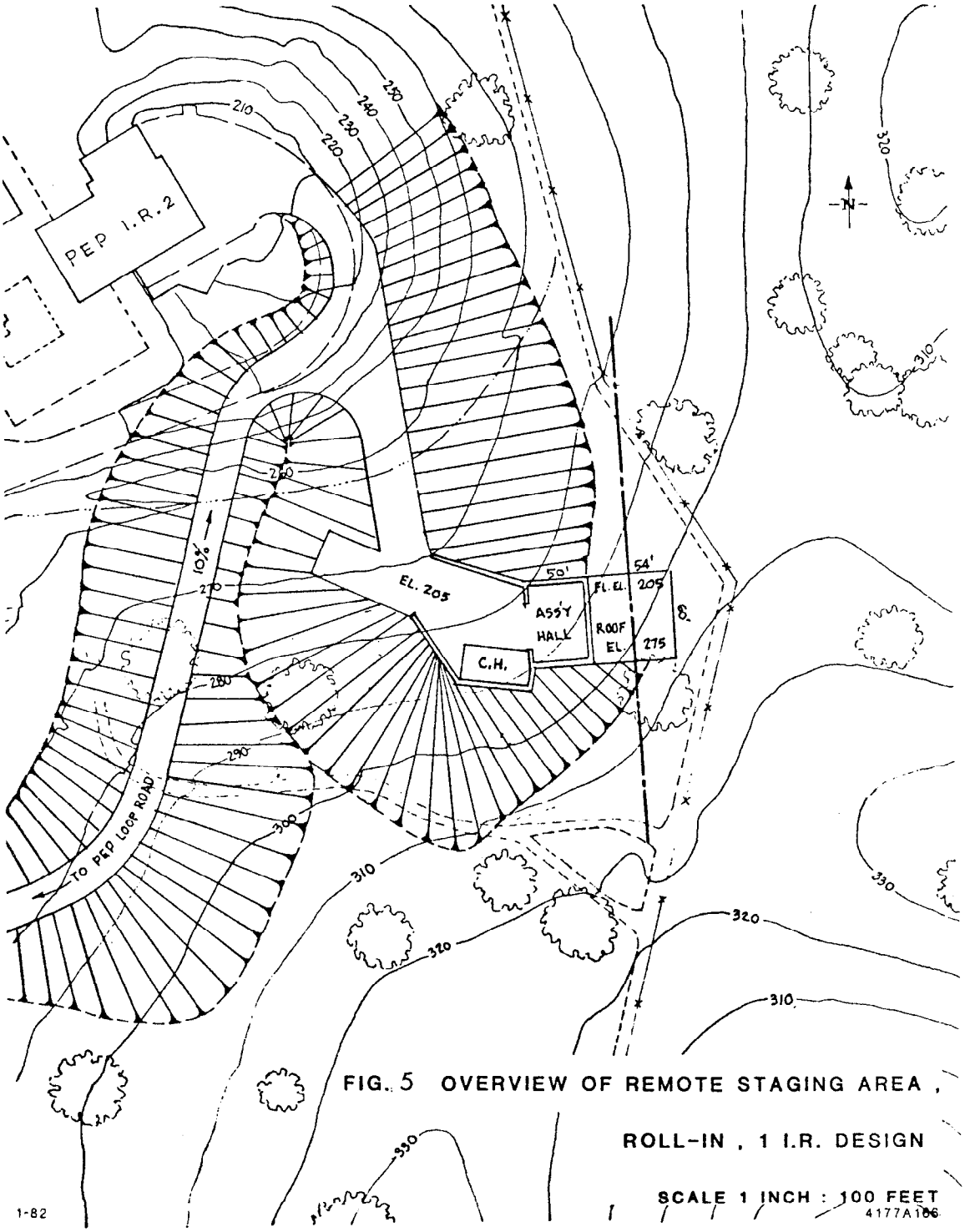

FIG. 5 OVERVIEW OF REMOTE STAGING AREA , ROLL-IN , 1 I.R. DESIGN

SCALE 1 INCH : 100 FEET

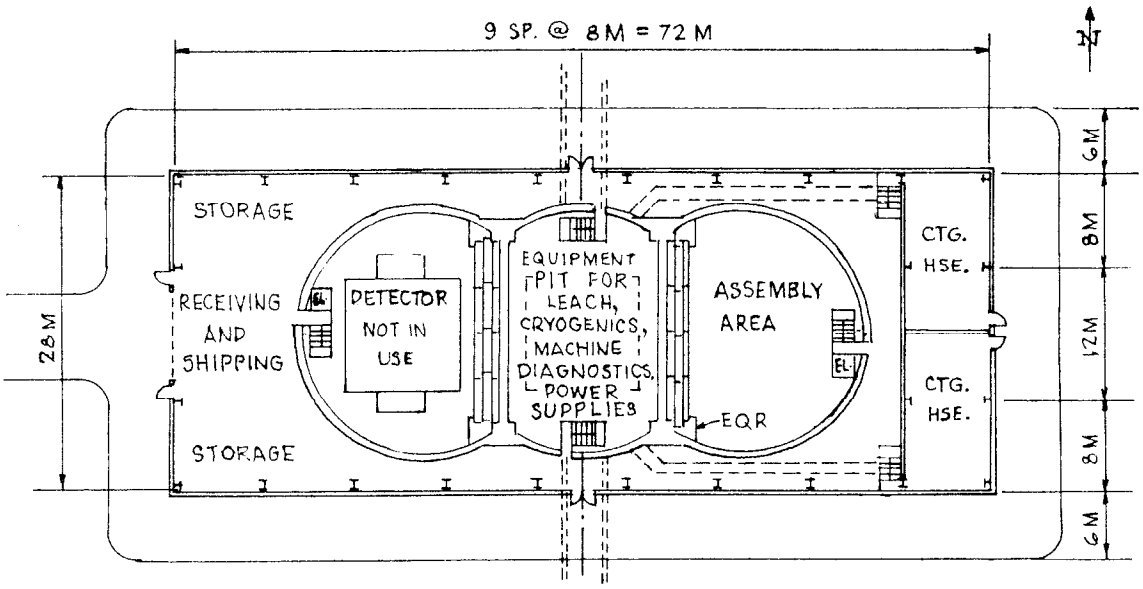

PLAN AT ELEV. 78 M

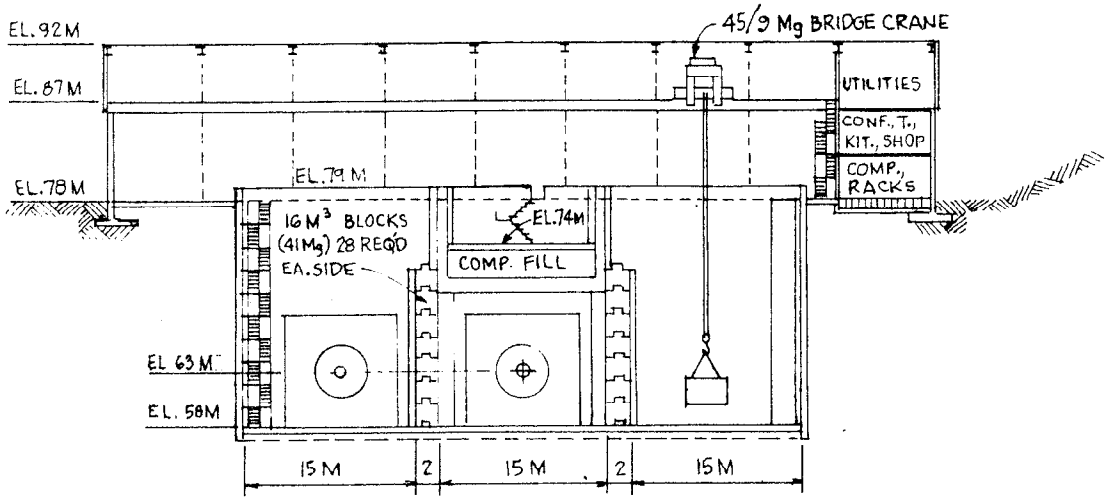

LONGITUDINAL SECTION

FIG. 6 PLAN AND ELEVATION VIEWS OF BELOW-GROUND, PUSH-PULL, IIR DESIGN

A metal building, about 30 m x 70 m, covers the pits. It contains a crane with one trolley having two hoists.

The locations of the counting houses or the use of the pit space above the vault have not been established. Fig. 6 shows one possibility where both counting houses are in the ground level building. The space above the vault is used for electronic trailers and/or cryogenic equipment. An alternative is to use that space for one of the counting houses.